Technical Report

TR-98-18

The interaction of sorbing and non-sorbing tracers with different Äspö rock types

Sorption and diffusion experiments in the laboratory scale

Johan Byegård, Henrik Johansson and Mats Skålberg
Department of Nuclear Chemistry
Chalmers University of Technology, Gotheburg, Sweden

Eva-Lena Tullborg
Terralogica AB, Gråbo, Sweden

November 1998

Svensk Kärnbränslehantering AB
Swedish Nuclear Fuel
and Waste Management Co
Box 5864
SE-102 40 Stockholm Sweden
Tel 08-459 84 00
+46 8 459 84 00
Fax 08-661 57 19
+46 8 661 57 19

The interaction of sorbing and non-sorbing tracers with different Äspö rock types

Sorption and diffusion experiments in the laboratory scale

Johan Byegård, Henrik Johansson and Mats Skålberg

Department of Nuclear Chemistry
Chalmers University of Technology, Gothenburg, Sweden

Eva-Lena Tullborg

Terralogica AB, Gråbo, Sweden

November 1998

Abstract

Laboratory experiments studying the sorption and diffusivity of different tracers in Äspö Hard Rock Laboratory (Äspö HRL) site specific conditions have been performed. The experiments were conducted by applying both the batch sorption and the through diffusion technique. The investigation was focused on slightly sorbing tracers, *i.e.*, alkaline metals (Na^+, Rb^+ and Cs^+) and alkaline earth metals (Ca^{2+}, Sr^{2+} and Ba^{2+}), but some presumed non-sorbing species have also been included. The dominating generic rock material from Äspö HRL, Äspö diorite and Fine grained granite, were used as well as some altered wall rock and mylonites from the Feature A fracture, the fracture where *in situ* migration studies have been performed during the First TRUE Stage (TRUE-1). Synthetic groundwater was used; similar to the high saline groundwater found at the 350m level at Äspö HRL and at the Feature A site.

The results of batch experiments show that the sorption of the tracers increase in the order $Na^+ < Ca^{2+} \approx Sr^{2+} < Rb^+ \approx Ba^{2+} < Cs^+$ with the sorption coefficient of Na^+ in the order of $(4\text{-}30)\cdot10^{-6}$ m^3/kg and for Cs^+ in the range of $(1\text{-}400)\cdot10^{-3}$ m^3/kg. The variations in sorption coefficients are due to differences in the composition of the geological material, contact time and particle size. Sorption is generally stronger for the Äspö diorite than for the Fine-grained granite which is explained by the much higher concentration of biotite in Äspö diorite than in Fine grained granite. In the altered material the biotite has been transformed to chlorite and a lower sorptivity is shown for those material compared to the fresh diorite and granite, respectively. Attempts to explain the sorption and desorption results to a surface sorption - diffusion model are presented.

The diffusion results show that the tracers were retarded in the same order as was expected from the measured batch sorption coefficients. Furthermore, the largest size fraction was the most representative when comparing batch sorption coefficients with sorption coefficients evaluated from the diffusion experiments. The observed effective diffusivities and transport porosities decreased with increasing sample lengths. It was also observed that the formation factor obtained for sorbing and non-sorbing tracers in the same sample is approximately equal.

A heteogeneous and mineral specific porosity distribution was found in the Äspö-diorite using the ^{14}C-PMMA method, whereas the porosity pattern of Fine-grained Granite was more uniformly distributed. The porous mineral areas were found to be consistent with the sorptive mineral areas in Äspö-diorite. A double porosity network of slow and fast migration pathways, with different sorption capabilites, was used to describe the diffusion of Cs and Ba.

The diffusivity and porosity were low in the Feature A sample containing mylonite compared to the generic material.

Sammanfattning

I syfte att studera sorption och diffusion av olika spårämnen under plats-specifika betingelser för Äspö Hard Rock Laboratory (Äspö HRL) har laboratorie-experiment utförts. Experimenten genomfördes som satsvisa sorptionsförsök och som genom-diffusionsförsök. Undersökningen fokuserades på svagt sorberande spårämnen, d.v.s. alkali-metaller (Na^+, Rb^+ and Cs^+) och alkaliska jordartsmetaller (Ca^{2+}, Sr^{2+} and Ba^{2+}), men några troliga icke-sorberande ämnen har också inkluderats. De dominerande generiska bergarterna från Äspö, Äspö-diorit och Finkornig granit samt omvandlat väggmaterial och mylonit från Struktur-A sprickan användes i experimenten. *In situ* migrationsstudier genomförs för närvarande i Struktur-A sprickan. Syntetiskt grundvatten liknande det högsalina grundvatten som återfinns på 350 m djup på Äspö samt vid Struktur A sprickan användes vid försöken.

Resultaten från de satsvisa experimenten visar att sorptionen av spårämnen ökar i ordningen $Na^+ < Ca^{2+} \approx Sr^{2+} < Rb^+ \approx Ba^{2+} < Cs^+$. Sorptionskoefficienten för Na^+ är ca $(4\text{-}30)\cdot10^{-6}$ m^3/kg och för Cs^+ ca $(1\text{-}400)\cdot10^{-3}$ m^3/kg. Variationen i sorptionskoefficienter beror på skillnader i sammansättning av det geologiska materialet, kontakttid och partikelstorlek. Sorptionen är generellt starkare för Äspö-diorit än för Finkorning granit vilket kan förklaras av den mycket högre halten av biotit i Äspö-diorit. Biotiten i det omvandlade materialet har ombildats till klorit vilket leder till en lägre sorptivitet i jämförelse med Äspö-diorit och Finkorning granit. En ytsorption-diffusionsmodell presenteras i ett försök att förklara sorptions- och desorptionsresultaten.

Diffusionsresultaten visar att spårämnena retarderades i samma ordning som förväntades från dom satsvis uppmätta sorptionskoefficienterna. Vidare fanns att den största partikelfraktionen var mest representativ i jämförelse mellan sorptionskoefficienter erhållna från skakförsök eller genom-diffusionsförsök. De uppmätta effektiva diffusiviteterna och transport-porositeterna minskade med ökande provlängder. Det observerades också att formationsfaktorn för sorberande och icke-sorberande spårämnen var approximativt lika i samma prov.

En heterogen och mineral-specifik porositetsfördelning observerades i Äspö-dioriten m.h.a. ^{14}C-PMMA-metoden, medan porositetsmönstret i den Finkorniga graniten var mer enhetligt fördelat. De porösa mineralytorna motsvarade de sorptiva mineralytorna i Äspö-diorit. Ett dubbelt porositets-nätverk bestående av långsamma och snabba diffusionsvägar med olika sorptionskapaciteter användes för att beskriva diffusionen av Cs och Ba.

Diffusiviteten och porositeten var lägre i Struktur-A materialet som innehöll mylonit än i det generiska materialet.

Contents

1 Introduction

Within the TRUE-1 project (Winberg 1994), research is presently being conducted in order to understand the transport and retention processes in a single fracture scale. The project comprises of *e.g.* fracture characterisation, experiments providing hydraulic information, tracer tests using non-sorbing tracers and also *in situ* experiments in order to study the behaviour of sorbing tracers in their transport in fractures of crystalline rock. The experiments are concentrated to the Feature A (Winberg 1996) fracture in the Äspö Hard Rock Laboratory.

One of the aims with the project is to study and model retardation using information from the different experimental scales; *i.e.* coupling of results obtained both in field experiments and laboratory experiments. From the breakthrough results of the sorbing tracers used in *in situ* experiments, information about the interaction of the groundwater and the rock matrix could be obtained. It may thus be possible to understand and quantify flow and retardation processes like flow wetted surface, matrix diffusion and the sorption capacity of fractures. To be able to interpret and model the *in situ* sorption results, supporting laboratory experiments are essential.

A suggestion for selection of sorbing tracers and some basic considerations have been given in earlier work (Byegård 1993). Before the use of sorbing tracers *in situ*, the following parameters must be investigated in laboratory experiments:

- The sorption mechanism. The desired sorption process should be a result of the interaction of solute and the rock matrix and not mainly reflecting properties solely dependent on the tracer itself, *e.g.* redox and precipitation reactions.
- The reversibility of the sorption of the tracers. For obtaining retardation data of tracers, it is important that both sorption and desorption occurs, *i.e.* that the tracer is not lost because of irreversible processes
- The strength of the sorption. The transport of the tracer in a fractured crystalline rock medium may be characterised by very large amounts of rock in contact with a low amount of groundwater. To be able to obtain a breakthrough within a reasonable time perspective, it is thus important that the strength of the sorption is not too high.
- The diffusion characteristics of the tracers. Transport of tracers in fractured rock is likely to be influenced by diffusion into the rock matrix, which will influence the sorption considerably.

In the present work, an investigation in the laboratory scale of the sorption and diffusion properties of different tracers is presented. The experimental conditions are selected in order to represent the chemical environment in and around the Feature A fracture. Quantitative information of the sorption and diffusion parameters is given, and the data are also evaluated in order to investigate the validity of some of the proposed sorption models.

2 Experimental Conditions

The experimental programme forming this investigation was divided into two series of different experimental conditions:

The first series of experiments were concentrated on generic rock material from the Äspö HRL. Before the Feature A was selected as the experimental site for the TRUE-1 experiment, the experimental programme was focused on obtaining sorption and diffusion data representing types "general" Äspö conditions. Therefore material was selected representing the two most important rock present at Äspö, Äspö diorite (ÄD) and Fine-grained granite (FGG). The groundwater used in the experiment with this geologic material was chosen in order to represent an average Äspö groundwater at 400m level. This investigation was focused on the sorbing cationic tracers and the only non-sorbing tracer (used as a reference tracer) was tritiated water, HTO.

In the second series of experiments, the main objective was to concentrate on the specific chemical and geological environment of the Feature A. When the Feature A was selected as the experimental site for the TRUE-1 experiment, a more elaborate investigation of the experimental conditions addressed directly on the Feature A environment was initiated (Winberg 1994). Geologically, it was found that the fracture walls consist of mylonite and layers of altered Äspö diorite and Fine-grained granite. Furthermore, the analysis of the sampled groundwater from the Feature A fracture showed that the composition was considerably different from the groundwater used in the first series of experiments. In this experiment series, the behaviour of both sorbing and presumed non-sorbing tracers were investigated.

The experimental techniques that have been applied in this experimental program are:

- Static batch experiments, investigating the sorption and desorption of the tracers on crushed and sieved geologic material, described in chapter 3.

- Through-diffusion experiments, using intact geologic material obtained form different drill cores, described in chapter 4.

2.1 GEOLOGIC MATERIAL

The generic geologic material used in this investigation was sampled in the Äspö tunnel. Two types of samples were collected. Samples were taken from intact drill cores (originating from the drilling of boreholes for the elevator shaft at 220 m), which were used for the preparation of the specimen in the diffusion experiments. Sampling of larger amounts of Äspö diorite and Fine-grained granite was performed directly from the tunnel walls. These samples were crushed and sieved, and was sent for geochemical and mineralogical analysis.

The Feature A site-specific material was obtained from the drillcores intersectioning the Feature A Fracture (KXTT1- KXTT4). At the KXTT1 intersection, two fractures with a distance of 1-2 cm were found. The rock piece in the drill core between these two fractures was used as the specimen in a diffusion cell, *i.e.*, a though-diffusion cell with mylotinised layers and altered material at both ends was thereby obtained. Mylonite and altered granite/diorite were sampled from the intersection of Feature A and KXTT2-KXTT4, respectively, and this material was after the crushing and sieving used for batch sorption experiments.

2.1.1 Geological characterisation

The retention that influence the mobility of radionuclides along flowpaths in a crystalline rock are determined both by the sorption capacity of the minerals in contact with the groundwater and of the network of interconnected pores in the fracture coating minerals and the adjacent wallrock. As a consequence of this, there is a need for characterisation not only of the mineral contents of the samples used for the laboratory studies, but also of the textures (porosity, orientation of minerals, etc.) of the different rock types used. A geological characterisation of the materials used in this investigation has therefore been performed and the results are given in the following sections.

2.1.1.1 Äspö diorite

Äspö diorite is the dominating rock type in the Äspö area. It is a medium-grained and porphyritic quartz monzodiorite/granodiorite, which contains K-feldspar phenocrysts, 1-2 cm in size. It is slightly foliated and the porosity is generally in the interval of 0.5±0.2 % (Stanfors *et al.* 1993a, Stanfors *et al.* 1993b).

Mineralogical composition has been determined from studies of thin section using transmissive light microscope. Plagioclase, K-feldspar, quartz, biotite and calcite were observed. Accessoric minerals were muscovite, titanite, apatite, fluorite, zircon and opaque phases (mostly magnetite). The plagioclase showed partly weak sausuritisation (plagioclase → albite+sericite+epidote). In the thin section analysis, the biotite showed a green color, indicative of a slight alteration. Chlorite was not present in the thin sections studied. Some microfractures sealed with calcite were observed.

The results of the analyses of the chemical composition of the different fractions of Äspö diorite (Table 2-1) show a significant difference between the coarse and the fine fractions. These differences are due to different original grain sizes of the minerals and also differences in brittleness between different types of minerals. The chemical analyses have been used in order to estimate the mineralogical composition in the different fractions. As the mineralogy of the rock is known and the compositions of the biotite and plagioclase have been analysed with microprobe (Banwart 1995), the following assumptions and simplifications could be made.

1. All Mg is hosted in the biotite
2. All Na is hosted in the plagioclase
3. All P is hosted in the apatite
4. K is partitioned between the biotite and the K-feldspars
5. Ti is partitioned between the biotite and titanite
6. Fe is partitioned between biotite, epidote, titanite and magnetite
7. The SiO_2 in access after subtracted for the amounts in feldspars, biotite and epidote is assumed to be quartz.

The result of the calculated mineralogical composition, described above, is given in Table 2.2. Significantly higher portions of biotite, titanite and apatite are found in the finest fractions, whereas the feldspars show the opposite trend. The calculated results are also in accordance with the trace element chemistry, *e.g.*, the Cs content correlates roughly with the calculated biotite content and Ba correlates with the calculated feldspar contents. The chondrite normalised rare earth elements (REE) diagrams for the Äspö diorite shows significant differences between the coarsest and the finest fractions of Äspö diorite (Fig. 2-1). The three larger fractions are largely similar in chemical composition and presumingly also in mineralogy.

Table 2-1. Chemical analyses of the different fraction sizes (mm) of Äspö diorite from Äspö Hard Rock Laboratory. Rb, Ba, Cs, U, Th, Hf and the Rare earth elements are analysed using INAA (Studsvik Nuclear, Radiometry, Nyköping). All other elements are analysed with ICP-MS (Svensk Grundämnesanalys AB, Luleå). All concentrations refer to single samples.

Element	ÄD-1 0.045-0.09	ÄD-2 0.09-0.25	ÄD-3 0.25-0.5	ÄD-4 0.5-1.0	ÄD-5 1-2	ÄD-6 2-4 (mm)
Main elements (%)						
SiO_2	60.1	61.3	60.0	60.6	60.1	60.7
Al_2O_3	14.6	16.3	16.3	18.7	18.1	18.0
CaO	4.5	4.4	4.5	4.4	4.4	4.2
Fe_2O_3	7.9	6.8	5.4	5.1	5.1	5.1
K_2O	3.3	3.0	3.3	3.3	3.2	3.2
MgO	3.1	2.3	2.3	2.2	2.2	2.1
MnO	0.2	0.1	0.1	0.1	0.1	0.1
Na_2O	3.2	4.0	4.6	4.7	4.7	4.6
P_2O_5	0.8	0.4	0.3	0.3	0.3	0.3
TiO_2	1.2	1.2	1.0	0.7	0.8	0.7
LOI	1.0	0.7	0.8	0.6	1.0	1.1
Trace elements (mg/kg)						
Rb	108	85	97	98	89	87
Cs	3.1	2.3	2.8	2.2	2.4	2.5
Sr	932	1070	1200	1250	1300	1250
Ba	1290	1495	1668	1597	1770	1728
Zr	1130	247	203	204	256	26
Hf	25.6	5.7	5.3	4.7	6.1	6.5
Th	14.3	10.7	7.8	4.7	5.2	7.2
U	5.1	2.4	2.6	1.2	2.1	1.9
La	73.7	77	60	46	47	47
Ce	173	183	146	93	104	97
Nd	79	85	70	42	46	45
Sm	13.4	15.5	13	6.9	8.4	7.6
Eu	2.6	3.2	2.2	1.5	1.6	1.6
Tb	1.6	1.7	1.3	0.8	1.0	1.0
Yb	3.6	3.2	2.6	1.7	2.0	1.9
Lu	0.6	0.5	0.4	0.2	0.3	0.3
Y	31.4	32.2	27.8	14.1	18.1	16.8

Table 2-2 Mineralogical analyses of the different fraction sizes (mm) of Äspö diorite from the Äspö Hard Rock Laboratory. The concentrations are given as weight %.

Element	ÄD-1 0.045-0.09	ÄD-2 0.09-0.25	ÄD-3 0.25-0.5	ÄD-4 0.5-1.0	ÄD-5 1-2	ÄD-6 2-4 (mm)
Biotite	25	18	19	18	18	17
Plagioclase	35	44	51	53	52	51
K-Feldspar	6	8	9	10	8.5	10
Quartz	22	19	12	10	13.5	15
Epidote	7	5.5	6	6	5.5	5
Apatite	2	1	0.5	1	1	1
Titanite	2	2	2	1	1	1
Opaque	2	2.5	1	1	1	1

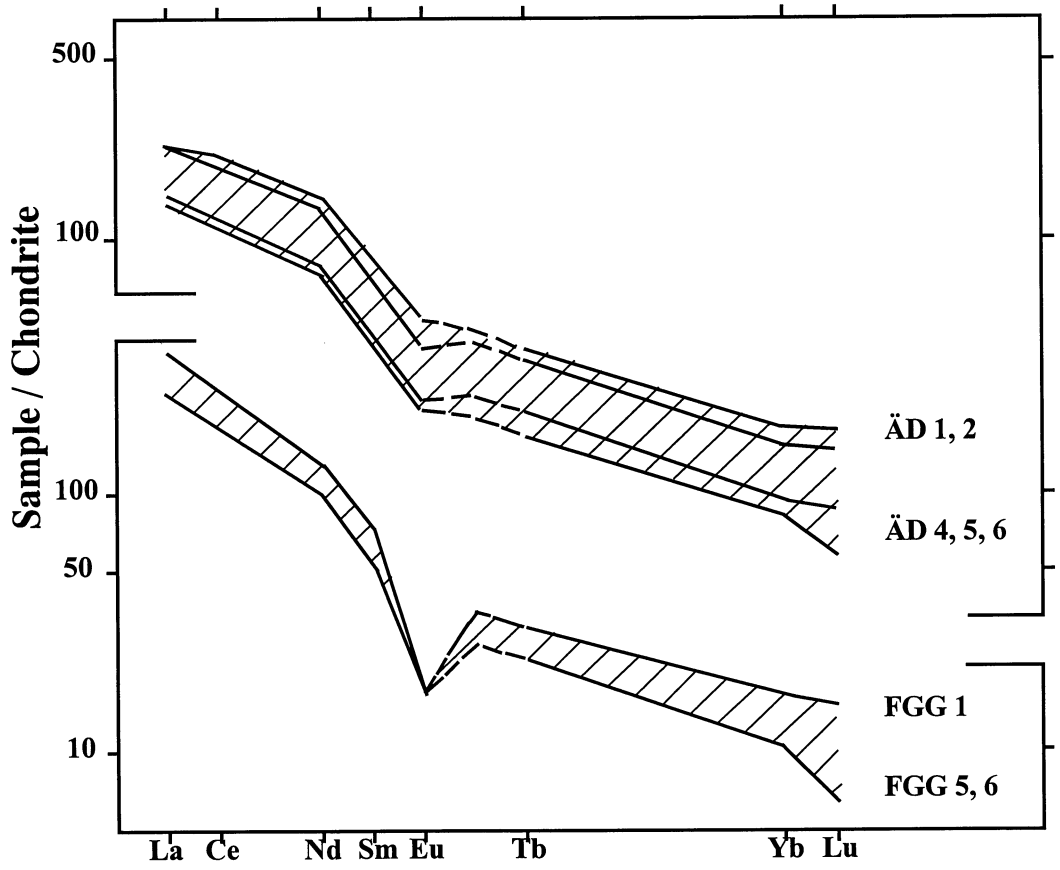

Figure 2-1. REE chondrite normalised diagram for fresh rock samples of Äspö diorite (ÄD) and Fine-grained granite (FGG). The intervals are shown as striped areas. Six different fractions of each rock type were analysed (cf. Tables 2-1 and 2-3). The highest REE contents were recorded in the finest fractions.

2.1.1.2 *Fine-grained granite*

The trace element analysis and a general mineralogical composition of the Fine-grained granite are given in Tables 2-3 and 2-5, respectively. Generally, the differences between the different size fractions are much lower for the Fine-grained granite than for the Äspö diorite. This observation is in accordance with the texture of the two rock types, *i.e.*, the Fine-grained granite is fine relatively homogeneous, while the Äspö diorite is characterised by its inhomogeneity both in mineral content and sizes of the grains. However, the two smaller fractions contain a slightly higher content of quartz, muscovite, magnetite and perhaps also chlorite. This is accompanied by a lower content of K-feldspar and plagioclase. The Fine-grained granite has a somewhat lower porosity than the Äspö diorite, 0.3±0.2 % (Stanfors *et al.* 1993a, Stanfors *et al.* 1993b).

The chondrite normalised REE diagrams for the Fine-grained granite shows that the different fractions of Fine-grained granites are very similar (Fig. 2-1). This indicates that the differences in the mineralogical composition of the fractions of the Fine-grained granite are lower than for Äspö diorite.

Table 2-3 **Chemical analyses of the different size fractions of Fine-grained granite from Äspö Hard Rock Laboratory. Rb, Ba, Cs, U, Th, Hf and the REEs are analysed using INAA (Studsvik Nuclear, Radiometry, Nyköping). All other elements are analysed with ICP-MS (Svensk Grundämnesanalys AB, Luleå). All concentrations refer to single samples.**

	FGG-1 0.045-0.09	FGG-2 0.09-0.25	FGG-3 0.25-0.5	FGG-4 0.5-1.0	FGG-5 1-2	FGG-6 2-4 (mm)
Main elements (%)						
SiO_2	74.5	75.7	72.8	72.7	73.3	73.2
Al_2O_3	12.0	11.8	13.9	13.8	13.5	13.3
CaO	1.1	1.2	1.3	1.3	1.3	1.1
Fe_2O_3	2.9	2.3	2.1	2.1	2.1	2.1
K_2O	5.9	5.7	6.2	6.1	6.1	6.0
MgO	0.5	0.4	0.5	0.5	0.5	0.4
MnO	0.07	0.07	0.08	0.05	0.05	0.04
Na_2O	2.1	2.3	2.9	2.9	2.7	2.7
P_2O_5	0.14	0.08	0.09	0.11	0.11	0.1
TiO_2	0.36	0.32	0.34	0.35	0.36	0.34
LOI	0.5	0.4	0.6	0.6	0.3	0.6
Trace elements (mg/kg)						
Rb	195	187	199	198	207	195
Cs	1.6	1.4	1.6	1.8	1.7	1.6
Sr	180	201	238	234	225	180
Ba	802	813	889	895	865	887
Zr	328	208	259	280	280	277
Hf	8.7	5.1	6.9	7.0	7.3	7.6
Nb	14.4	17.2	18.1	20.0	20.5	12.6
Th	34.8	32.7	27.2	25.8	24.1	24.1
U	7.0	3.6	3.0	3.3	3.0	3.2
La	120	117	112	93	84	91
Ce	230	234	220	190	164	174
Nd	78	83	77	71	59	62
Sm	13.0	12.6	12.0	11.3	9.7	9.7
Eu	1.2	1.2	1.2	1.1	1.2	1.1
Tb	1.4	1.2	1.3	1.2	1.1	1.1
Yb	3.3	2.4	2.1	2.3	2.3	2.1
Lu	0.5	0.4	0.3	0.4	0.3	0.3
Y	25.9	20.3	21.3	23.4	22.0	19.7

2.1.1.3 *Feature A Site Specific Material.*

Feature A is a reactivated mylonite hosted in Äspö diorite. Wall rock samples of the intersection of the fracture and four different boreholes were obtained (Fig. 2-2). This site-specific material from the Feature A fracture has been analysed chemically (results, Table 2-4) and from the analysis results, estimation of mineralogical composition (Table 2-5) and thin sections of the material (Fig. 2-3), some general observations can be made.

The altered geologic material from the *KXTT2* drill core is an altered Äspö diorite containing epidote and chlorite and also some traces of biotite. This sample is the only one of the site-specific sample which contains biotite. Compared to fresh Äspö diorite, an albitisation (breakdown of plagioclase to form albite) has occurred which has resulted in a mobilisation of. Ca. This can probably explain the increased concentration of Ca in the adjacent mylonite. A rough estimation of the mineralogy indicates that there are similarities with the mineralogy of non-altered Äspö diorite, except for a higher content of chlorite and epidote. It is also possible that the water content of the biotite residue is higher than for biotite in the non-altered Äspö diorite.

The mylonite from the *KXTT2* drill core contains mainly epidote, K- and Na-feldspars and quartz. No biotite is present and formation of Fine-grained muscovite has appeared. The sample contains approximately 50 % epidote, which is associated with high concentration of Sr.

Due to calcite impurities of the mylonite layer of the *KXTT3* sample, only an altered geologic material was isolated for the sorption experiment. The altered geologic material located inside the mylonite was found to originate from Äspö diorite This sample has the same composition as the altered granite from the T2 drill core, except for that the biotite has been completely altered to chlorite.

The altered material from the *KXTT4* drill core deviates from the other altered materials; it is an altered Fine-grained granite. Compared to a non-altered sample of the same rock type, the content of muscovite, chlorite and epidote is higher.

The mylonite from the *KXTTT4* drill core is extremely fine grained and has a high concentration of epidote. The muscovite content of is rather low and the dominating minerals are epidote, quartz, albite and K-feldspar.

For the diffusion experiment on site specific material, sample *KXTT1*:15.77m was chosen. This sample consist of altered and partly mylonitised Äspö diorite limited by two natural fracture surfaces coated with chlorite. These natural fracture surfaces are the one exposed to fluid in the diffusion experiment described in this report. The foliation and the bands of mylonite are orientated parallel with the fracture surfaces which means perpendicular to the measured diffusion paths (cf. Fig 2-4). The mineralogical composition of the entire sample can be described as an altered and fractured Äspö diorite with all biotite replaced with chlorite (similar to T3:14.10m) interlayered with millimetre thick shear bands of mylonite (epidote, sericite some chlorite, and quartz) and recrystallised quartz. Also a recrystallisation of magnetite is observed. A few sealed

microfractures cross cut the foliation and the mylonites. It is difficult to identify the minerals in these microfractures but it seams to be epidote, chlorite and probably also some FeOOH.

Altered Äspö diorite has a higher porosity than the fresh, 1.0 % compared with 0.45% (Eliasson 1993), whereas the mylonitic parts are extremely fine grained and has a lower porosity (probably in the order of 0.25%).

The chondrite normalised REE diagram (Fig. 2.3) for the site specific material show that the samples of altered Äspö diorite and mylonites are where similar which suggests that the Äspö diorite is the original host rock for both mylonite samples. The sample of altered Fine-grained granite shows another pattern including the typical pronounced negative Eu-anomaly.

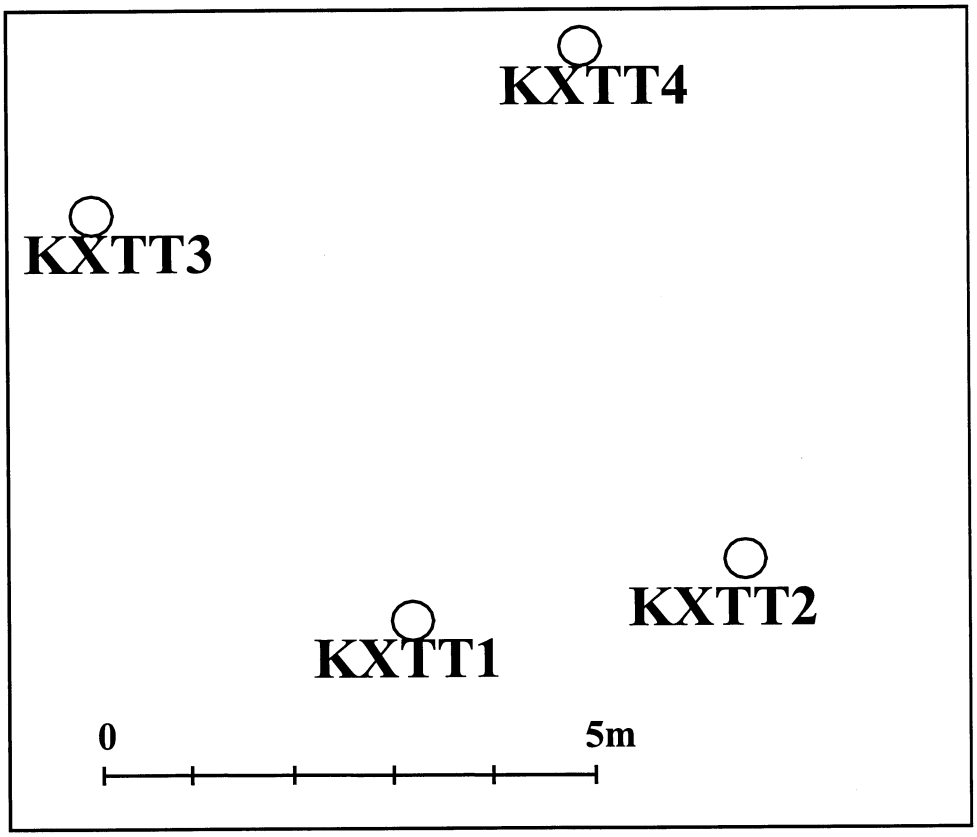

Figure 2-2 Sections in the plane of Feature A showing the relative positions of the places from where the Feature A site –specific material were sampled

Table 2-4 Chemical analyses of site-specific material from the TRUE study site. The drillcores are KXTT2, KXTT3 and KXTT4. Rb, Ba, Cs, U, Th, Hf and the rare earth elements are analysed using INAA (Studsvik Nuclear, Radiometry, Nyköping) . All other elements are analysed with ICP-MS (Svensk Grundämnesanalys AB, Luleå). All concentrations refer to single samples.

	T2:15.10 Altered ÄD	T2:15.10 Mylonite	T3:14.10 Altered ÄD	T4:12.10 Altered FGG	T4 12.10 Mylonite
Main elements (%)					
SiO_2	63.8	61.6	62.6	76.0	62.6
Al_2O_3	16.6	16.1	16.3	13.3	13.0
CaO	3.5	7.2	4.4	1.1	11.1
Fe_2O_3	4.1	5.9	5.4	0.85	7.6
K_2O	2.2	2.2	1.8	3.6	0.7
MgO	1.8	1.6	1.9	0.3	0.9
MnO	0.08	0.11	0.09	0.02	0.13
Na_2O	5.6	3.4	5.3	4.6	0.9
P_2O_5	0.28	0.31	0.36	0.04	0.26
TiO_2	0.7	0.74	0.85	0.13	0.72
LOI	2.4	1.4	1.8	0.8	2.0
Trace elements (ppm)					
Rb	85	89	78	72	32
Cs	2.0	1.7	0.64	0.4	0.2
Sr	785	1760	1260	441	2950
Ba	926	1359	691	1528	308
Zr	228	229	314	82	217
Hf	6.2	5.7	7.3	2.3	5.5
Nb	15.3	15.8	14.7	6.2	14.5
Th	10.3	11.8	8.2	26.3	10.2
U	3.7	5.0	3.0	4.4	3.6
La	43	57	91	29	82
Ce	98	124	172	59	157
Nd	47	58	68	26	62
Sm	8.2	10.0	10.7	6.3	10.6
Eu	1.5	2.0	1.9	0.5	1.9
Tb	1.0	1.2	1.3	1.6	1.3
Yb	2.4	2.8	2.4	2.4	2.6
Lu	0.3	0.4	0.35	0.25	0.36
Y	19.8	24.5	22.4	31.3	24.2

Table 2-5 Average mineralogical composition (weight %) of the mylonites, the altered material, Fine-grained granite, Äspö diorite from Äspö Hard Rock Laboratory.

Mineral	ÄD	Alt.ÄD T2:15.10	Mylonite T2:15.10	Alt.ÄD T3:14.10	FGG	Alt.FGG T4:12.10	Mylonite T4:12.10
Biotite	18	9	2	-	1	-	-
Plagioclase	47	-	-	-	23	-	-
Albite	-	40	40	38	-	30	10
K-feldspar	10	12	10	10	38	20	8
Quartz	14	14	14	15	30	35	22
Epidote	5	7	20	15	1	5	42
Chlorite	-	8	6	15	1	3	7
Sericite	-	2	4	2	3	3	5
Ass*	6	8	4	5	3	4	6

* Accessoric phases like titanite, apatite, magnetite, pyrite, Fe-oxyhydroxides and calcite

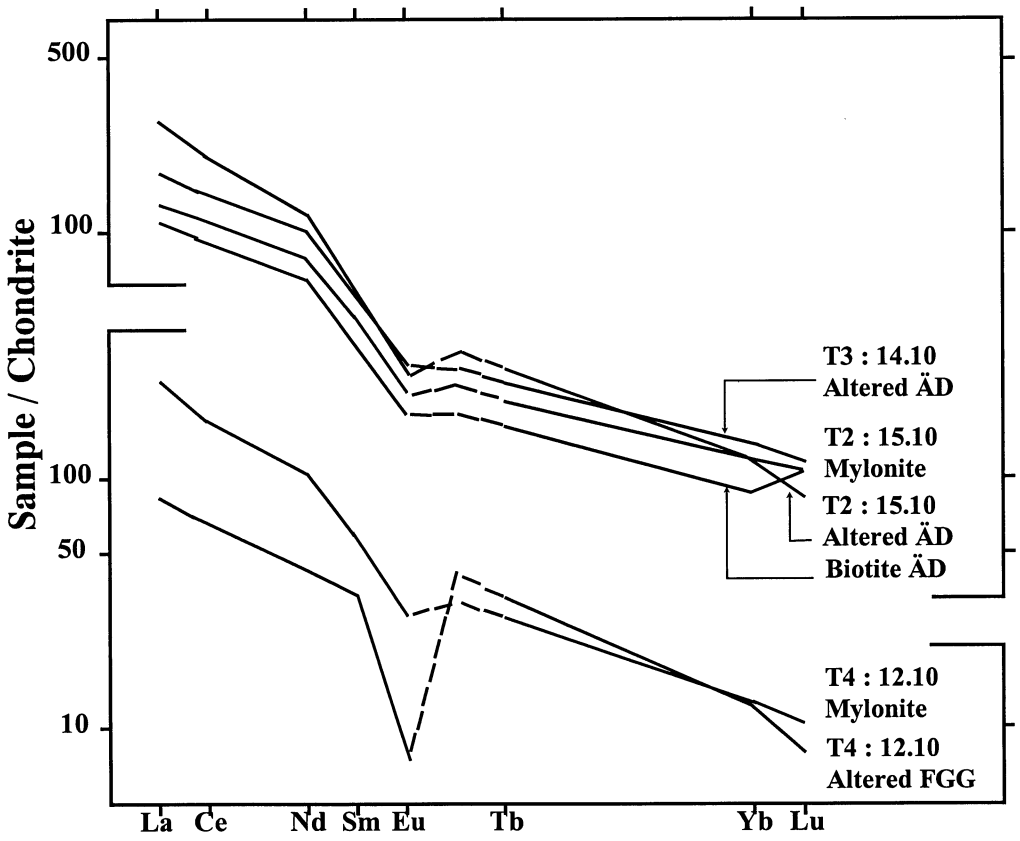

Figure 2-3. *Chondrite normalised REE pattern for the site-specific material from the TRUE site.*

Fresh Äspö diorite (ÄD)

Fresh Fine-grained granite (FGG)

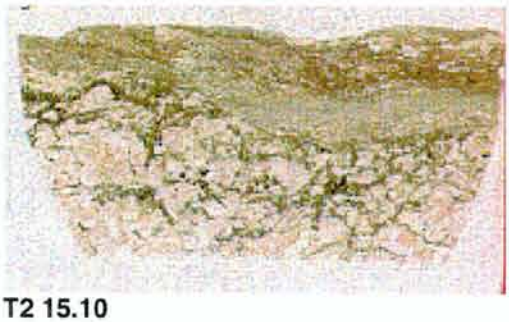

T2 15.10
Mylonite (top)
Altered ÄD (bottom)

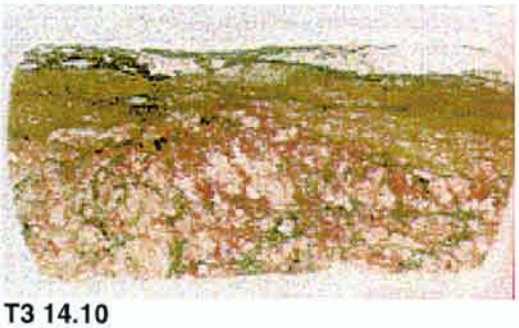

T3 14.10
Mylonite, not in the experiment (top)
Altered ÄD (bottom)

T4 12.10
Mylonite (top)
Altered FGG (bottom)

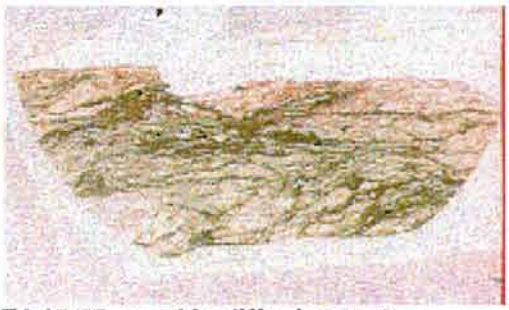

T1 15.77, used in diffusion test

T1 15.77

Figure 2-4. Thin section of fresh samples (Äspö diorite and Fine-grained granite) and altered and mylonitised samples from the Feature A fracture (see text for details). Two samples from Feature A T1:15.77 are shown. One represents the sample used for diffusion experiment and the other show the same fracture and the adjacent wall rock. The black dots on the picture of the T4 samples are rests from the SEM/EDS studies.

2.2 GROUNDWATERS

In the investigation, two types of synthetic groundwaters have been used, see table 2.7 for compositions. The first type was used in the first series of investigations using only generic rock material. The composition is chosen in order to simulate the natural groundwater from the 350 m level at Äspö, sampled at SA2600A 940307 (Smellie *et al.*, 1995). The use of the second type of groundwater was motivated by a later analysis performed of the groundwater sampled from the Feature A fracture, (Nilsson 1997). The analysis showed a lower salinity in the Feature A fracture water.

Synthetic groundwater (and not water sampled *in situ*) was chosen in order to avoid iron oxide precipitation which often occurs when a natural deep granitic groundwater is sampled and thereby coming into contact with air. All contact between the synthetic groundwater and the rock material was performed inside an N_2-fed glovebox.

Table 2-7 Compositions of the two different synthetic groundwaters used in the batch sorption experiments and the diffusion experiments.

Ion	General Äspö groundwater, 340 m depth	Feature A specific groundwater
Li^+ (mg/kg)	1.3	0.75
Na^+	2400	1735
K^+	10	12.7
Rb^+	0.026	0.056
Cs^+	0.001	0.005
Mg^{2+}	50	85.6
Ca^{2+}	2540	1310
Sr^{2+}	35	21.4
Ba^{2+}	0.14	0.080
Cl^-	8350	5400
Br^-		22
SO_4^{2-}	170	305
$H_4SiO_{4(aq)}$	16	20
HCO_3^-	17	57
pH	7.5	7.5
Ionic Strength	0.25	0.17

2.3 TRACERS

In the first series of experiments studying diffusion and sorption using generic material as the solid phase, only tritiated water was used as the non-sorbing reference tracer. As sorbing tracers, cations were selected which were expected to have cation exchange as their major sorption mechanism. In order to minimise the influence of non-linear sorption, radioactive tracers were used which made it possible to study the sorption without having to make any changes of the natural concentrations in the groundwaters. (see Byegård 1993 for the further discussion on the selection of sorbing tracers). The radioisotopes used were $^{22}Na^{+}$, $^{45}Ca^{2+}$, $^{86}Rb^{+}$, $^{85}Sr^{2+}$, $^{137}Cs^{+}$ and $^{133}Ba^{2+}$; selected with respect to their half-lives and radiation detection characteristics.

In the second series of experiments, tracers presumed to act non-sorbing was also included in the investigation, *i.e.*, anions, fluorescent dye tracers and metal complexes. Due to the shortage of site-specific geologic material, experiments had to be performed using all tracers in the same cocktail.

3 Batch Sorption Experiments

In the present investigation, two series of batch experiments were performed. The different objectives of the two experiments are described under section 2.

3.1 EXPERIMENTAL

3.1.1 Rock Material

In the first series of experiments, the main type of generic rock material from the Äspö area; Äspö diorite and Fine-grained granite, were used. The rock samples were crushed and sieved into the fractions described in Table 3-1.

The Feature A site-specific material, which was used in the second series of experiments, are described in section 2. In this experiment, only the 1-2mm fraction was used. For comparison, samples of the generic rock types (ÄD and FGG) were also involved in this experiment. Furthermore, two types of biotite and a cation exchanger (Dowex 50Wx8) were used for comparison of the cation exchange characteristics of the rock materials used. One of the biotite samples consisted of magnetically enriched biotite from the Äspö diorite, 0.25-0.5 mm fraction, and the other type consisted of big flakes (1-5 mm) from large monomineralic biotite crystals, obtained from Swedish Museum of Natural Science.

Table 3-1 Size fractions and the corresponding surface areas for Äspö diorite and Fine-grained granite. The geometric surface is given assuming a spherical form of the crushed material.

Size Fraction (mm)	Geometric Surface (m^2/g)	BET Surface (m^2/g)	
		ÄD	FGG
0.045 - 0.090	0.030	0.33	0.23
0.090 - 0.25	0.011	0.23	0.15
0.25 - 0.50	0.0054	0.077	0.077
0.50 - 1.0	0.0027	0.050	0.046
1.0 - 2.0	0.0013	0.038	0.036
2.0 - 4.0	0.00067	0.024	0.06

3.1.2 Synthetic Groundwater

For the first series of experiments with generic rock material a synthetic groundwater was produced which matched the composition of groundwater sampled from the 400m level in Äspö. For the second series of experiment, using mainly Feature A site-specific geologic material, a synthetic groundwater with the same composition as the sampled Feature A water was produced. The compositions of the synthetic groundwaters are shown in Table 2-7.

3.1.3 Tracers

In the first series of experiments, the radioactive tracers $^{22}Na^{+}$, $^{45}Ca^{2+}$, $^{86}Rb^{+}$, $^{85}Sr^{2+}$, $^{137}Cs^{+}$ and $^{133}Ba^{2+}$ were used. They were all obtained from NEN. An aliquot of the stock solution was taken out and was mixed with ~10 ml of synthetic groundwater. From this solution, 0.5 ml was spiked to each of the sorption samples. The concentrations of the tracers were set so that no increase of the background concentrations were obtained, *i.e.* the concentrations given in Table 2-7 were used.

In the second series of experiments, the same tracers were used, except for that the γ-radioactive $^{47}Ca^{2+}$ replaced $^{45}Ca^{2+}$. This tracer was obtained by neutron irradiation of natural $CaCl_2 \cdot 2H_2O$. The irradiated calcium was dissolved in a water were additions of the other species present in the synthetic groundwater already had been performed. By this way, a synthetic radioactive groundwater was produced.

The second series of experiment was also aimed to obtain information of some presumed non-sorbing species. Prior to irradiation, the $CaCl_2 \cdot 2H_2O$ was therefore mixed with KBr and KReO4 in order to obtain the radioactive tracers $^{82}Br^{-}$ and $^{186}ReO_4^{-}$, respectively. Furthermore, Tb_2O_3, Yb_2O_3 and Lu_2O_3 were irradiated individually, and thereafter dissolved and complexed with DTPA, EDTA and DOTA, respectively. The procedure for the complexation has been described by Byegård 1993(2). $^{131}I^{-}$, obtained from NEN, and the fluorescent dye tracers Uranine, Rhodamine WT and Amino G Acid were used as non-sorbing tracer. The concentrations of the $^{186}ReO_4^{-}$ and the metal complexes were chosen in order to obtain a concentration of 10 µg/l of the Re, Tb, Yb and Lu metals, respectively. The $^{131}I^{-}$ was added as carrier-free radioisotope while the dye tracers were added to obtain a concentration of each tracer of 10 µg/l.

3.1.4 Sorption Experiment

In the first series of batch laboratory, the samples were pre-equilibrated for 1-2 months experiment before the radioactive tracers were added to the mixture. The samples regularly consisted of 2 g of solid phase in contact with 8 ml of the synthetic groundwater. Since it was suspected that the Cs sorption would be strong, only 1 g of solid phase was used in these samples. The total sorption time for the samples, *i.e.* the time until the rinsing and desorption of the solid phase was started, varied form 1-30 days.

In the experiment studying the sorption of different tracers on Feature A site-specific material, 2g of solid phase was equilibrated with 8.5g of synthetic groundwater. The synthetic groundwater was exchanged 3 times before the addition of tracer was performed. A total pre-equilibration time of 5 months was applied. For the Dowex 50x8 sample, higher cation exchange capacity was presumed and consequently the groundwater was exchanged 6 times for this sample. The addition of tracers to the sample was performed by taking away 6 ml of the synthetic groundwater in each test tube and replace that with 6 ml of the synthetic radioactive groundwater. The sorption time were the same for all samples, *i.e.* 10 days.

In both experiment series, the crushed and sieved granite was put together with the synthetic groundwater in gloveboxes continuously fed with nitrogen gas (<0.1% O_2). All the sampling, weighing of the samples and changes of the water was performed without taking the samples out of the glove-box. The temperature in the glove box was ambient (20-25° C). In the experiments, blank samples were also used which contained tracer spiked groundwater without any solid phase. No continuous stirring of the samples was applied. The samples were instead manually shaken; once or twice during the days directly after the tracer injection and more sporadically during the rest of the experiment time. However, prior to the sampling, the samples were always thoroughly shaken.

3.1.5 Sampling

Sampling was performed with regular intervals, both during the sorption and the desorption phase of the experiments. During the sampling, 0.5 ml was taken out from each sample. The exact amount taken was registered by weighing.

3.1.6 Rinsing

When the sorption part of the experiment was ended, desorption experiment was performed. The whole initial tracer solution was extracted and replaced with synthetic groundwater without any spike of radioactive tracers. However, after taking out as much as possible of the spiked groundwater, a little portion of spiked water was remaining (~0.5g water per gram solid phase). Adding new groundwater directly after the removal of the spiked groundwater would thus have resulted in a considerable concentration in the desorption solution of tracers which originates from the spiked sorption groundwater. Since the sorption of some of the tracers was very low, the desorbed part of the tracer would not have been possible to quantify because of the presence of orders of magnitude higher concentration of tracers originating from the non-removed tracer solution.

Instead of directly adding new synthetic groundwater after the removal of the initial tracer solution, the solid phase was repeatedly rinsed with distilled water in order to "dilute away" the remaining portion of spiked groundwater. After each removal of the distilled water, sampling was conducted on the water. The solid phases were rinsed 3

times in the first series of experiment and 4 times in the second series of experiment, resulting in that <0.1% of the initial spike solution was left when the desorption experiment started. Sampling and measurement of the rinsing solution was performed in order to study if deviations from the expected dilution the remaining tracer. Such behaviour would be indicative of desorption of the tracers during the rinsing process.

3.1.7 Solid Phase Measurements

Since very low sorption was found for some of the cationic tracers, *i.e.*, Na^{+}, Sr^{2+} and Ca^{2+}, the loss in the aqueous phase could not be statistically verified. For the tracers used that emitted γ-radiation, *i.e.* $^{22}Na^{+}$ and $^{85}Sr^{2+}$, measurements of the solid phase were performed after the rinsing. In that way, a better quantification of the total amount of sorbed tracer could be obtained.

In the experiments using the Feature A site-specific material, no such measurements were performed. Because of the use of several tracers in the same batch, some of them with short half-lives, the experimental time did not allow solid phase measurements.

3.1.8 Desorption experiments

The desorption experiments was performed by addition of non-spiked synthetic groundwater to the solid phases after the rinsing. Sampling was performed in regular intervals, as described for the sorption experiment.

3.1.9 Measurements

3.1.9.1 Radioactivity Measurements

In the first series of sorption experiment, using generic material, not more than one tracer was used in a single batch. Therefore detectors that measured the total radioactivity present in the samples could be used for the quantification of the sorption and desorption. For the tracers $^{22}Na^{+}$, $^{86}Rb^{+}$, $^{85}Sr^{2+}$, $^{137}Cs^{+}$ and $^{133}Ba^{2+}$, the measurements were performed using a NaI(Tl)-scintillation detector (Intertechnique, CG 4000) while the $^{45}Ca^{2+}$, lacking γ-radiation, was measured using a liquid scintillation detector (LKB Wallac, Rackbeta 1219)

In the second series of experiment using Feature A site-specific material, the limited amount of rock material made it necessary to use all tracers of interest in the same batch. Therefore, a detector with high selectivity for different γ-energies had to be used, *i.e.*, High Purity Germanium detector (EG & G Ortec).

3.1.9.2 *Fluorescence Measurements*

The measurements of the fluorescent dye tracers were conducted by Geosigma AB.

3.1.10 Calculation of the sorption coefficient

The results of the sorption experiments are mainly expressed as the K_d-value; *i.e.* the sorption is a function of the ratio of the mass of the solid material versus the volume of the water phase. If the sorption reaction is given as:

$$M^{\nu+}{}_{aq} \rightleftarrows M^{\nu+}{}_{s} \qquad 3\text{-}1$$

where:

$M^{\nu+}{}_{aq}$ = Cation in the aqueous phase
$M^{\nu+}{}_{s}$ = Cation in the solid phase

the sorption coefficient, K_d, is defined as:

$$K_d = \frac{[M^{\nu+}]_s}{[M^{\nu+}]_{aq}} \qquad 3\text{-}2$$

where:

$[M^{\nu+}]_{aq}$ = Concentration of the cation in the aqueous phase (mole·m^{-3})
$[M^{\nu+}]_s$ = Concentration of the cation in the solid phase (mole·kg^{-1})
K_d = Distribution coefficient (m^3· kg^{-1})

One way of determining the sorption coefficient is to measure the distribution of a radioactive isotope of the cation $M^{\nu+}$ between the two phases. Usually, a small volume of the aqueous phase is sampled from a batch containing the mixture of aqueous and solid phase, spiked with a radioactive tracer. The same small volume is also sampled from a batch that contains the same amount of radioactivity spiked to a sample containing no solid phase. From measurement of the radioactive counting rate of the samples, the K_d can be calculated as:

$$K_d = \left(\frac{R_0}{R_{aq}} - 1 \right) \cdot \frac{V}{m} \qquad 3\text{-}3$$

where:

R_0 = Counting rate of the sampled water from samples with no solid phase present

R_{aq} = Counting rate of the sampled water from samples with solid phase present
V = Volume of the aqueous phase (m^3)
m = Mass of the solid phase (kg)

The sorption can also be considered to be a surface dependent reaction. In a such a case, the sorption coefficient is given as K_a, *i.e.*:

$$K_a = \frac{[M^{\nu+}]_a}{[M^{\nu+}]_{aq}} \qquad 3\text{-}4$$

where:

$[M^{\nu+}]_a$ = Concentration of the cation in the solid phase (mole· m^{-2})
K_a = Distribution coefficient (m)

From experimental data, K_a is calculated analogously with the procedure above, *i.e.*;

$$K_a = \left(\frac{R_0}{R_{aq}} - 1 \right) \cdot \frac{V}{A} \qquad 3\text{-}5$$

where:

A = Area of the solid phase (m^2)

K_a can be expressed using the geometric surface area of the crushed material used (usually by assuming spherical particles). One can also obtain a more exact measure of the surface area by using BET measurements (Brunauer *et al.* 1938). In this work, it has, however, been decided to give the sorption coefficients as mass dependent sorption coefficients, *i.e.*, K_d.

For some of the tracers where the loss in the aqueous phase during the sorption experiment could not be quantified, measurement of the radioactivity of the solid phase was performed. In this case the sorption coefficient was calculated according to:

$$K_d = \frac{R_s}{R_{aq}} \cdot \frac{V_s}{m} \qquad 3\text{-}6$$

where:

R_s = Counting rate of the solid phase measurement
V_s = Volume of the sampled aqueous phase (m^3)

3.1.11 Calculation of the desorption coefficient

The distribution coefficient obtained from desorption studies, $K_{d(des)}$, can be calculated in two different ways. If a strong desorbing agent is used, it is a reasonable assumption that all desorbable tracer will be desorbed from the geologic material after the first contact with the desorption solution. In such cases, the desorption coefficient, $K_{d(des1)}$, is given from:

$$K_{d(des1)} = \frac{[M^{\nu+}]_{des}}{[M^{\nu+}]_{aq}} \cdot \frac{V}{m} \qquad 3\text{-}7$$

where:

$[M^{\nu+}]_{des}$ = Concentration of the $M^{\nu+}$ cation in the desorption phase (mole/dm^3)

Calculation of the desorption $K_{d(des1)}$ from experimentally obtained data can thus be performed according to:

$$K_{d(des1)} = \frac{R_{des}}{R_{aq}} \cdot \frac{V}{m} \qquad 3\text{-}8$$

where:

R_{des} = Counting rate of the sampled desorption solution

However, in the desorption experiments in this investigation, synthetic groundwater of the same composition as the original aqueous phase has been used as the desorption medium. In the case of a large loss of tracer in the sorption experiment, one can therefore not expect a complete desorption in one single batch desorption. A linear sorption model gives that, *e.g.*, for a sorption of 50 % of the originally added tracer, 50 % of the sorbed tracer, *i.e.*, 25 % of the originally added tracer, should be desorbed in the first desorption batch. By using repetitive batches of the desorption, *i.e.*, changing the water phase repetitively, a desorption coefficient could be calculated, according to:

$$K_{d(des1)} = \frac{\sum_{p=1}^{n} R_{des(p)}}{R_{aq}} \cdot \frac{V}{m} \qquad 3\text{-}9$$

where:

$R_{des(p)}$ = Counting rate of the sampled desorption solution after the (p-1)th exchange of the desorption solution

However, in most of the desorption studies performed within this experimental programme, slow desorption kinetics did not allow contact with more than one desorption solution. An alternative way of calculating the desorption coefficient is to

use the desorbed amount in the first desorption batch to make an estimation of the total amount of desorbable and non-desorbable tracer. Assuming a fast, fully reversible sorption, the expected counting rate in the first desorption synthetic groundwater, $R_{des(exp)}$ can be calculated according to:

$$R_{des(exp)} = R_{aq} - \frac{R_{aq}^{\ 2}}{R_s} \qquad 3\text{-}10$$

where:

R_s = Counting rate of the sampled water from samples with no solid phase present (sorption experiment).

R_{aq} = Counting rate of the sampled water from samples with solid phase present (sorption experiment).

Equation 3-10 is valid only if the same volume of the sorption and desorption solution is applied.

The expected desorption counting rate, $R_{des(exp)}$, is compared to the counting rate actually obtained, $R_{des(1)}$. It is assumed that lower obtained counting rate is because of non- or slowly reversible sorption, and the percentage of the non- or very slowly desorbable tracer, N_{ndes}, is calculated according to:

$$N_{ndes}\,(\%) = \left(1 - \frac{R_{des(1)}}{R_{des(exp)}}\right) \cdot 100 \qquad 3\text{-}11$$

A desorption coefficient, $K_{d(des2)}$ can then be defined using only the desorbable part of the sorbed tracer. It can be calculated according to:

$$K_{d(des2)} = \frac{(100 - N_{ndes})}{100} \cdot K_d \qquad 3\text{-}12$$

where:

K_d = Sorption coefficient, see (3-2) and (3-3), ($m^3 \cdot kg^{-1}$)

The difference of the two desorption coefficients is that the $K_{d(des1)}$ only uses the experimentally observed desorbed tracer while the $K_{d(des2)}$ uses an extrapolation of the first batch desorption experiment in order to determine the total part of desorbable tracer. The $K_{d(des1)}$ can be regarded as the minimum value of desorbable part of the tracer while the $K_{d(des2)}$ represents the maximum desorbable part of the tracer.

3.1.12 Calculation of cation exchange capacity and selectivity coefficient

The cations used in this study, *i.e.* Na^+, Ca^{2+}, Rb^+, Sr^{2+}, Cs^+ and Ba^{2+} are expected to sorb with cation exchange as the major sorption mechanism. Sorption via cation exchange mechanism can be described as:

$$\nu_2 M_1^{\nu 1+} + \nu_1 \left(M_2 - S_{\nu_2}\right) \quad \rightleftarrows \quad \nu_2 \left(M_1 - S_{\nu_1}\right) + \nu_1 M_2^{\nu 2+} \qquad 3\text{-}13$$

where:

$M_1^{\nu 1+}$	=	Cation with the charge ν_1+
$M_2^{\nu 2+}$	=	Cation with the charge ν_2+
S	=	Cation exchange site with the charge -1

The concentration of a cation in the solid phase can be calculated using the distribution coefficient measured in a desorption experiment and the known concentration of the tracer in the water phase, *i.e.*;

$$\left(M_n - S_{\nu_n}\right) = K_{d(des)_n} \cdot \left[M_n^{\nu_n +}\right] \cdot 1 \cdot 10^6 \qquad 3\text{-}14$$

where:

$(M_n\text{-}S)$	=	Concentration of $M_n^{\nu_n +}$ in the solid phase (μeq/g)
$[M_n^{\nu_n +}]$	=	Concentration of the $M_n^{\nu_n +}$ cation in the aqueous phase (M)
$K_{d(des)_n}$	=	Desorption coefficient for the $M_n^{\nu_n +}$ cation, ($m^3 \cdot kg^{-1}$)

The concentration of cation exchange sites of a solid material is described by the cation exchange capacity, CEC (*μ*eq/g), *i.e.*;

$$CEC = \sum_n \nu_n \left(M_n - S_{\nu_n}\right) \qquad 3\text{-}15$$

The selectivity for sorption of $M_1^{\nu 1+}$ in preference to $M_2^{\nu 2+}$, by cation exchange, can be expressed by the selectivity coefficient, K_s,

$$K_s = \frac{\left(\frac{\nu_1 \cdot \left(M_1 - S_{\nu_1}\right)}{CEC}\right)^{\nu_2} \cdot \left[M_2^{\nu_2 +}\right]^{\nu_1}}{\left(\frac{\nu_2 \cdot \left(M_2 - S_{\nu_2}\right)}{CEC}\right)^{\nu_1} \cdot \left[M_1^{\nu_1 +}\right]^{\nu_2}} \qquad \left(M^{(\nu_1 - \nu_2)}\right) \qquad 3\text{-}16$$

where:

$\left(\frac{\nu_n \cdot \left(M_n - S_{\nu_n}\right)}{CEC}\right)$ =The part of the CEC occupied by the cation $M_n^{\nu_n+}$, fractional occupancies(-)

$[M_n^{\nu_n+}]$ = Concentration of the $M_n^{\nu_n+}$ cation in the aqueous phase (M)

3.2 Results and Discussion

3.2.1 Non-Sorbing Tracers

The results of the experiments studying losses of the presumed non-sorbing tracers from the water phases are given in Table 3-2 The results are given as C/C_0-values where C_0 refers to the initial concentration in the blank sample, *i.e.*, water-phase without any solid phase present. A C/C_0-value of 1 thus indicates that no loss of the tracer due to sorption on the solid phase has occurred. In Table 3-3 the results of the desorption part of the experiment are given. In this case, a C/C_0-value higher than 0 thus indicates that tracer has sorbed on the solid phase during the sorption experiment and desorbed during the desorption experiment.

3.2.1.1 Anions

The results of the sorption experiment studying the loss of the anions (Table 3-2) do not verify any sorption of any of the anions used, *i.e.*, $^{82}Br^-$, $^{131}I^-$ and $^{186}ReO_4^-$. The only exception is $^{131}I^-$ on separated biotite where a loss can be found. One drawback is the short half-lives of $^{82}Br^-$ (1.35 days) and $^{186}ReO_4^-$ (3.78 days) which cause a low activity and high uncertainty in the measurements. This makes it difficult to quantify any small losses in the sorption experiment (*i.e.*, statistically verify a small deviation from a C/C_0-value of 1, indicative of sorption).

The desorption experiments show that any desorption of $^{82}Br^-$ or $^{186}ReO_4^-$ is below the detection limit. However, desorption of $^{131}I^-$ in the range of 1-5% of the original concentration of the water phase indicates that $^{131}I^-$ is leached from the solid material during the desorption process. However, this could be a result of diffusion in to pores of the crushed material. $^{131}I^-$ is the only one of the anionic tracers for which the half-life makes it possible to study low concentrations in the desorption studies after a desorption performed for a longer time.

3.2.1.2 Metal Complexes

The results of the sorption and desorption studies on metal complexes are difficult to use for any conclusions since speciation studies performed after the injection of tracers showed that the complexation procedure did not work. By cation and anion exchange studies of the stock solutions (Table 3-4) it was shown that a considerable part of the metal ions were not in the anionic form. The concentrations of the injected metal complexes were therefore very low and difficult to quantify.

Comparing the results from the sorption part of the experiment, it is indicated that losses of Tb-DTPA and Yb-EDTA occur to an extent, which is higher than what can be explained from the results of the speciation studies. However, the loss of the Lu-DOTA is not as severe as for the other metal complex tracers.

The desorption studies show that no or very low amounts of metal complex tracers are desorbed. The species that sorb are probably the non-complexed metal ions which either were non-complexed already at the experiment start (see above) or have undergone decomplexation during the contact. Because of hydrolysis, precipitation and/or generally strong sorption of the non-complexed cation, no or very low desorption of the tracers can therefore be observed.

3.2.1.3 Fluorescent dye tracers

The fluorescent dye tracers (Uranine, Amino G Acid and Rhodamine WT) were used in concentrations of 10 ppb. In the sorption experiment, 0.5 ml was sampled which had to be diluted before spectrofluorometric measurements could be performed. The results from the sorption experiments indicate that the major part (>90%) of all the fluorescent dye tracers were lost in all sorption samples, even the samples with no solid phase present. However, it was found that the concentration in the samples from the rinsing of the solid phase and the desorption samples had about the same concentration and fluctuation as the sorption samples. Considering these facts, the results from the sorption studies of the fluorescent dye tracers can not be considered reliable. The same type of problem occurred for the measurement of the samples from the experiment studying the sorption on the borehole equipment (Ittner and Byegård, 1997). A possible explanation for the experiment failure is that the tracers were measured too long time after the sampling, (~6 months). Limited stability due to light sensitivity might explain the detected low fluorescence.

Table 3-2 Results of the sorption test of the presumed non-sorbing tracers, anions and metal complexes. The results of the investigation are given as C/C_0 values; *i.e.*, the part of the added tracer that remained in the solution after a contact time of 9 days.

Material	$^{82}Br^-$	$^{131}I^-$	$^{186}ReO_4^-$	^{160}Tb-DTPA	^{169}Yb-EDTA	^{177}Lu-DOTA
ÄD	1.07±0.03	1.00±0.02	1.24±0.18	0.21±0.06	0.55±0.30	0.94±0.07
FGG	1.07±0.03	1.01±0.02	1.24±0.20	0.37±0.07	0.67±0.37	0.92±0.07
Mylonite, T2	0.91±0.02	0.92±0.02	1.09±0.17	0.11±0.07	0.53±0.31	0.75±0.06
Mylonite, T4	0.99±0.04	0.97±0.02	1.42±0.23	<0.12	<0.23	0.72±0.07
Alt. ÄD, T2	1.05±0.03	0.96±0.02	1.08±0.20	0.17±0.07	<0.23	0.78±0.07
Alt. ÄD, T3	1.05±0.03	0.98±0.02	0.90±0.16	<0.16	0.50±0.29	0.63±0.06
Alt. FGG, T4	0.99±0.03	0.99±0.02	1.09±0.20	0.17±0.08	0.33±0.32	0.76±0.07
Biotite, ÄD	0.94±0.02	0.86±0.02	0.95±0.15	0.22±0.06	<0.36	0.51±0.05
Biotite, Flakes	0.96±0.02	0.96±0.02	0.99±0.16	0.21±0.06	<0.43	0.95±0.07
Dowex 50Wx8	1.06±0.02	0.99±0.01	1.22±0.14	0.27±0.02	0.47±0.15	0.89±0.05

Table 3-3 The results of the desorption test of the presumed non-sorbing tracers, anions and metal complexes. The results of the investigation are given as C/C_0 values, *i.e.*, the part of the added tracer in the sorption experiment that was desorbed after a desorption contact time of 7 days.

	$^{82}Br^-$	$^{131}I^-$	$^{186}ReO_4^-$	^{160}Tb-DTPA	^{169}Yb-EDTA	^{177}Lu-DOTA
Blank	<0.03	0.008±0.0002	<0.01	0.006±0.001	0.004±0.002	<0.002
ÄD	<0.02	0.007±0.0004	<0.06	0.003±0.001	<0.01	0.018±0.003
FGG	<0.02	0.009±0.0005	<0.06	<0.002	0.02±0.009	<0.008
Mylonite, T2	<0.004	0.020±0.001	<0.01	<0.003	<0.01	0.04±0.003
Mylonite, T4	<0.003	0.015±0.001	<0.03	0.01±0.001	<0.01	0.04±0.003
Alt. ÄD, T2	<0.003	0.016±0.001	<0.03	<0.003	0.02±0.01	0.04±0.003
Alt. ÄD, T3	<0.01	0.012±0.001	<0.03	0.005±0.002	<0.012	0.09±0.006
Alt. FGG, T4	<0.03	0.010±0.001	<0.04	0.01±0.001	<0.01	0.05±0.003
Biotite, ÄD	<0.01	0.044±0.001	<0.06	<0.01	<0.03	0.12±0.009
Biotite, Flakes	<0.01	0.011±0.001	<0.05	<0.004	<0.02	<0.01
Dowex 50Wx8	<0.04	0.012±0.001	<0.06	0.005±0.003	<0.02	<0.01

Table 3-4 Result of the ion exchange speciation studies performed on the stock solutions of the metal complex tracers.

Complex	% Filtered (non-soluble)	% Sorbed by cation-exchanger (non-complexed)	% Sorbed by anion-exchanger (complexed)	% Passing both filtration and ion exchange
^{160}Tb-DTPA	28-30	3-10	47-69	13
^{169}Yb-EDTA	32-43	4-26	42-50	0.7-3
^{177}Lu-DOTA	25-27	12-26	47-56	7

3.2.2 Sorbing Tracers

3.2.2.1 Sorption Coefficient

Sorption coefficients are given for the tracers for which a K_d could be calculated from the loss of tracer concentration in the aqueous phase or where solid phase measurements could be performed. The results for the generic Äspö material experiment are given in Table 3-3 (Äspö diorite) and Table 3-4 (Fine-grained granite). The results for the Feature A site-specific material experiment are given in Table 3-5.

Table 3-5 Sorption coefficients, K_d (m^3/kg) obtained in the generic Äspö material experiment using Äspö diorite as solid phase. For Na^+ and Sr^{2+} the K_d has been calculated from solid phase measurements (Eq. 3-6) while for the other tracers the K_d has been calculated from measurements of the loss in the aqueous phase (Eq. 3-3). When uncertainties are given, they are based on the standard deviation of 2-4 samples (2σ confidence level).

Fraction size (mm)	Contact time (d)	Na^+	Ca^{2+}	Rb^+	Sr^{2+}	Cs^+	Ba^{2+}
0.045-0.090	1		$<70\cdot10^{-6}$	$5.0\pm0.3\cdot10^{-3}$	$97\cdot10^{-6}$	$54\pm3\cdot10^{-3}$	$2.6\pm0.06\cdot10^{-3}$
	2			$6.8\cdot10^{-3}$		$75\cdot10^{-3}$	$3.3\cdot10^{-3}$
	6				$98\cdot10^{-6}$		
	7	$10\cdot10^{-6}$					
	14	$10\cdot10^{-6}$	$<70\cdot10^{-6}$	$8.1\pm1.4\cdot10^{-3}$	$100\cdot10^{-6}$	$290\pm1\cdot10^{-3}$	$4.3\pm0.03\cdot10^{-3}$
	36			$8.8\cdot10^{-3}$		$410\cdot10^{-3}$	$5.1\cdot10^{-3}$
0.090-0.25	1			$4.1\cdot10^{-3}$		$14\cdot10^{-3}$	$1.6\cdot10^{-3}$
	6						
	14	$9\cdot10^{-6}$		$6.7\cdot10^{-3}$	$77\cdot10^{-6}$	$110\cdot10^{-3}$	$3.1\cdot10^{-3}$
	36			$7.4\cdot10^{-3}$		$140\cdot10^{-3}$	$4.1\cdot10^{-3}$
0.25-0.5	1		$<70\cdot10^{-6}$	$3.0\pm0.1\cdot10^{-3}$	$70\cdot10^{-6}$	$26\pm2\cdot10^{-3}$	$1.1\pm0.01\cdot10^{-3}$
	2			$3.8\cdot10^{-3}$		$32\cdot10^{-3}$	$1.5\cdot10^{-3}$
	6				$73\cdot10^{-6}$		
	7	$10\cdot10^{-6}$					
	14	$10\cdot10^{-6}$	$<60\cdot10^{-6}$	$4.9\pm0.1\cdot10^{-3}$	$73\cdot10^{-6}$	$150\pm1\cdot10^{-3}$	$2.1\pm0.02\cdot10^{-3}$
	36			$5.5\cdot10^{-3}$		$170\cdot10^{-3}$	$2.8\cdot10^{-3}$
0.5-1	1			$1.8\cdot10^{-3}$		$6.8\cdot10^{-3}$	$0.68\cdot10^{-3}$
	6						
	14	$8\cdot10^{-6}$		$3.3\cdot10^{-3}$	$50\cdot10^{-6}$	$38\cdot10^{-3}$	$1.5\cdot10^{-3}$
	36			$4.0\cdot10^{-3}$		$44\cdot10^{-3}$	$1.9\cdot10^{-3}$
1.0-2.0	1		$<50\cdot10^{-6}$	$1.1\pm0.2\cdot10^{-3}$	$35\cdot10^{-6}$	$6.5\pm1.3\cdot10^{-3}$	$0.48\pm0.07\cdot10^{-3}$
	2			$1.6\cdot10^{-3}$		$5.1\cdot10^{-3}$	$0.56\cdot10^{-3}$
	6				$37\cdot10^{-6}$		
	7	$5\cdot10^{-6}$					
	14	$7\cdot10^{-6}$	$<30\cdot10^{-6}$	$1.9\pm0.4\cdot10^{-3}$	$36\cdot10^{-6}$	$30\pm4\cdot10^{-3}$	$0.90\pm0.03\cdot10^{-3}$
	36			$2.8\cdot10^{-3}$		$53\cdot10^{-3}$	$1.1\cdot10^{-3}$
2.0-4.0	1			$0.79\cdot10^{-3}$		$2.7\cdot10^{-3}$	$0.40\cdot10^{-3}$
	6						
	14	$7\cdot10^{-6}$		$1.4\cdot10^{-3}$	$29\cdot10^{-6}$	$8.2\cdot10^{-3}$	$0.74\cdot10^{-3}$
	36			$2.0\cdot10^{-3}$		$9.6\cdot10^{-3}$	$1.0\cdot10^{-3}$

Table 3-6 Sorption coefficients, K_d (m^3/kg) obtained in the generic Äspö material experiment using Fine-grained granite as solid phase. For Na^+ and Sr^{2+} the K_d has been calculated from solid phase measurements (Eq. 3-6) while for the other tracers the K_d has been calculated from measurements of the loss in the aqueous phase (Eq. 3-3). When uncertainties are given, they are based on the standard deviation of 2-4 samples (2σ confidence level).

Fraction Size (mm)	Contact time (d)	Na^+	Ca^{2+}	Rb^+	Sr^{2+}	Cs^+	Ba^{2+}
0.045-0.090	1		$<70\cdot10^{-6}$	$1.9\pm0.03\cdot10^{-3}$	$78\cdot10^{-6}$	$26\pm0.2\cdot10^{-3}$	$1.9\pm0.04\cdot10^{-3}$
	2			$2.3\cdot10^{-3}$			$2.1\cdot10^{-3}$
	6				$84\cdot10^{-6}$		
	7	$27\cdot10^{-6}$				$53\cdot10^{-3}$	
	14	$27\cdot10^{-6}$		$2.8\pm0.1\cdot10^{-3}$	$84\cdot10^{-6}$	$57\pm1\cdot10^{-3}$	$2.7\pm0.06\cdot10^{-3}$
	36			$3.0\cdot10^{-3}$			$3.0\cdot10^{-3}$
0.090-0.25	1			$1.0\cdot10^{-3}$		$15\cdot10^{-3}$	$0.90\cdot10^{-3}$
	6						
	7					$30\cdot10^{-3}$	
	14	$13\cdot10^{-6}$			$45\cdot10^{-6}$	$30\cdot10^{-3}$	
	36			$2.1\cdot10^{-3}$			$1.8\cdot10^{-3}$
0.25-0.5	1		$<70\cdot10^{-6}$	$0.77\pm0.04\cdot10^{-3}$	$27\cdot10^{-6}$	$11\pm0.3\cdot10^{-3}$	$0.66\pm0.06\cdot10^{-3}$
	2			$0.98\cdot10^{-3}$			$0.75\cdot10^{-3}$
	6				$30\cdot10^{-6}$		
	7	$7\cdot10^{-6}$				$17\cdot10^{-3}$	
	14	$13\cdot10^{-6}$		$1.2\pm0.06\cdot10^{-3}$	$31\cdot10^{-6}$	$19\pm2\cdot10^{-3}$	$1.1\pm0.1\cdot10^{-3}$
	36			$1.6\cdot10^{-3}$			$1.3\cdot10^{-3}$
0.5-1	1			$0.54\cdot10^{-3}$		$7.2\cdot10^{-3}$	$0.41\cdot10^{-3}$
	6						
	7						
	14	$4\cdot10^{-6}$			$21\cdot10^{-6}$	$10\cdot10^{-3}$	
	36			$1.2\cdot10^{-3}$		$11\cdot10^{-3}$	$0.94\cdot10^{-3}$
1.0-2.0	1		$<28\cdot10^{-6}$	$0.36\pm0.01\cdot10^{-3}$	$14\cdot10^{-6}$	$6.1\pm0.1\cdot10^{-3}$	$0.28\pm0.02\cdot10^{-3}$
	2			$0.44\cdot10^{-3}$			0.31
	6				$15\cdot10^{-6}$		
	7	$4\cdot10^{-6}$				$7.9\cdot10^{-3}$	
	14	$5\cdot10^{-6}$		$1.4\pm0.02\cdot10^{-3}$	$18\cdot10^{-6}$	$8.3\pm0.3\cdot10^{-3}$	$0.60\pm0.04\cdot10^{-3}$
	36			$0.86\cdot10^{-3}$			$0.75\cdot10^{-3}$
2.0-4.0	1			$0.30\cdot10^{-3}$		$5.3\cdot10^{-3}$	$0.19\cdot10^{-3}$
	6						
	7					$6.4\cdot10^{-3}$	
	14	$4\cdot10^{-6}$			$14\cdot10^{-6}$	$6.7\cdot10^{-3}$	
	36			$0.82\cdot10^{-3}$			$0.65\cdot10^{-3}$

Table 3-7 Sorption coefficients, K_d (m^3/kg) obtained in the experiment applying Feature A site-specific conditions. The K_d has been calculated from measurements of the loss in the aqueous phase (Eq. 3-3) for all the tracers. The uncertainties are based on γ-spectrometric counting statistics (2σ confidence level).

Material	Contact time (d)	Na^+	Ca^{2+}	Rb^+	Sr^{2+}	Cs^+	Ba^{2+}
Mylonite	0.75	$<50\cdot10^{-6}$	$<400\cdot10^{-6}$	$0.8\pm0.4\cdot10^{-3}$	$<300\cdot10^{-6}$	$2.8\pm0.3\cdot10^{-3}$	$0.7\pm0.1\cdot10^{-3}$
KXTT2	5.4	$<70\cdot10^{-6}$	$<200\cdot10^{-6}$	$0.9\pm0.3\cdot10^{-3}$	$<200\cdot10^{-6}$	$5.7\pm0.3\cdot10^{-3}$	$0.6\pm0.1\cdot10^{-3}$
	8.4	$<200\cdot10^{-6}$	$<500\cdot10^{-6}$	$2.0\pm0.4\cdot10^{-3}$	$<300\cdot10^{-6}$	$8.0\pm0.6\cdot10^{-3}$	$1.3\pm0.1\cdot10^{-3}$
Mylonite	0.75	$<200\cdot10^{-6}$	$<500\cdot10^{-6}$	$<0.29\cdot10^{-3}$	$<50\cdot10^{-6}$	$0.8\pm0.2\cdot10^{-3}$	$0.3\pm0.1\cdot10^{-3}$
KXTT4	5.4	$<70\cdot10^{-6}$	$<40\cdot10^{-6}$	$<0.37\cdot10^{-3}$	$<200\cdot10^{-6}$	$0.9\pm0.1\cdot10^{-3}$	$0.3\pm0.1\cdot10^{-3}$
	8.4	$<300\cdot10^{-6}$	$<700\cdot10^{-6}$	$<0.54\cdot10^{-3}$	$<300\cdot10^{-6}$	$1.2\pm0.2\cdot10^{-3}$	$0.4\pm0.1\cdot10^{-3}$
Altered	0.75	$<200\cdot10^{-6}$	$<200\cdot10^{-6}$	$0.9\pm0.4\cdot10^{-3}$	$<200\cdot10^{-6}$	$5.3\pm0.4\cdot10^{-3}$	$0.5\pm0.1\cdot10^{-3}$
ÄD	5.4	$<10\cdot10^{-6}$	$<200\cdot10^{-6}$	$0.9\pm0.4\cdot10^{-3}$	$<300\cdot10^{-6}$	$11\pm0.8\cdot10^{-3}$	$0.7\pm0.1\cdot10^{-3}$
KXTT2	8.4	$<100\cdot10^{-6}$	$<60\cdot10^{-6}$	$0.9\pm0.4\cdot10^{-3}$	$<40\cdot10^{-6}$	11 ± 110^{-3}	$1.2\pm0.1\cdot10^{-3}$
Altered	0.75	$<200\cdot10^{-6}$	$<400\cdot10^{-6}$	$<0.92\cdot10^{-3}$	$<400\cdot10^{-6}$	$1.8\pm0.3\cdot10^{-3}$	$0.8\pm0.2\cdot10^{-3}$
ÄD	5.4	$<200\cdot10^{-6}$	$<1000\cdot10^{-6}$	$<0.80\cdot10^{-3}$	$<500\cdot10^{-6}$	$2.3\pm0.2\cdot10^{-3}$	$1.2\pm0.1\cdot10^{-3}$
KXTT3	8.4	$<60\cdot10^{-6}$	$<600\cdot10^{-6}$	$<0.69\cdot10^{-3}$	$<100\cdot10^{-6}$	$3.1\pm0.2\cdot10^{-3}$	$1.8\pm0.1\cdot10^{-3}$
Altered	0.75	$<200\cdot10^{-6}$	$<500\cdot10^{-6}$	$<0.82\cdot10^{-3}$	$<200\cdot10^{-6}$	$0.4\pm0.2\cdot10^{-3}$	$0.5\pm0.1\cdot10^{-3}$
FGG	5.4	$<100\cdot10^{-6}$	$<200\cdot10^{-6}$	$<0.51\cdot10^{-3}$	$<100\cdot10^{-6}$	$1.0\pm0.2\cdot10^{-3}$	$<0.3\cdot10^{-3}$
KXTT4	8.4	$<200\cdot10^{-6}$	$<300\cdot10^{-6}$	$<0.51\cdot10^{-3}$	$<400\cdot10^{-6}$	$1.5\pm0.2\cdot10^{-3}$	$0.4\pm0.1\cdot10^{-3}$
Äspö	0.75	$<50\cdot10^{-6}$	$<400\cdot10^{-6}$	$<0.70\cdot10^{-3}$	$<300\cdot10^{-6}$	$5.0\pm0.3\cdot10^{-3}$	$0.4\pm0.1\cdot10^{-3}$
Diorite	5.4	$<50\cdot10^{-6}$	$<100\cdot10^{-6}$	$1.4\pm0.3\cdot10^{-3}$	$<200\cdot10^{-6}$	$12\pm0.4\cdot10^{-3}$	$0.9\pm0.1\cdot10^{-3}$
	8.4	$<30\cdot10^{-6}$	$<50\cdot10^{-6}$	$1.4\pm0.4\cdot10^{-3}$	$<200\cdot10^{-6}$	$14\pm1\cdot10^{-3}$	$1.2\pm0.1\cdot10^{-3}$
Fine	0.75	$<60\cdot10^{-6}$	$<700\cdot10^{-6}$	$1.2\pm0.5\cdot10^{-3}$	$<100\cdot10^{-6}$	$5.9\pm0.6\cdot10^{-3}$	$0.5\pm0.1\cdot10^{-3}$
Grained	5.4	$<60\cdot10^{-6}$	$<700\cdot10^{-6}$	$<0.66\cdot10^{-3}$	$<60\cdot10^{-6}$	$1.9\pm0.2\cdot10^{-3}$	$0.5\pm0.1\cdot10^{-3}$
Granite	8.4	$<10\cdot10^{-6}$	$<600\cdot10^{-6}$	$<0.59\cdot10^{-3}$	$<100\cdot10^{-6}$	$1.6\pm0.2\cdot10^{-3}$	$0.6\pm0.1\cdot10^{-3}$
Biotite	0.75	$<300\cdot10^{-6}$	$<100\cdot10^{-6}$	$23\pm5\cdot10^{-3}$	$<500\cdot10^{-6}$	$72\pm15\cdot10^{-3}$	$4.9\pm0.3\cdot10^{-3}$
Sep, ÄD	5.4	$<40\cdot10^{-6}$	$<200\cdot10^{-6}$	$16\pm3\cdot10^{-3}$	$<200\cdot10^{-6}$	$190\pm70\cdot10^{-3}$	$6.5\pm0.4\cdot10^{-3}$
0.25-0.5	8.4	$<400\cdot10^{-6}$	$<500\cdot10^{-6}$	$30\pm7\cdot10^{-3}$	$<200\cdot10^{-6}$	$>250\cdot10^{-3}$	$8.1\pm0.5\cdot10^{-3}$
Biotite	0.75	$<80\cdot10^{-6}$	$<700\cdot10^{-6}$	$5.5\pm0.9\cdot10^{-3}$	$<100\cdot10^{-6}$	$71\pm12\cdot10^{-3}$	$5.4\pm0.4\cdot10^{-3}$
Flakes	5.4	$<100\cdot10^{-6}$	$<300\cdot10^{-6}$	$9.6\pm1.7\cdot10^{-3}$	$<200\cdot10^{-6}$	$130\pm30\cdot10^{-3}$	$5.6\pm0.4\cdot10^{-3}$
1-5 mm	8.4	$<300\cdot10^{-6}$	$<900\cdot10^{-6}$	$8.8\pm1.3\cdot10^{-3}$	$<900\cdot10^{-6}$	$190\pm70\cdot10^{-3}$	$8.8\pm0.5\cdot10^{-3}$
Dowex	0.75	$11\pm0.2\cdot10^{-3}$	$180\pm30\cdot10^{-3}$	$42\pm4\cdot10^{-3}$	$250\pm40\cdot10^{-3}$	$38\pm2\cdot10^{-3}$	$480\pm90\cdot10^{-3}$
50Wx8	5.4	$11\pm0.2\cdot10^{-3}$	$290\pm100\cdot10^{-3}$	$31\pm2\cdot10^{-3}$	$270\pm40\cdot10^{-3}$	$41\pm2\cdot10^{-3}$	$960\pm180\cdot10^{-3}$
20-50 m	8.4	$11\pm0.2\cdot10^{-3}$	$280\pm60\cdot10^{-3}$	$36\pm3\cdot10^{-3}$	$280\pm40\cdot10^{-3}$	$38\pm2\cdot10^{-3}$	$670\pm150\cdot10^{-3}$

3.2.2.2 *Desorption Coefficients*

The desorption coefficients generic Äspö material experiment are presented in Table 3-6 (Äspö diorite) and Table 3-7 (Fine-grained granite). The results for the experiment using Feature A site-specific material are given in Table 3-8. Generally, in the cases where no sorption could be statistically verified during the sorption part of the experiment, no $K_{d(des2)}$ could be calculated and only $K_{d(des1)}$ are given (cf. section 3.1.11).

Table 3-8 **Desorption coefficients, $K_{d(des1)}$ and $K_{d(des2)}$ (m^3/kg), obtained for the tracers in contact with Äspö diorite, compared to the sorption coefficients K_d (m^3/kg) for corresponding contact time (cf. section 3.1.10 and 3.1.11). The desorption coefficients are given using the desorption obtained using the longest desorption time applied for each sample.**

		Na^+		Ca^{2+}			Rb^+		
Fraction size (mm)	Sorp time (d)	$K_{d(des1)}$	K_d	$K_{d(des1)}$	K_d		$K_{d(des1)}$	$K_{d(des2)}$	K_d
0.045-0.09	1				$<7\cdot10^{-5}$				
	2			$5.5\cdot10^{-5}$			$1.3\cdot10^{-3}$	$3.3\cdot10^{-3}$	$6.8\cdot10^{-3}$
	7	$1.0\cdot10^{-5}$	$1.0\cdot10^{-5}$						
	14	$1.1\cdot10^{-5}$	$1.0\cdot10^{-5}$	$6.3\cdot10^{-5}$	$<7\cdot10^{-5}$		$1.1\cdot10^{-3}$	$3.0\cdot10^{-3}$	$8.1\cdot10^{-3}$
	36			$6.3\cdot10^{-5}$			$1.1\cdot10^{-3}$	$3.3\cdot10^{-3}$	$8.8\cdot10^{-3}$
0.25-0.50	1				$<7\cdot10^{-5}$				
	2			$4.6\cdot10^{-5}$			$1.1\cdot10^{-3}$	$2.1\cdot10^{-3}$	$3.8\cdot10^{-3}$
	7	$1.1\cdot10^{-5}$	$1.0\cdot10^{-5}$						
	14	$1.1\cdot10^{-5}$	$1.0\cdot10^{-5}$	$5.5\cdot10^{-5}$	$<6\cdot10^{-5}$		$1.3\cdot10^{-3}$	$2.6\cdot10^{-3}$	$4.9\cdot10^{-3}$
	36			$5.5\cdot10^{-5}$			$1.0\cdot10^{-3}$	$2.1\cdot10^{-3}$	$5.5\cdot10^{-3}$
1.0-2.0	1				$<5\cdot10^{-5}$				
	2			$3.4\cdot10^{-5}$			$6.3\cdot10^{-4}$	$8.5\cdot10^{-4}$	$1.6\cdot10^{-3}$
	7	$6.0\cdot10^{-6}$	$5.0\cdot10^{-6}$						
	14	$8.0\cdot10^{-6}$	$7.0\cdot10^{-6}$	$3.7\cdot10^{-5}$	$<3\cdot10^{-5}$		$7.4\cdot10^{-4}$	$1.0\cdot10^{-3}$	$1.9\cdot10^{-3}$
	36			$4.2\cdot10^{-5}$			$5.0\cdot10^{-4}$	$8.0\cdot10^{-4}$	$2.8\cdot10^{-3}$

		Sr^{2+}		Cs^+			Ba^{2+}		
Fraction size (mm)	Sorp time (d)	$K_{d(des1)}$	K_d	$K_{d(des1)}$	$K_{d(des2)}$	K_d	$K_{d(des1)}$	$K_{d(des2)}$	K_d
0.045-0.09	1	$6.7\cdot10^{-5}$	$9.7\cdot10^{-5}$						
	2			$1.4\cdot10^{-3}$	$5.2\cdot10^{-2}$	$1.5\cdot10^{-1}$	$1.1\cdot10^{-3}$	$1.9\cdot10^{-3}$	$3.3\cdot10^{-3}$
	6	$1.2\cdot10^{-4}$	$9.8\cdot10^{-5}$						
	14	$8.3\cdot10^{-5}$	$1.0\cdot10^{-4}$	$2.0\cdot10^{-3}$	$1.4\cdot10^{-1}$	$2.9\cdot10^{-1}$	$1.0\cdot10^{-3}$	$1.9\cdot10^{-3}$	$4.3\cdot10^{-3}$
	36			$2.1\cdot10^{-3}$	$2.1\cdot10^{-1}$	$4.1\cdot10^{-1}$	$1.0\cdot10^{-3}$	$2.0\cdot10^{-3}$	$5.1\cdot10^{-3}$
0.25-0.50	1	$5.5\cdot10^{-5}$	$7.0\cdot10^{-5}$						
	2			$1.9\cdot10^{-3}$	$3.2\cdot10^{-2}$	$6.5\cdot10^{-2}$	$8.1\cdot10^{-4}$	$1.0\cdot10^{-3}$	$1.5\cdot10^{-3}$
	6	$7.1\cdot10^{-5}$	$7.3\cdot10^{-5}$						
	14	$5.8\cdot10^{-5}$	$7.3\cdot10^{-5}$	$3.0\cdot10^{-3}$	$1.2\cdot10^{-1}$	$1.5\cdot10^{-1}$	$7.8\cdot10^{-4}$	$1.1\cdot10^{-3}$	$2.1\cdot10^{-3}$
	36			$2.1\cdot10^{-3}$	$9.0\cdot10^{-2}$	$1.7\cdot10^{-1}$	$8.4\cdot10^{-4}$	$1.3\cdot10^{-3}$	$2.8\cdot10^{-3}$
1.0-2.0	1	$2.2\cdot10^{-5}$	$3.5\cdot10^{-5}$						
	2			$1.0\cdot10^{-3}$	$4.6\cdot10^{-3}$	$1.0\cdot10^{-2}$	$4.7\cdot10^{-4}$	$5.1\cdot10^{-4}$	$5.6\cdot10^{-4}$
	6	$3.6\cdot10^{-5}$	$3.7\cdot10^{-5}$						
	14	$3.0\cdot10^{-5}$	$3.6\cdot10^{-5}$	$1.7\cdot10^{-3}$	$1.7\cdot10^{-2}$	$3.0\cdot10^{-2}$	$5.5\cdot10^{-4}$	$6.1\cdot10^{-4}$	$9.0\cdot10^{-4}$
	36			$1.8\cdot10^{-3}$	$2.7\cdot10^{-2}$	$5.3\cdot10^{-2}$	$4.8\cdot10^{-4}$	$5.6\cdot10^{-4}$	$1.1\cdot10^{-3}$

Table 3-9 **Desorption coefficients, $K_{d(des1)}$ and $K_{d(des2)}$ (m^3/kg), obtained for the tracers in contact with Fine-grained granite, compared to the sorption coefficients K_d (m^3/kg) for corresponding contact time (see text for details). The desorption coefficients are given using the desorption obtained using the longest desorption time applied for each sample.**

		Na^+		Ca^{2+}			Rb^+		
Fraction size (mm)	Sorp time (d)	$K_{d(des1)}$	K_d	$K_{d(des1)}$	K_d		$K_{d(des1)}$	$K_{d(des2)}$	K_d
0.045-0.09	1				$<7\cdot10^{-5}$				
	2			$2.9\cdot10^{-5}$			$8.3\cdot10^{-4}$	$1.3\cdot10^{-3}$	$2.3\cdot10^{-4}$
	7	$3.0\cdot10^{-5}$	$2.7\cdot10^{-5}$						
	14	$2.6\cdot10^{-5}$	$2.7\cdot10^{-5}$	$3.0\cdot10^{-5}$			$9.1\cdot10^{-4}$	$1.4\cdot10^{-3}$	$2.8\cdot10^{-3}$
	36			$3.3\cdot10^{-5}$			$6.0\cdot10^{-4}$	$9.3\cdot10^{-4}$	$3.0\cdot10^{-3}$
0.25-0.50	1				$<7\cdot10^{-5}$				
	2			$1.1\cdot10^{-5}$			$4.9\cdot10^{-4}$	$5.7\cdot10^{-4}$	$9.8\cdot10^{-4}$
	7	$8.0\cdot10^{-6}$	$7.0\cdot10^{-6}$						
	14	$1.3\cdot10^{-5}$	$1.3\cdot10^{-5}$	$1.3\cdot10^{-5}$			$6.1\cdot10^{-4}$	$7.2\cdot10^{-4}$	$1.2\cdot10^{-3}$
	36			$1.4\cdot10^{-5}$			$2.7\cdot10^{-4}$	$3.4\cdot10^{-4}$	$1.6\cdot10^{-3}$
1.0-2.0	1				$<3\cdot10^{-5}$				
	2			$8.1\cdot10^{-6}$			$2.3\cdot10^{-4}$	$2.8\cdot10^{-4}$	$4.4\cdot10^{-4}$
	7	$5.0\cdot10^{-6}$	$4.0\cdot10^{-6}$						
	14	$5.0\cdot10^{-6}$	$5.0\cdot10^{-6}$	$1.3\cdot10^{-5}$			$4.8\cdot10^{-4}$	$5.3\cdot10^{-4}$	$8.1\cdot10^{-4}$
	36			$1.2\cdot10^{-5}$			$1.2\cdot10^{-4}$	$1.3\cdot10^{-4}$	$8.6\cdot10^{-4}$

		Sr^{2+}		Cs^+			Ba^{2+}		
Fraction size (mm)	Sorp time (d)	$K_{d(des1)}$	K_d	$K_{d(des1)}$	$K_{d(des2)}$	K_d	$K_{d(des1)}$	$K_{d(des2)}$	K_d
0.045-0.09	1	$5.7\cdot10^{-5}$	$7.8\cdot10^{-5}$	$2.9\cdot10^{-3}$	$1.2\cdot10^{-2}$	$2.6\cdot10^{-2}$			
	2						$1.0\cdot10^{-3}$	$1.4\cdot10^{-3}$	$2.1\cdot10^{-3}$
	6	$7.6\cdot10^{-5}$	$8.4\cdot10^{-5}$						
	7			$6.6\cdot10^{-3}$	$4.8\cdot10^{-2}$	$5.3\cdot10^{-2}$			
	14	$6.7\cdot10^{-5}$	$8.4\cdot10^{-5}$	$3.9\cdot10^{-3}$	$3.0\cdot10^{-2}$	$5.7\cdot10^{-2}$	$8.1\cdot10^{-4}$	$1.2\cdot10^{-3}$	$2.7\cdot10^{-3}$
	36						$9.2\cdot10^{-4}$	$1.5\cdot10^{-3}$	$3.0\cdot10^{-3}$
0.25-0.50	1	$2.0\cdot10^{-5}$	$2.7\cdot10^{-5}$	$1.7\cdot10^{-3}$	$3.9\cdot10^{-3}$	$1.1\cdot10^{-2}$			
	2						$5.3\cdot10^{-4}$	$5.9\cdot10^{-3}$	$7.5\cdot10^{-3}$
	6	$2.9\cdot10^{-5}$	$3.0\cdot10^{-5}$						
	7			$3.8\cdot10^{-3}$	$1.1\cdot10^{-2}$	$1.7\cdot10^{-2}$			
	14	$2.6\cdot10^{-5}$	$3.1\cdot10^{-5}$	$2.2\cdot10^{-3}$	$7.1\cdot10^{-3}$	$1.9\cdot10^{-2}$	$5.7\cdot10^{-4}$	$6.7\cdot10^{-4}$	$1.1\cdot10^{-3}$
	36						$3.7\cdot10^{-4}$	$4.4\cdot10^{-4}$	$1.3\cdot10^{-3}$
1.0-2.0	1	$8.4\cdot10^{-6}$	$1.4\cdot10^{-5}$	$8.3\cdot10^{-4}$	$1.4\cdot10^{-3}$	$6.1\cdot10^{-3}$			
	2						$2.4\cdot10^{-4}$	$2.4\cdot10^{-4}$	$3.1\cdot10^{-4}$
	6	$1.5\cdot10^{-5}$	$1.5\cdot10^{-5}$						
	7			$1.9\cdot10^{-3}$	$3.7\cdot10^{-3}$	$7.9\cdot10^{-3}$			
	14	$1.6\cdot10^{-5}$	$1.8\cdot10^{-5}$	$1.0\cdot10^{-3}$	$2.1\cdot10^{-3}$	$8.3\cdot10^{-3}$	$4.2\cdot10^{-4}$	$4.5\cdot10^{-4}$	$6.0\cdot10^{-4}$
	36						$3.2\cdot10^{-4}$	$3.5\cdot10^{-4}$	$7.5\cdot10^{-4}$

Table 3-10 Desorption coefficients, $K_{d(des1)}$ and $K_{d(des2)}$ (m^3/kg), obtained for the tracers in contact with Feature A geologic material, compared to the sorption coefficients K_d (m^3/kg). The desorption coefficients are given using 9 days of sorption and 7 days of desorption.

	Na^+			Ca^{2+}			Rb^+		
Material	$K_{d(des1)}$	$K_{d(des2)}$	K_d	$K_{d(des1)}$	$K_{d(des2)}$	K_d	$K_{d(des1)}$	$K_{d(des2)}$	K_d
Mylonite, KXTT2	$6.8\cdot10^{-6}$		$<2\cdot10^{-4}$	$2.7\cdot10^{-5}$		$<5\cdot10^{-4}$	$5.1\cdot10^{-4}$	$8.2\cdot10^{-4}$	$2.0\cdot10^{-3}$
Mylonite, KXTT4	$2.6\cdot10^{-6}$		$<3\cdot10^{-4}$	$1.7\cdot10^{-5}$		$<7\cdot10^{-4}$	$1.3\cdot10^{-4}$	$4.2\cdot10^{-4}$	$5.4\cdot10^{-4}$
Alt. Diorite, KXTT2	$2.9\cdot10^{-6}$		$<1\cdot10^{-4}$	$2.7\cdot10^{-5}$		$<6\cdot10^{-5}$	$4.4\cdot10^{-4}$	$5.9\cdot10^{-4}$	$8.9\cdot10^{-4}$
Alt. Diorite, KXTT3	$4.4\cdot10^{-6}$		$<6\cdot10^{-5}$	$<5\cdot10^{-5}$		$<6\cdot10^{-4}$	$3.9\cdot10^{-4}$		$<7\cdot10^{-4}$
Alt. Granite, KXTT4	$1.1\cdot10^{-6}$		$<2\cdot10^{-4}$	$<2\cdot10^{-5}$		$<3\cdot10^{-4}$	$1.3\cdot10^{-4}$	$4.7\cdot10^{-4}$	$5.1\cdot10^{-4}$
Äspö diorite	$3.8\cdot10^{-6}$		$<3\cdot10^{-5}$	$5.4\cdot10^{-5}$		$<4\cdot10^{-5}$	$5.9\cdot10^{-4}$	$8.6\cdot10^{-4}$	$1.4\cdot10^{-3}$
Fine-grained granite	$6.0\cdot10^{-6}$		$<1\cdot10^{-5}$	$<2\cdot10^{-5}$		$<5\cdot10^{-4}$	$2.5\cdot10^{-4}$		$<6\cdot10^{-4}$
Biotite, ÄD-sep	$3.6\cdot10^{-6}$		$<4\cdot10^{-4}$	$8.3\cdot10^{-5}$		$<6\cdot10^{-4}$	$2.0\cdot10^{-3}$	$2.4\cdot10^{-2}$	$3.0\cdot10^{-2}$
Biotite, flakes 1-5 mm	$3.4\cdot10^{-6}$		$<3\cdot10^{-4}$	$5.7\cdot10^{-5}$		$<9\cdot10^{-4}$	$6.9\cdot10^{-4}$	$3.3\cdot10^{-3}$	$8.8\cdot10^{-3}$
Dowex 50Wx8	$2.0\cdot10^{-3}$	$1.0\cdot10^{-2}$	$1.1\cdot10^{-2}$	$5.6\cdot10^{-3}$	$4.4.\cdot10^{-1}$	$2.8\cdot10^{-1}$	$3.4\cdot10^{-3}$	$4.1\cdot10^{-2}$	$3.6\cdot10^{-2}$

	Sr^{2+}			Cs^+			Ba^{2+}		
Material	$K_{d(des1)}$	$K_{d(des2)}$	K_d	$K_{d(des1)}$	$K_{d(des2)}$	K_d	$K_{d(des1)}$	$K_{d(des2)}$	K_d
Mylonite, KXTT2	$5.0\cdot10^{-5}$		$<3\cdot10^{-4}$	$1.1\cdot10^{-3}$	$3.3\cdot10^{-3}$	$8.0\cdot10^{-3}$	$5.0\cdot10^{-4}$	$6.8\cdot10^{-4}$	$1.3\cdot10^{-3}$
Mylonite, KXTT4	$2.6\cdot10^{-5}$		$<2\cdot10^{-4}$	$4.0\cdot10^{-4}$	$5.4\cdot10^{-4}$	$1.2\cdot10^{-3}$	$2.3\cdot10^{-4}$	$2.5\cdot10^{-4}$	$3.7\cdot10^{-4}$
Alt. Diorite, KXTT2	$4.1\cdot10^{-5}$		$<4\cdot10^{-5}$	$1.2\cdot10^{-3}$	$4.9\cdot10^{-3}$	$1.1\cdot10^{-2}$	$7.2\cdot10^{-4}$	$9.6\cdot10^{-4}$	$1.2\cdot10^{-3}$
Alt. Diorite, KXTT3	$9.0\cdot10^{-5}$		$<9\cdot10^{-5}$	$9.3\cdot10^{-4}$	$1.7\cdot10^{-3}$	$3.1\cdot10^{-3}$	$8.9\cdot10^{-4}$	$1.3\cdot10^{-3}$	$1.8\cdot10^{-3}$
Alt. Granite, KXTT4	$1.0\cdot10^{-5}$		$<4\cdot10^{-4}$	$3.5\cdot10^{-4}$	$5.0\cdot10^{-4}$	$1.5\cdot10^{-3}$	$2.0\cdot10^{-4}$	$2.2\cdot10^{-4}$	$4.1\cdot10^{-4}$
Äspö diorite	$1.1\cdot10^{-4}$		$<2\cdot10^{-4}$	$1.4\cdot10^{-3}$	$6.8\cdot10^{-3}$	$1.4\cdot10^{-2}$	$7.4\cdot10^{-4}$	$1.0\cdot10^{-3}$	$1.2\cdot10^{-3}$
Fine-grained granite	$3.1\cdot10^{-5}$		$<1\cdot10^{-4}$	$4.8\cdot10^{-4}$	$7.1\cdot10^{-4}$	$1.6\cdot10^{-3}$	$4.5\cdot10^{-4}$	$5.4\cdot10^{-4}$	$6.3\cdot10^{-4}$
Biotite, ÄD-sep	$1.6\cdot10^{-4}$		$<2\cdot10^{-4}$	$1.2\cdot10^{-3}$	$7.0\cdot10^{-2}$	$1.9\cdot10^{-1}$	$9.6\cdot10^{-4}$	$4.3\cdot10^{-3}$	$8.1\cdot10^{-3}$
Biotite, flakes 1-5 mm	$9.4\cdot10^{-5}$		$<9\cdot10^{-4}$	$1.8\cdot10^{-3}$	$1.1\cdot10^{-1}$	$1.9\cdot10^{-1}$	$1.4\cdot10^{-3}$	$6.8\cdot10^{-3}$	$8.8\cdot10^{-3}$
Dowex 50Wx8	$3.7\cdot10^{-3}$	$2.9\cdot10^{-1}$	$2.8\cdot10^{-1}$	$3.0\cdot10^{-3}$	$3.7\cdot10^{-2}$	$3.8\cdot10^{-2}$	$3.3\cdot10^{-3}$	$6.1\cdot10^{-1}$	$6.7\cdot10^{-1}$

3.2.2.3 *Sorption Behaviour of the Different Cations*

The sorption of Na is very low (<0.1%) in these comparatively high saline waters. Since the sorption of Na is small, the radioactivity measured during the desorption process is only slightly higher than the background levels and the uncertainties are therefore significant.

The sorption of Ca is somewhat higher than for Na, but is still too low to be able to statistically verify any loss of the tracer in the aqueous phase in the sorption experiment. The sorption of Ca was studied using the radioactive tracer ^{45}Ca. Since the decay of this isotope is not associated with any γ-radiation, quantification of the sorbed amount of Ca could not be performed by measurements of the solid phase. The only way that the Ca sorption was quantified was therefore by the desorption experiment.

The sorption of Sr is also low and the activities measured during the desorption are very low and are therefore associated with high uncertainties. In the investigation of sorption of Sr on generic material, the sorption has been quantified by measuring the concentration of $^{85}Sr^{2+}$ in the solid phase after the spiked synthetic groundwater has been removed. The sorption coefficients obtained from the solid phase measurement and the desorption results agree fairly well, indicating a fast reversible sorption of Sr. The desorption behaviour of Sr and Ca are very similar, which is expected from the general chemical similarity of these cations.

The cations that have the strongest sorption are Cs, Rb and Ba, listed in the order of decreasing sorption. The sorption for all these cations are possible to quantify from the loss in the aqueous phase in the sorption part of the experiment, with the exception of Rb in some of the geologic materials used in the Feature A site-specific material experiment. Significant differences between the sorption and desorption coefficients are observed, indicating a significant part of the sorption being non- or slowly reversible. The reversibility decreases with stronger sorption; Cs with the absolute strongest sorption has the lowest desorption.

3.2.2.4 *Sorption Dependence on the Geologic Material*

Some general conclusions can be made regarding the sorptivity of the different geologic materials used in this investigation (Fig. 3-1 to 3-3):

- The results from the generic rock material shows that Äspö diorite is significantly more sorptive than the Fine-grained granite.
- It is shown that among the Feature A site specific materials, all the altered material and the mylonites show a lower sorptivity compared to their corresponding fresh rock types (*i.e.*, Äspö diorite for the KXTT2 and KXTT3 samples, Fine-grained granite for the KXTT4 samples). It is indicated that alteration and mylonitisation causes a reduction in the sorptivity.
- Comparing the altered Äspö diorites, the altered Fine-grained granites and the fresh rock materials (Table 2-5), a trend of higher sorptivity with higher concentration of biotite is observed. However, the mylonite from the KXTT2

sample is comparatively sorptive, although the geological characterisation shows that all biotite of that sample has been completely altered.

- The sorption on the pure biotite samples is much higher than any of the other rock types involved in this investigation. This confirms that the biotite concentration is an important parameter for the prediction of the sorption capacity of different rock types.

- The Dowex 50Wx8 cation exchanger is extremely much more sorptive than any of the geological material, and any comparison between them is therefore difficult. However, the Dowex 50Wx8 cation exchanger shows a strong preference of divalent cations compared to monovalent cations and a slow increase of the sorption is observed for ions with larger ionic radius. This is a behaviour which is expected for a non-selective cation exchanger. For the geologic material involved in this investigation, a selective cation exchange behaviour is indicated. A trend of increased sorption as one moves to the bottom of the left corner of the periodic table is observed.

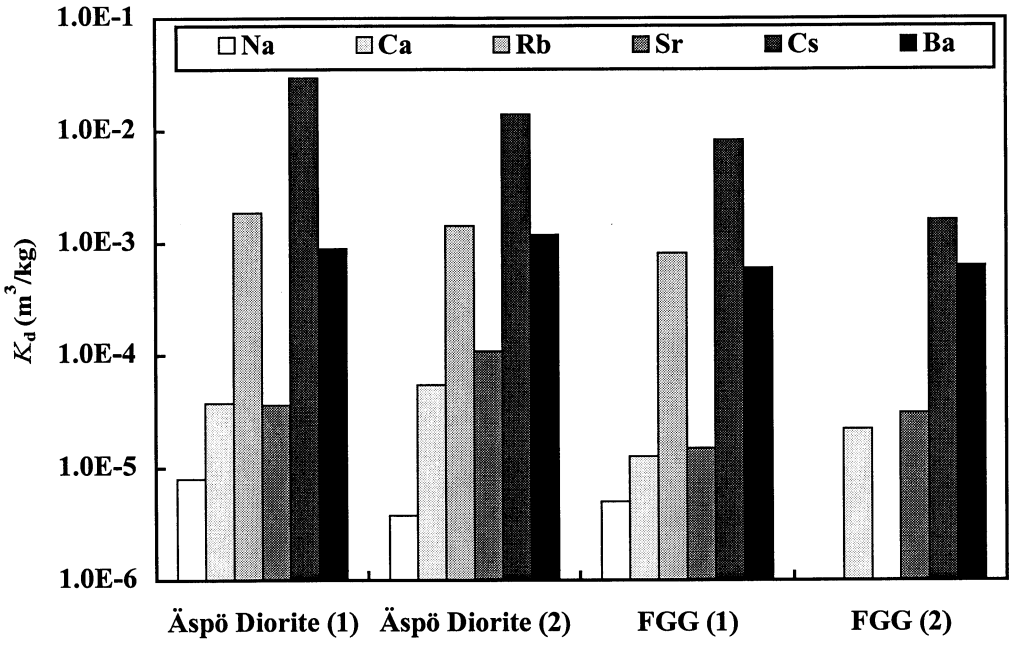

Figure 3-1 Sorption coefficients for the Äspö diorite and Fine-grained granite, 1-2 mm size fraction, 7-14 days contact time. The notation (1) refers to the first experiment series and (2) to the second experiment series, using different water compositions in the different experiment series, see Table 2-7. For series (2), sorption K_d is used for all tracers, except for Ca where $Kd_{(des1)}$ is presented. For series (1), sorption K_d is used for Cs, Rb and Ba, while $Kd_{(des1)}$ is presented for Na, Ca and Sr.

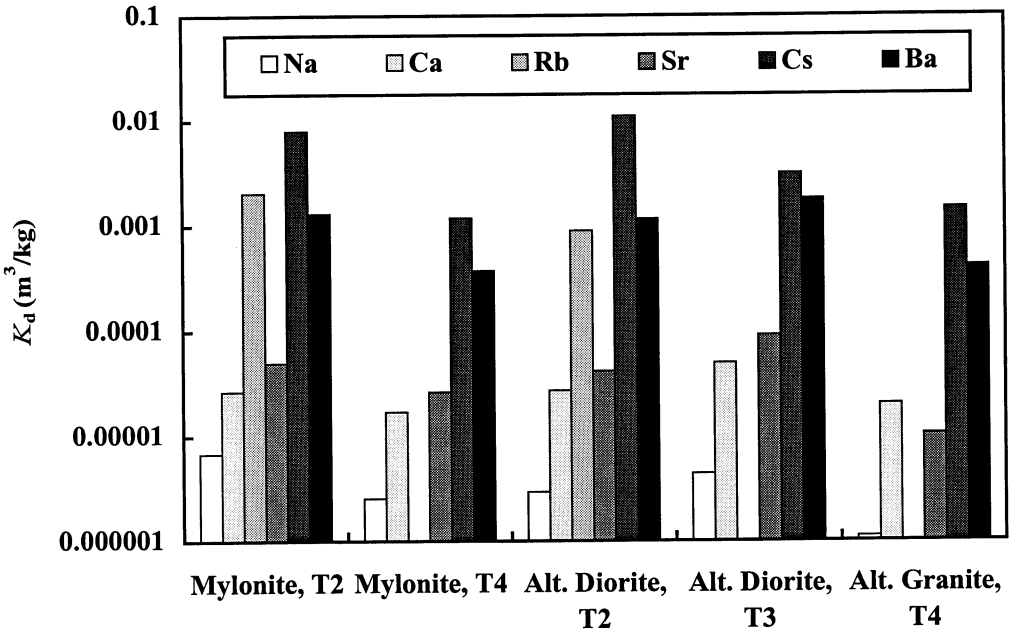

Figure 3-2 The sorption coefficients for the Feature A site-specific material, 1-2 mm size fraction, 9 days contact time. Sorption K_d is used for Cs, Rb and Ba, while $Kd_{(des1)}$ is presented for Na, Ca and Sr.

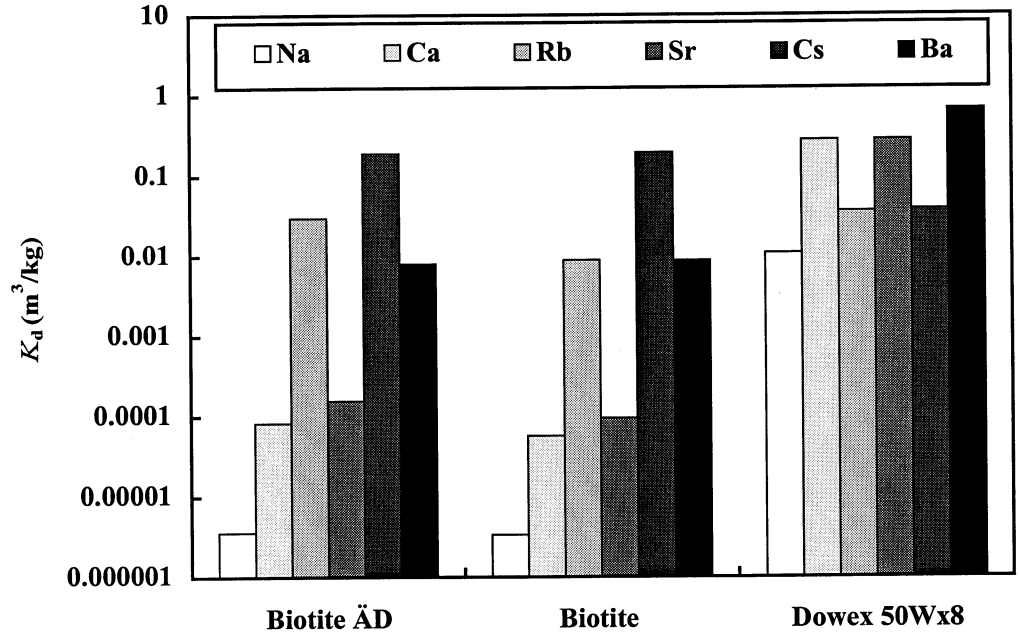

Figure 3-3 Sorption coefficients for the Biotite, compared to Dowex 50Wx8 cation exchanger, 9 days contact time. For the cation exchanger sorption Kd is used for all tracers. For the biotite sorption Kd is used for Cs, Rb and Ba, while $Kd_{(des1)}$ is presented for Na, Ca and Sr.

3.2.2.5 *Sorption Dependence on the Contact Time*

As can be seen in Figs 3-4 to 3-6, the sorption coefficients for Cs, Ba and Rb are steadily increasing with increasing contact time for the geological material. Alternative explanations can be presented for the observed behaviour:

1. Diffusion of the tracer. It is possible some cation exchange sites are located in the microfractures of the crushed geologic material and are thus not immediately available for the tracer in the solution. The number of available sorption sites will therefore increase with increasing contact time.

2. Degradation or weathering of the geologic material, creating more available sorption surfaces with increasing contact time.

3. Slow kinetics for the sorption. The cations used in this experiment are believed to sorb with a cation exchange mechanism, which generally is considered to be a fairly fast process. However, studies have shown that *e.g.* Cs^+ exchange in the layers of mica is a slow process (Cornell, 1993).

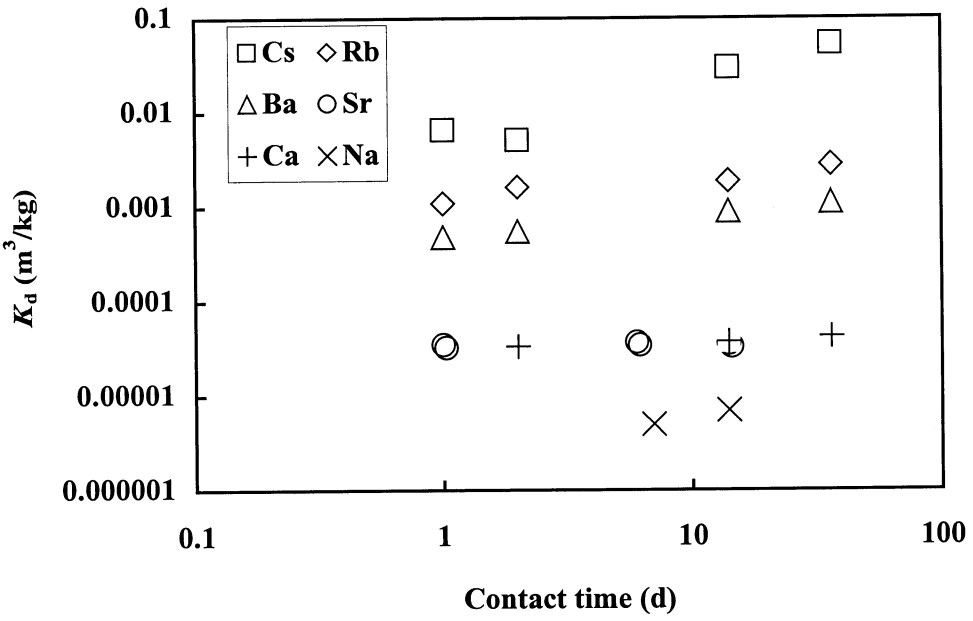

Figure 3-4 Sorption coefficients versus contact time for the 1-2 mm fraction of the Äspö diorite. Sorption K_d is presented for all tracers except for Ca where the $K_{d(des1)}$ is given.

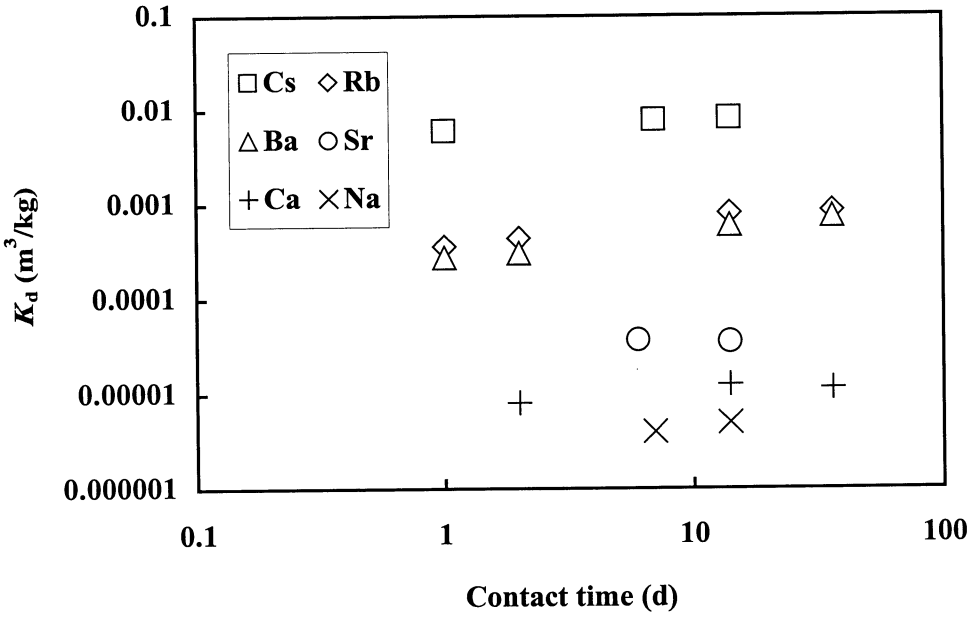

Figure 3-5 *Sorption coefficients versus contact time for the 1-2 mm fraction of the Fine-grained granite. Sorption K_d is presented for all tracers except for Ca where the $K_{d(des1)}$ is given.*

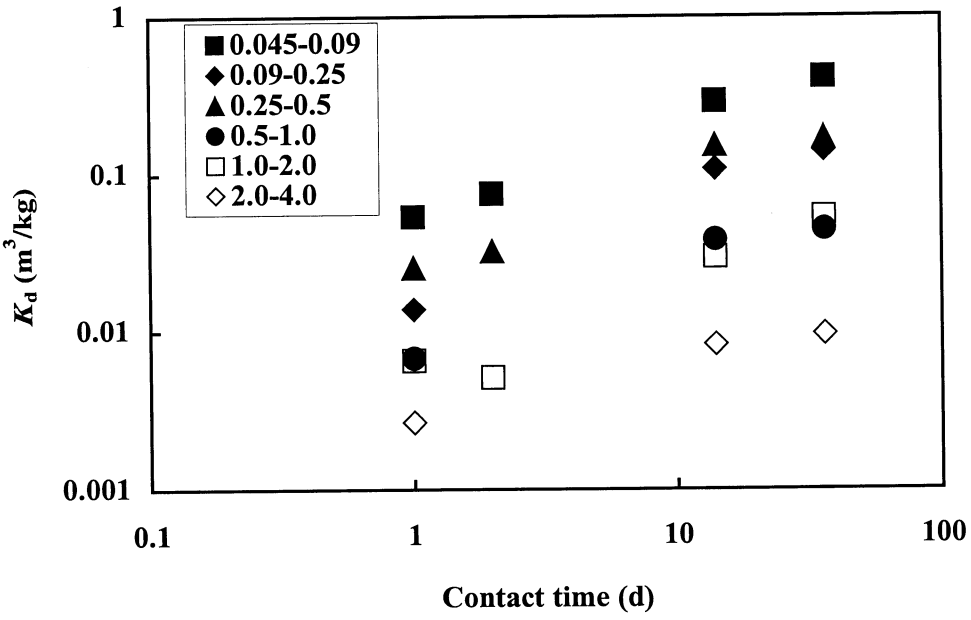

Figure 3-6 Sorption of Cs versus contact time for the different size fractions of the Äspö diorite.

It can be assumed that diffusion takes place in the boundary between the different mineral grains. Since the larger size fractions of the crushed rock consist of polymineralic grains, one would according to this assumption expect a time dependent sorption. The smaller size fractions are likely to consist of monomineralic grains and the numbers of inner surfaces would therefore be rather low. For the smaller size fractions, one should therefore expect a fast sorption equilibrium between the outer surfaces and the aqueous phase; *i.e.*, a very small increase of the sorption with increasing contact time should be observed. However, in fact the sorption seems to increase with increasing contact time more for the smaller size fractions than for the large size fractions. One explanation to this could be that the crushing of the rock material increases the availability of the small grains with high porosity. It can, however, be concluded that if diffusion is an important parameter, it takes place in the smaller size fractions as well as in the larger size fractions.

Degradation or weathering does not seem to be processes which solely can explain the time dependence in the sorption. For Cs sorption on the smallest size fraction of Äspö diorite, the sorption coefficient increases with 50% from 1 to 2 days of contact time. It does not seem likely that the degradation or weathering should make the total amount of available surfaces to increase with that high rate; especially not since the geological material was pre-equilibrated with the synthetic groundwater for 40 days before the addition of tracer was performed.

Since the samples were not continuously stirred, it may be possible that the time dependence of the sorption can be explained by slow diffusion in the water phase. However, this is contradicted by the results of the Dowex cation exchanger in the second series experiment, which was treated the same way as all the geological samples. No time dependence can be verified for the Dowex cation exchanger, although the sorption for all the cations is very high. Hence, no evidence can be presented that the water phase diffusion of the tracers has any major impact on the sorption rate.

3.2.2.6 *Sorption Dependence on the Particle Size*

The sorption results show increased sorption of the used cationic tracers when smaller size fractions of the solid phase are used. Smaller particles provide a larger contact area that probably results in a larger sorption capacity, at least in the short term perspective.

The crushing of the rock material causes that the more brittle minerals, *e.g.*, biotite, are enriched in the smaller size fractions. This is observed for the mineralogical composition of the Äspö diorite, Table 2-2. The biotite concentration differ from 17% (2-4 mm fraction) to 25% (0.045-0.090 mm fraction). However, the K_d (36 days contact time) for Cs^+ for these fractions are 0.01 m^3/kg and 0.4 m^3/kg, respectively, which shows that the differences in sorption between the size fractions are larger than what solely can be explained by the mineral enrichment.

One proposed assumption is that sorption on crushed geologic material may be interpreted as fast equilibrium with an outer surface of the crushed grains and slower diffusion-controlled sorption on the inner surfaces. The distribution coefficient, K_d, could thus be divided into two parts; an inner $K_{d,i}$ and an outer K_a. Assuming that the geologic material can be characterised as spherical particles, the K_d can be expressed as

$$K_d = K_{d,i} + K_a \cdot \frac{6}{\rho \cdot < d_p >} \qquad 3\text{-}17$$

where:

ρ = Density of the solid phase (kg/m^3)
$<d_p>$ = Average particle diameter of the solid phase (m)

Plots of K_d versus the inverse of the particle diameter have been constructed for the most weakly sorbing cation tracers, *i.e.*, Na^+, $Sr^{2+}$and Ca^{2+} (Fig 3-7 and Table 3-11). $K_{d,i}$ and K_a were fitted to the sorption results of the different size fractions. The mineralogical composition of the two smallest size fractions of Äspö diorite deviates considerably from the average composition (Table 2-1). It is also observed that strong deviations from the outer/inner surface sorption model occur for those fractions. For the fitting of the sorption results of Äspö diorite, only the four largest size fractions have therefore been used.

For Na^+, $Sr^{2+}$and Ca^{2+} no pronounced increase of the sorption with contact time is observed and it is indicated that an outer/inner surface model can explain the results obtained for those tracers

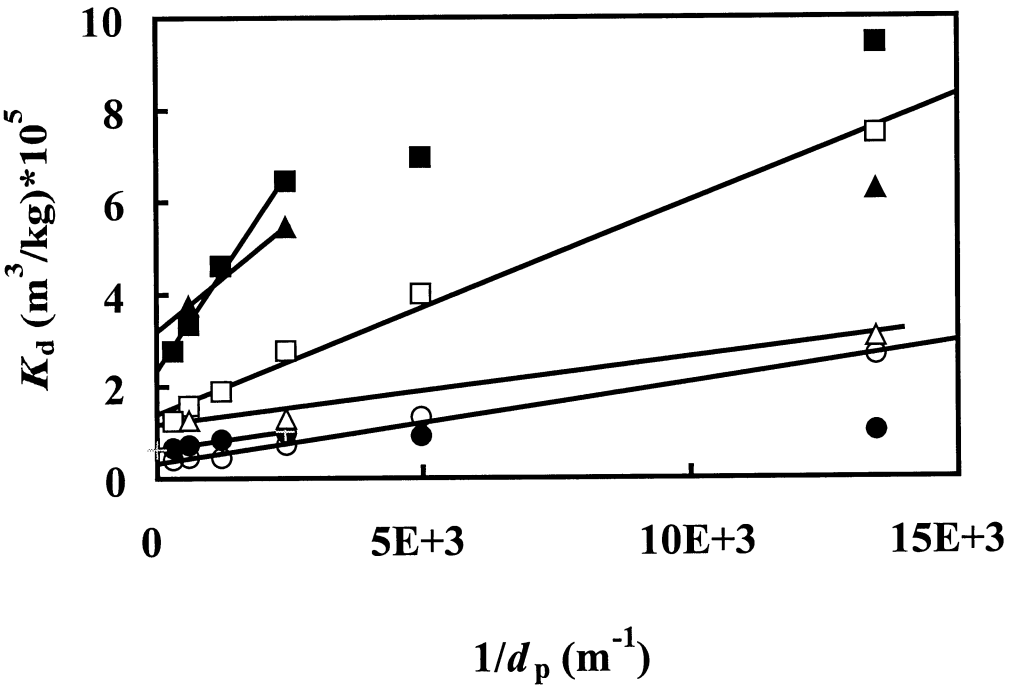

Figure 3-7 Desorption $K_{d(des1)}$ for Na^+ (● Äspö diorite, ○ Fine-grained granite), Ca^{2+} (▲ Äspö diorite, Δ Fine-grained granite and Sr^{2+} (■ Äspö diorite, □ Fine-grained granite) versus the inverse of the mean particle diameter. The lines are the fit of eq. (3.19) to the size fractions. For Äspö diorite only the 4 largest size fractions have been used. For sorption of Ca^{2+} on Äspö diorite only two fractions are used and the line is therefore not a fitting but a straight line between the two data points.

Table 3-11 Extrapolated $K_{d,i}$ and K_a for Na^+, Ca^{2+} and Sr^{2+}.

Tracer	Rock Type	$K_{d,i}$ (m^3/kg)	K_a (m)
Na^+	ÄD	$6.3 \cdot 10^{-6}$	$6.9 \cdot 10^{-7}$
	FGG	$3.3 \cdot 10^{-6}$	$7.9 \cdot 10^{-7}$
Ca^{2+}	ÄD	$3.2 \cdot 10^{-5}$	$4.3 \cdot 10^{-6}$
	FGG	$1.2 \cdot 10^{-5}$	$6.7 \cdot 10^{-7}$
Sr^{2+}	ÄD	$2.8 \cdot 10^{-5}$	$7.8 \cdot 10^{-6}$
	FGG	$1.1 \cdot 10^{-5}$	$3.0 \cdot 10^{-6}$

For a more strongly sorbing species, the diffusion should have a very low impact of the sorption, *i.e.*, the tracer should sorb only on the absolute outer surface of the crushed material. According to this assumption, the $K_{d,i}$ could therefore be neglected and one would expect to obtain outer-surface dependent sorption behaviour. Plots of the K_d versus the inverse of the average particle diameter would according to this model give a straight line with the intercept at zero and no change in the slope with the contact time. However, plots for the sorption of Cs (Figs. 3-8 to 3-9) do not confirm such behaviour. For the Fine-grained granite, an intercept significantly over zero is observed and no straight line dependence is observed for the Äspö diorite.

The assumption of a spherical shape of the grains of the crushed geologic material is certainly an oversimplification. An alternative way of measuring surfaces is the BET technique (Brunauer, 1938) which makes use of gas (in this case Kr) sorption in order to obtain a measure of the surface area. It is likely to assume that the obtained BET surface corresponds to the total surface, *i.e.*, the sum of the inner and outer surfaces. A difference between the BET surface and the geometric surface can, according to the proposed inner and outer surface model, be caused mainly by two phenomena:

1. Existence of an inner surface, accessed only by diffusion.
2. An uneven outer surface deviating from an ideal smooth spherical form.

Measurements have been performed on the crushed Fine-grained granite and Äspö diorite used in these investigations. The dependence of BET surface area on the particle diameter is shown in Fig. 3-10. In the case of a clear distinction between outer surfaces and inner surfaces of the crushed material, one would expect a straight line dependence of the BET surface versus the geometric surface. The intercept should then give the inner surface of the material. However, no clear straight line behaviour can be observed, which slightly contradicts such a model. Anyway, the graph clearly indicates that for the smaller size fractions, the inner surfaces are very small compared to the outer surfaces. This makes it difficult to use a diffusion model to explain the observed increase in the K_d with contact time.

Plotting the sorption coefficients for Cs on Fine-grained granite versus the BET surface (Fig. 3-11) indicates a linear relationship. The corresponding plot for the Äspö diorite is more complex (Fig. 3-12). A possible explanation to this is that crushing and sieving of the heterogeneous and large grained Äspö diorite have caused some mineral separation. No such behaviour is to be expected for the Fine-grained granite which is relatively homogeneous. The results of the mineralogical characterisation of the different size fractions of the generic geologic material (Table 2-5) support this conclusion.

Comparing the graphs of the K_d of Cs^+ versus the BET-surface (Figs. 3-11 and 3-12) with the corresponding graphs using a spherical geometrical surface (Figs 3-8 and 3-9), it is indicated that a better correlation is obtained in the former case. Even when a longer contact time is used, straight line behaviour with an intercept of ~0 is observed. This observation alone indicates that the total surface of the crushed material is outer surfaces, *i.e.*, directly accessed for sorption. The explanation for the time dependent sorption would then be kinetically hindered sorption reactions instead of diffusion.

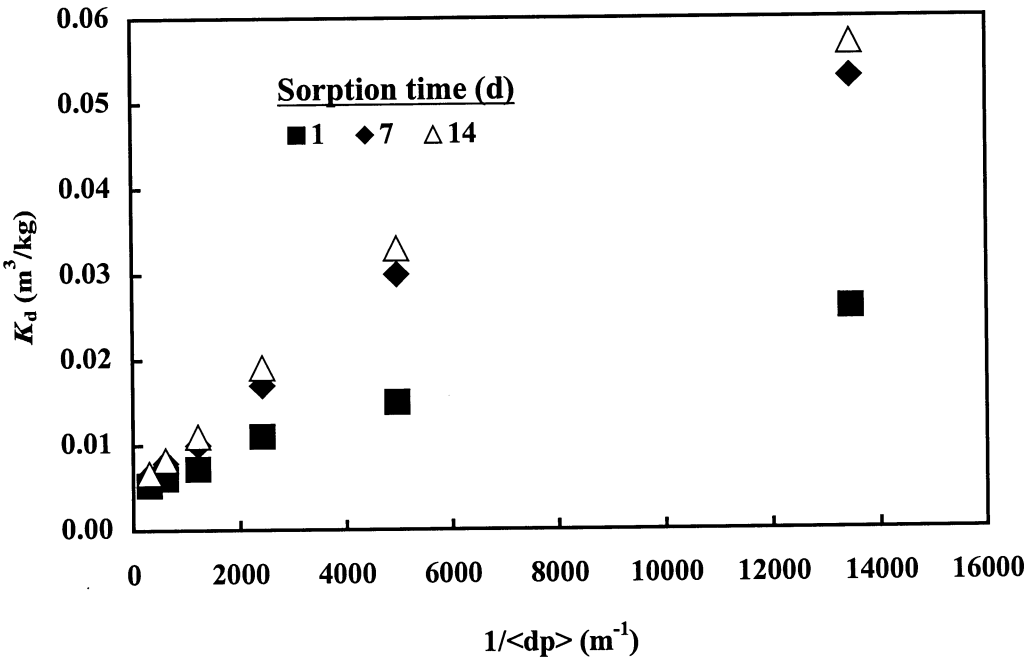

Figure 3-8 Sorption coefficients, K_d for Cs^+ on Fine-grained granite versus the inverse of the average particle size of the different size fractions.

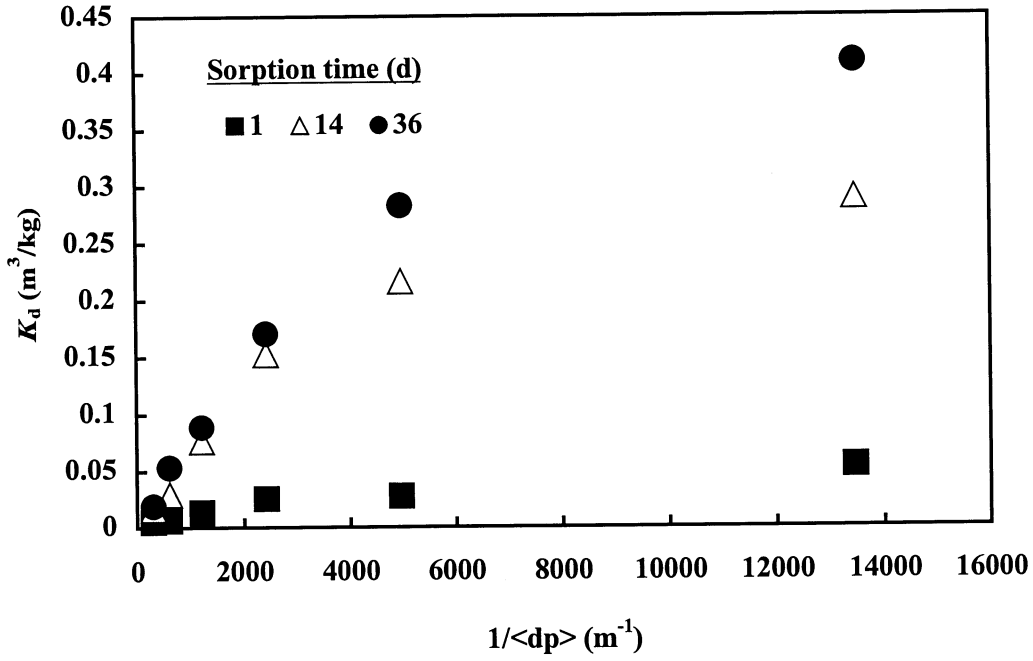

Figure 3-9 Sorption coefficients, K_d for Cs^+ on Äspö diorite versus the inverse of the average particle size of the different size fractions.

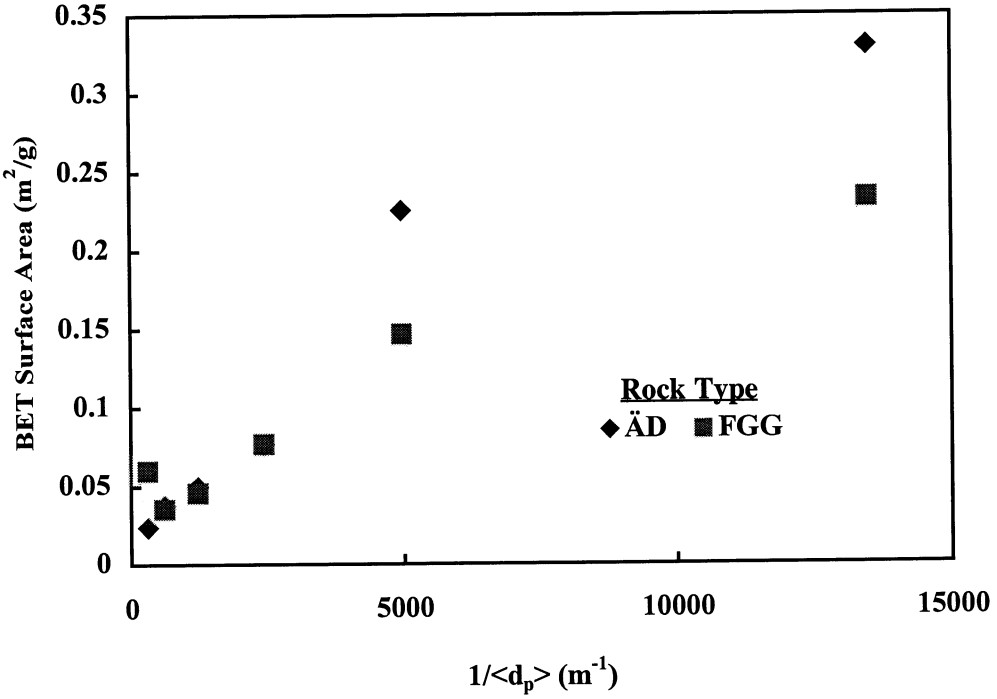

Figure 3-10 BET surface versus the inverse of the average particle size of the Äspö diorite and the Fine-grained granite.

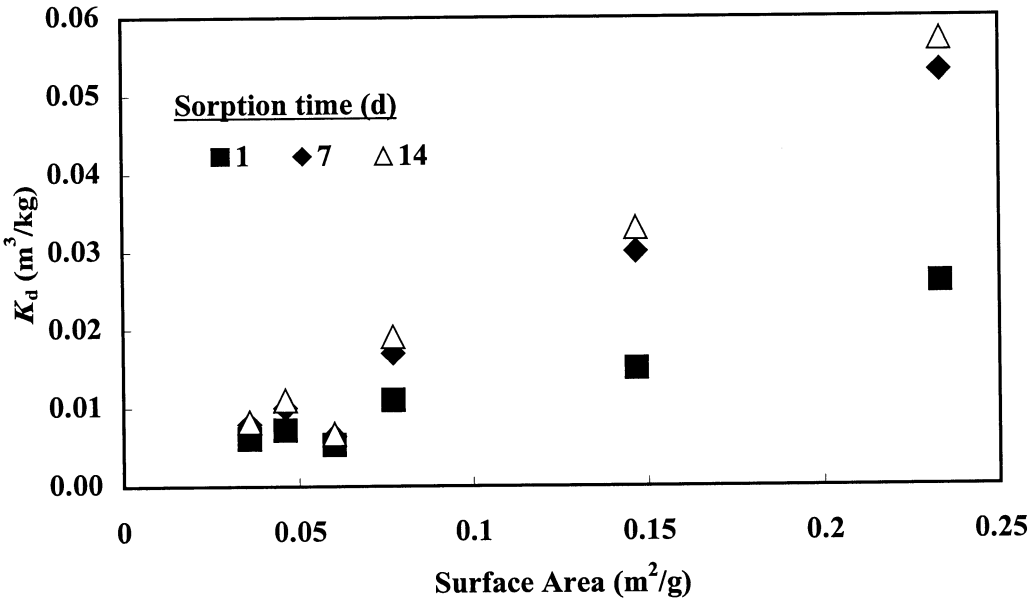

Figure 3-11 *Sorption coefficients for Cs versus the BET surface area for Fine-grained granite.*

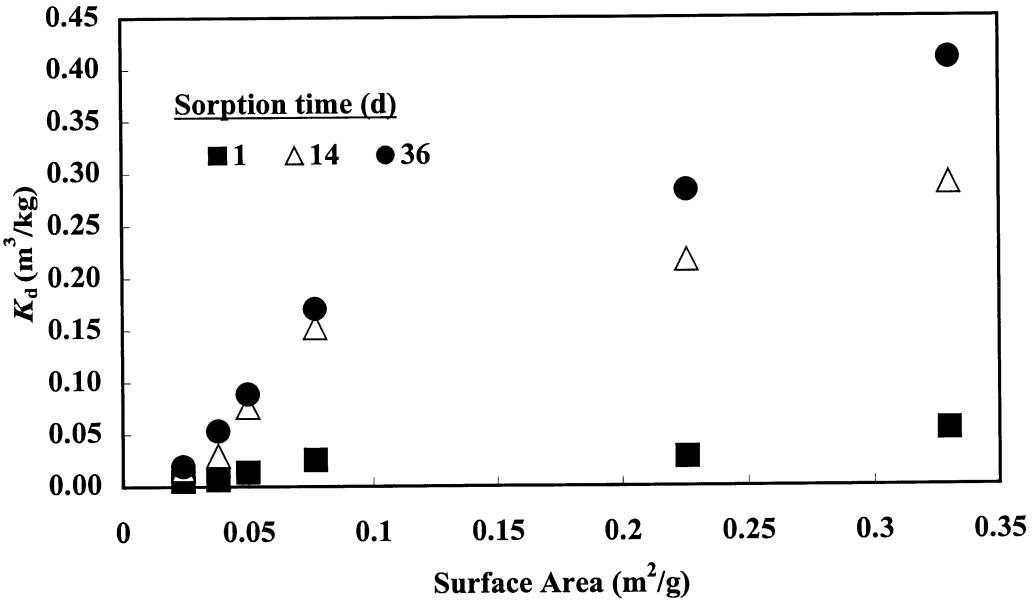

Figure 3-12 *Sorption coefficients for Cs versus the BET surface area for Äspö diorite.*

3.2.2.7 *Desorption and Reversibility in the Sorption*

Comparison of the sorption coefficients and the desorption coefficients (Tables 3-8 to 3-10) gives an indication of the reversibility of the sorption in the short term scale. For the tracers that sorb very weakly, *i.e.*, Na, Sr and Ca, no non-reversibility can be verified. However, the low sorption of these tracers makes it difficult to detect any non- or slowly reversible sorption at all.

For the stronger sorbing cationic tracers, *i.e.*, Rb, Ba and Cs, observations of non- or slowly reversible sorption are obvious. One can also see that in some cases, the desorption decreases with increasing desorption time. This effect is more pronounced for the strongly sorbing Cs than for the other cations. Furthermore, the effect is observed to be stronger for the Äspö diorite than for the Fine-grained granite and also more pronounced for the smaller fraction size than for the larger fractions. A general conclusion is that stronger sorption leads to higher part of apparent non-desorbable part of the sorbed tracer.

There are a number of possible explanations for the observed sorption/desorption behaviour. It is possible that a continuous diffusion of the tracers in to the microscopic fractures of the solid material is taking place. In this case, there would be a concentration gradient towards the centre of the grains, which can explain the observed re-uptake of desorbed tracer during the desorption step. However, this can not explain the observed differences between the size fractions of the geologic materials. One would instead expect a larger part of non-desorbable tracer in the larger size fractions, since these consist of several mineral grains with lots of diffusion pockets between them. The smaller size fractions are believed to a larger degree consist of monomineralic grains. The sorption on the smaller particles would therefore, according to this explanation, occur only on the outer surfaces. No diffusion would therefore be necessary for the desorption of the tracers sorbed on the smaller size fractions. Contrary to the observed result, one would therefore expect a lower amount of non- or slowly reversible sorption in the smaller size fractions compared to the larger size fractions. In line with the conclusions made for the time dependence of the sorption (see section 3.2.2.5), it must be concluded that if diffusion is occurring, it takes place both in the larger and the smaller size fractions.

An alternative explanation is that the crushing process opens up more pores and microfractures in the solid material. If that is the case, the porosity and the diffusivity can be higher in the smaller fractions than in the larger fractions, which could explain differences observed for the desorption behaviour of the different size fraction of the rock material. Such an explanation would indicate that the crushed material in general and the smaller sizes in particular are not representative for the characteristics of the *in situ* rock material.

It is also likely that the crushing and sieving of the geologic material, cause enrichment of more easily crushed minerals (*e.g.* biotite) in the smaller size fractions. This can be observed in Table 2-2 where it is seen that for Äspö diorite, the biotite concentration increases with decreasing fraction size of the material. It has been found that the desorption of Cs and other strongly electropositive cations from mica are kinetically hindered due to the "trap" that the cations are in when they sorb in the layers of *e.g.*

biotite (Cornell 1993). However, the increase in the biotite content as one move from the largest to the smallest size fraction is only a factor 1.5. The observed differences in sorption and/or effect of non- or slowly reversible sorption is far more pronounced than that.

3.2.2.8 *Cation Exchange Sorption Model*

The concentrations in the solid phases of all the different cations involved in this study have been calculated using eq. (3.15). Estimations of the CEC and the selectivity coefficients have been performed and the results are given in Table 3-12 for the generic material and in Table 3-13 for the material used in the Feature A site specific material. The values are given using the following assumptions and restrictions:

1. The CEC is assumed to consist only of the cations involved in this study, *i.e.*, Na^+, Ca^{2+}, Rb^+, Sr^{2+}, Cs^+ and Ba^{2+}. Cations present in the synthetic groundwater for which no estimation of the sorption and desorption has been performed (*e.g.* Mg^{2+}, K^+, Li^+ and H^+) are thus not involved in the cation exchange capacity calculations. A similar investigation (Byegård *et al.* 1993) performed using Finnsjön granodiorite and a high saline groundwater indicated that Mg^{2+} and K^+ occupied approximately 10 and 5 %, respectively, of the cation exchange capacity. It was also indicated that a small desorption could occur during the rinsing between sorption and desorption experiment.

2. In these investigations, the solid phases were equilibrated with the synthetic groundwater for up to 5 months before addition of the tracers were conducted. It is therefore assumed that no change of the water phase composition occurred during the experiment, *i.e.*, cation exchange sorption caused desorption of the same composition as the tracers that were sorbed.

3. Due to the non- or slowly reversible sorption, the obtained sorption and desorption coefficients were not the same. In the cation exchange model calculation, only the fast reversible part of the sorption has been included. In the calculations the $K_{d(des2)}$ desorption coefficients were used if available. However, for the tracers where a decrease of the concentration of the radioactive tracer in the water phase in the sorption experiment could not be statistically verified, $K_{d(des1)}$ was used instead.

4. The values are given for the longest desorption time applied for each sample.

The investigation of the generic material shows that the CEC is higher for Äspö diorite than for Fine-grained granite, probably because of the presence of much higher biotite concentration in Äspö diorite. Generally, the smaller size fractions have higher CEC than the larger size fractions. It is also indicated that CEC is slightly increased with increasing contact time, indicating that some cation exchange sites are only available through diffusion. The results based on the 1-2 mm fraction used in experiments with somewhat different water compositions gives similar CEC, indicating that the cation exchange model is valid for the present cations.

The investigations of the Feature A site specific materials (mylonites and granites) indicate that the alteration has significantly decreased the CEC. However, the KXTT2 samples which originate from Äspö diorite has higher CEC than the KXTT4 samples which originate from Fine-grained granite. It can therefore be concluded that the CEC depends strongly on the concentration of biotite and that alteration to chlorite decreases the CEC. This is also supported by the investigation of magnetically separated biotite from Äspö diorite that has significantly higher CEC than the other materials present in this investigation. A chlorite sample included in the investigation of Finnsjön conditions (Byegård *et al.* 1993) gave the CEC of 9.3 μeq/g (0.1-0.063 mm size fraction).

Table 3-12 Apparent cation exchange capacities and selectivity coefficients (cf. Section 3.2.2.7) obtained in the generic rock material experiments.

Rock Material	Size fraction (mm)	Sorp. time (d)	CEC (μeq/g)	Selectivity Coefficients				
				Na^+	Rb^+	Sr^{2+}	Cs^+	Ba^{2+}
ÄD	0.045-0.09	1-2	7.6±0.4	0.04±0.03	$9\pm1\cdot10^3$	1±0.6	$5\pm0.6\cdot10^5$	30±2
		14	9.1±0.6	0.1±0.05	$8\pm0.4\cdot10^3$	2±0.4	$9\pm0.2\cdot10^7$	60±2
	0.25-0.5	1-2	6.2±0.2	0.02±0.01	$5\pm0.3\cdot10^3$	1±1	$3\pm0.4\cdot10^5$	20±0.3
		14	8.1±0.6	0.1±0.06	$4\pm0.2\cdot10^3$	2±1	$3\pm0.07\cdot10^7$	30±1
	1-2	1-2	4.5±0.1	0.01±0.007	$1\pm0.3\cdot10^3$	0.6±0.3	$4\pm1\cdot10^4$	10±3
		14	5.5±0.6	0.1±0.08	$7\pm3\cdot10^2$	2±0.5	$1\pm0.4\cdot10^6$	20±1
FGG	0.045-0.09	1-2	5.1±1.0	0.5±0.3	$4\pm1\cdot10^3$	3±0.6	$5\pm0.7\cdot10^5$	50±7
		14	6.8±1.0	2±1	$2\pm0.1\cdot10^3$	4±1	$9\pm0.6\cdot10^6$	60±4
	0.25-0.5	1-2	1.6±0.1	0.2±0.1	$6\pm1\cdot10^3$	4±2	$5\pm0.3\cdot10^5$	50±9
		14	3.1±0.6	2±1	$8\pm1\cdot10^2$	5±4	$3\pm0.5\cdot10^6$	40±9
	1-2	1-2	1.2±0.1	0.08±0.04	$3\pm1\cdot10^3$	3±2	$1\pm0.05\cdot10^5$	30±4
		14	2.1±0.3	0.5±0.2	$3\pm1\cdot10^2$	2±0.6	$3\pm0.3\cdot10^5$	20±3

Table 3-13 Apparent cation exchange capacities and selectivity coefficients in relation to Ca^{2+} obtained for the Feature A site-specific rock material experiments (cf. Section 3.2.2.7).

Rock Material	CEC (μeq/g)	Selectivity Coefficients				
		Na^+	Rb^+	Sr^{2+}	Cs^+	Ba^{2+}
Mylonite KXTT2	2.2±0.5	0.4±0.1	$5\pm1\cdot10^4$	2±0.5	$8\pm2\cdot10^4$	30±6
Mylonite KXTT4	1.3±0.5	0.2±0.1	$4\pm1\cdot10^2$	2±0.6	$6\pm2\cdot10^3$	14±7
Altered ÄD KXTT2	2.2±0.6	0.1±0.02	$2\pm1\cdot10^3$	1±0.4	$2\pm0.4\cdot10^5$	30±9
Altered ÄD KXTT3	<2.4					
Altered FGG KXTT4	<1.1					
ÄD	4.2±0.9	0.03±0.01	$1\pm0.4\cdot10^3$	2±0.4	$8\pm2\cdot10^4$	20±4
FGG	<0.8					
Biotite, sep. ÄD	14±3	0.01±0.003	$8\pm2\cdot10^4$	2±0.4	$1\pm0.2\cdot10^6$	20±5
Biotite flakes 1-5 mm	9±1	0.03±0.01	$5\pm1\cdot10^3$	2±0.3	$3\pm0.4\cdot10^6$	60±10
Dowex 50Wx8	$1.7\pm3\cdot10^4$	0.01±0.002	0.2±0.03	0.5±0.1	0.2±0.03	2±0.4

3.2.3 Behaviour of the Tracers during the Rinsing Process

During the rinsing process, the ionic strength of the aqueous phase is decreased, approximately one order of magnitude for each rinsing step. In the case of no additional sorption or desorption occurring during the rinsing, the amount of tracers in the water phase should decrease with the same rate. Such behaviour would prove cationic exchange behaviour of the tracers, *i.e.* an addition of other cations is necessary in order for the sorbed cations to desorb. On the other hand, a pronounced desorption of the cations during the rinsing process could indicate that the major sorption mechanism is not cation exchange. Alternative mechanisms for the decrease of the concentrations of the tracers in the water phase are:

1. Precipitation. The alkaline earth metals, Ca, Sr and Ba, are likely to be close to saturation with respect to their carbonates, fluorides and sulphates, respectively. During the rinsing, the concentrations of the mentioned anions decrease and the saturation of the alkaline earth metals complexes decrease. Any precipitate formed during the contact of the solid phase to the original high saline groundwater should thus dissolve during the rinsing process.

2. A distribution equilibrium independent of the water phase composition, analogous to *e.g.* distribution of an extractable tracer between an organic and an aqueous liquid phase. In such a case, the ratio of concentration of the tracer between the phases is always constant and independent of the water phase composition. By doing repeated changes of the water phase, one would in such a case desorb the tracer from the solid phase.

The results of the rinsing, Fig. 3-13 and 3-14 and Table 3-14, show that a slight desorption is occurring during the rinsing process. One simple explanation to this could be that microscopic particles are physically detached from the surfaces of the solid phase and these particles can not be centrifuged to the bottom of the test tubes. Such an explanation would demand that the proportion of the sorbed tracer which is desorbed, would be the same for all the different cationic tracers. However, it is observed that the percentages vary between the different tracers; *e.g.* the most strongly sorbed tracer Cs is less desorbed than the weaker sorbed Rb, which contradicts this explanation.

The explanation of a formed solid phase being dissolved during the rinsing process, is contradicted by the observation of desorption of Cs and Rb. These cations are known not to form any insoluble precipitates at all. The proposed mechanism can not explain their behaviour. Furthermore, since the desorption is increased >2 orders of magnitude when the distilled water is replaced by saline synthetic groundwater, it is obvious that the cation exchange sorption mechanism plays an important role in the sorption characteristics. It is therefore excluded that the sorption for the most part is controlled by a simple phase distribution equilibrium with no cation exchange mechanism involved.

An explanation to the observed desorption during the decrease of the ionic strength has been proposed by Byegård *et al.* (1995). It is proposed that exchange of the sorbed cations occurs due to exchange with the H^+ ions in the solution. During the decrease of the ionic strength, the H^+-concentration will remain relatively constant (neutral pH, $[H^+]$

$= \sim 10^{-7}$ M). Since the concentrations of the other cations decrease during the rinsing, the selectivity coefficient relation (eq. 3.16) yields that the part of the cation exchange capacity occupied by protons will increase with lowered ionic strength.

Table 3-14 The amounts of the sorbed tracers which was desorbed during the rinsing. Negative value (found for Ca and Ba) means that the concentrations found in the rinsing solution was lower than expected from the dilution, indicating a increasing sorption during the rinsing process

Tracer	Size fraction (mm)	Percent of sorbed which was desorbed during the rinsing
Ca	1-2	-5
Rb	1-2	8
Ba	1-2	-4
Cs	1-2	0.9
Cs	0.25-0.5	0.2
Cs	0.045-0.09	0.6

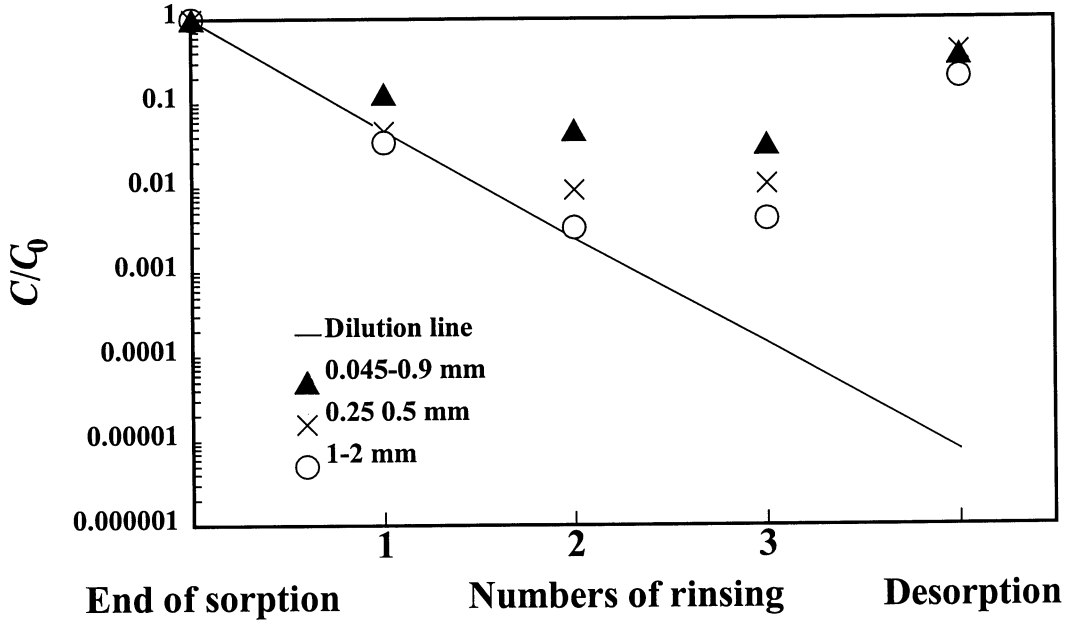

Figure 3-13 Behaviour of Cs during the rinsing process (see text for details) on the different size fractions of Äspö diorite. The dilution line represents the concentration expected from the hypothesis of no desorption during the rinsing process.

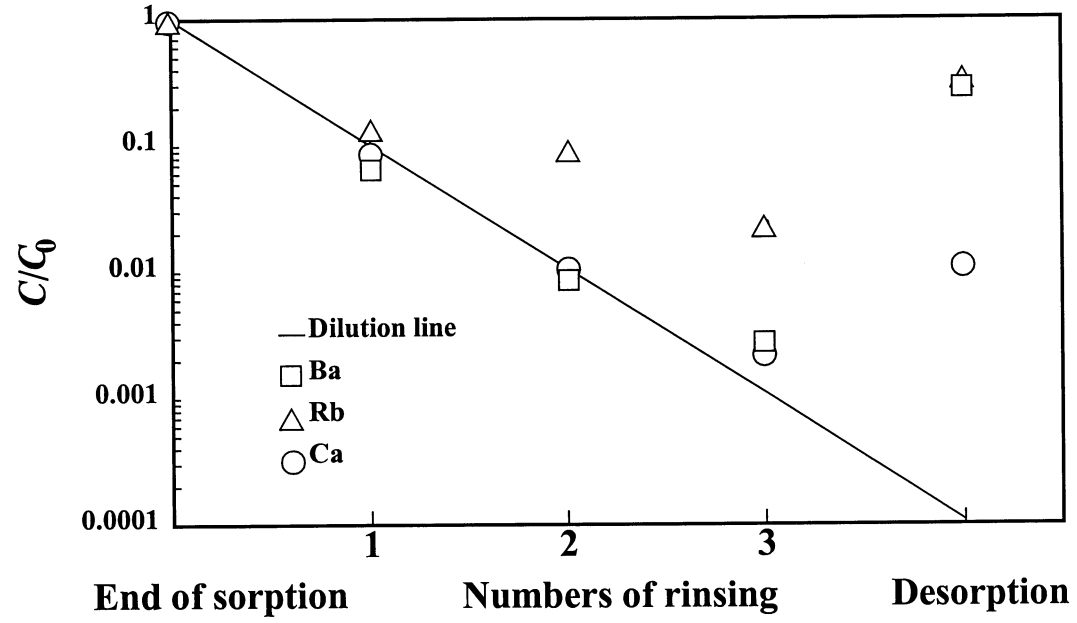

Figure 3-14 Behaviour of Ba, Rb and Ca during the rinsing process (see text for details) on the 1-2 mm size fractions of Äspö diorite. The dilution line represents the concentration expected from the hypothesis of no desorption during the rinsing process.

3.2.4 Modelling

3.2.4.1 First Order Kinetics Model

An attempt has been made to model the sorption of Cs using first order kinetics. Generally, when introducing a radioactive tracer cation to a mixture of groundwater and rock material, the equilibrium conditions can be written as

$$[M]_{aq} \underset{k_{-1}}{\overset{k_1}{\rightleftarrows}} [M]_s \qquad 3\text{-}18$$

where

$[M]_{aq}$ = Concentration of the tracer in the aqueous phase (mole·m^{-3})
$[M]_s$ = Concentration of the tracer in the solid phase (mole·kg^{-1})
k_1 = Rate constant for the sorption reaction (s^{-1})
k_{-1} = Rate constant for the desorption reaction (kg·m^{-3}·s^{-1})

The rate expression for the sorption is given as

$$\frac{d[M]_{aq}}{dt} = -k_1 \cdot [M]_{aq} + k_{-1} \cdot [M]_s \qquad 3\text{-}19$$

In the case of equilibrium, no change of the concentration occurs, *i.e.*,:

$$\frac{d[M]_{aq}}{dt} = -k_1 \cdot [M]_{aq} + k_{-1} \cdot [M]_s = 0 \qquad 3\text{-}20$$

Rearranging 3-20 yields

$$\frac{k_1}{k_{-1}} = \frac{[M]_s}{[M]_{aq}} = K_d \qquad 3\text{-}21$$

where

K_d = Distribution coefficient, see eq.3-2, (m^3·kg^{-1})

The total concentration of tracer in the system is constant, *i.e.*,

$$[M]_{aq} = [M]_{tot} - [M]_s \cdot \frac{m}{V} \qquad 3\text{-}22$$

where:

$[M]_{tot}$ = Total concentration of the tracer, defined for the aqueous phase (mole·m^{-3})
m = Mass of the solid phase (kg)

V = Volume of the aqueous phase (m^3)

The analytical solution to equation 3-19, using the boundary condition 3-22, is (Weast *et al.* 1966)

$$[M]_{aq,t} = \frac{\exp\left((t-t_0)\cdot\left(-k_1-k_{-1}\cdot\frac{V}{m}\right)\right)\cdot\left(k_{-1}\cdot[M]_{tot}\cdot\frac{V}{m}+[M]_{aq,0}\cdot\left(-k_1-k_{-1}\cdot\frac{V}{m}\right)\right)}{\left(-k_1-k_{-1}\cdot\frac{V}{m}\right)}+$$

$$+\frac{\left(-k_{-1}\cdot[M]_{tot}\cdot\frac{V}{m}\right)}{\left(-k_1-k_{-1}\cdot\frac{V}{m}\right)} \qquad 3-23$$

where:

$[M]_{aq,t}$ = Concentration of the tracer in the aqueous phase at time t (mole·m^{-3})
$[M]_{aq,0}$ = Concentration of the tracer in the aqueous phase at the starting time t_0 (mole·m^{-3})

Calculation has been performed using the results of the sorption and desorption of Cs^+ on the smallest (0.045-0.090 mm) fraction of the Äspö diorite. The smallest fraction was chosen since this fraction was most likely to consist of monomineralic grains. Therefore, time dependent loss of the tracer from the aqueous phase caused by diffusion in the mineral grain boundary should not be significant and chemical kinetics should be the major time dependent sorption process.

Calculation was first performed in order only to fit equation 3-18 to the experimentally obtained sorption curve, *i.e.*, not including the corresponding desorption results. In this case $[M]_{aq,0} = [M]_{tot}$ and $[M]_{tot}$ equals the total added concentration of tracer. The t_0 corresponds to the time when the tracer injection was performed. In a second series of calculations, fitting of the results of the desorption curves was included in the calculations. For the desorption calculations $[M]_{aq,0} = 0$ and $[M]_{tot}$ equals the concentration of tracer remaining in the system at the time t_0, *i.e.*, the time where the change to non-spiked water phase occurred in the experiment. The calculation was performed using AMOEBA (Press *et al.* 1986) as the fitting routine and equation 3-18 was fitted to the experimentally obtained sorption data by changing the k_1 and k_{-1} constants according to the least square differences.

The results of the calculations are shown in Figure 3-15 and Table 3-15. Using only the sorption data, a reasonable fit of the results can be obtained. However, the time dependence in both the sorption and desorption observed in the experimental data can not be fitted by the model. The conclusion must be that first order kinetics can not solely explain the time dependence observed in the sorption of Cs^+.

It is possible that the time dependence in the sorption could be explained by introducing more complex kinetics, *e.g.*, second order kinetics. However, in the case of tracers of

low concentration in the groundwater it is shown from the cation exchange characteristics that these cations occupy a very low number of the cation exchange sites. Second order kinetics caused by sorption dependent decrease of both the tracer concentration and the available sorption sites seem therefore not likely. However, one possibility is that the different minerals have cation exchange sites with different selectivity for different cations. It is also possible that the kinetics of the cation exchange is different for different materials. However, modelling addressing such heterogeneity in the solid material is considered beyond the scope of this study.

Table 3-15 Rate constants obtained from the fitting of the sorption and desorption results for Cs on the 0.045-0.090 mm size fraction of the Äspö diorite to a first order kinetics model

Results used in fitting	k_1 (s^{-1})	k_{-1} ($kg \cdot m^{-3} \cdot s^{-1}$)	K_d ($m^3 \cdot kg^{-1}$) ($=k_1/k_{-1}$)
Sorption	$2.2 \cdot 10^{-5}$	$6.2 \cdot 10^{-5}$	0.35
Sorption + Desorption	$4.3 \cdot 10^{-4}$	$1.5 \cdot 10^{-3}$	0.28

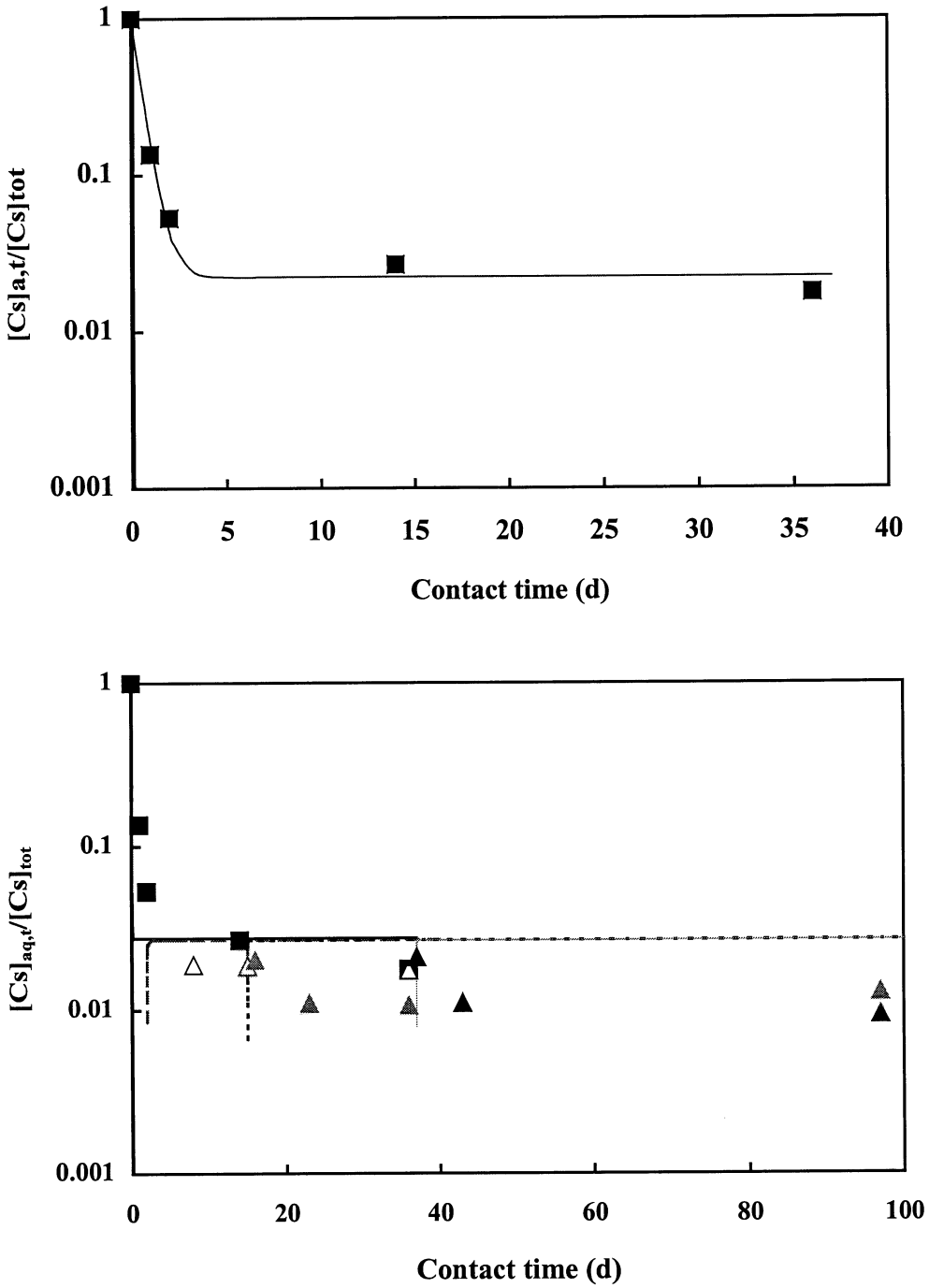

Figure 3-15 Experimental results and results of first order kinetics calculations of Cs sorption on the 0.045-0.090 mm size fraction of Äspö diorite. The experimentally obtained values are given with symbols and the sorption and desorption curves calculated from a first order kinetics is given with the solid and dashed lines. The upper graph represents the results of the fitting using only the sorption results, while the lower graph represents fitting using both the desorption and sorption results. The squares represents the sorption results and the white, grey and black triangles represents the desorption results obtained after a contact time of 2, 17 and 37 days, respectively.

3.2.4.2 *Homogeneous Diffusion-Sorption Model*

An attempt has been made to model the sorption of Cs using a homogeneous diffusion-sorption model. In this case the diffusion into the pores in the particles of the solid phase results in a time dependence of the uptake of tracer from the solution. All loss of the tracer in the aqueous phase is therefore dependent on the diffusion in the solid phase, *i.e.*, no surface sorption in the boundary of the solid and aqueous phase is considered. The sorption is assumed to be linear, and is represented by a single K_d value. If the crushed particles are considered as porous bodies of spherical shape, an analytical solution to the diffusion equation (Crank 1975) was suggested by Skagius *et al.* (1982) for the determination of D_a and K_d:

$$\frac{M_s}{M_{s,\infty}} = 1 - \sum_{n=1}^{\infty} \frac{6\alpha(\alpha+1)\cdot\exp(-D_a\cdot q_n^2\cdot t/r^2)}{9+9\alpha+q_n^2\alpha^2} \qquad 3\text{-}24$$

where:

M_s = Total amount of solute in sphere after time t
$M_{s,\infty}$ = Total amount of solute in sphere after infinite time
r = Radius of sphere

and the q_n values are the non-zero roots of:

$$\tan q_n = \frac{3q_n}{3+\alpha q_n^2} \qquad 3\text{-}25$$

and:

$$\alpha = \frac{V}{m\cdot K_d} \qquad 3\text{-}26$$

where:

V = Volume of the spiked solution
m = Mass of the solid phase.

The concentration, C, in the solution after time t is given by a mass balance

$$\frac{C}{C_0} = 1 - \frac{M_s}{M_{s,\infty}}\left(\frac{m\cdot K_d/V}{1+m\cdot K_d/V}\right) \qquad 3\text{-}27$$

D_a and K_d for Cs sorption on Fine-grained granite and Äspö diorite were evaluated by curve fitting to the experimental data minimising the error sum of squares. D_e was calculated from:

$$D_e = D_a(\varepsilon + K_d\cdot\rho) \qquad 3\text{-}28$$

For Cs, the sorption is so strong that the porosity (ε) can be neglected compared to the $K_d \cdot \rho$ term. Since this analytical solution can not address desorption, only the sorption part of the experiment has been calculated.

An example of the fits to the data is presented in Fig.3-16 and the evaluated parameters for all data are presented in Table 3-16. The evaluated sorption coefficients agree well with the data presented in Tables 3-5 and 3-6. A wide range, 2-3 decades, in the calculated effective diffusion coefficients are observed. The diffusivity increases with increasing particle sizes. Most likely, the low diffusivities in the small particle sizes are a result of diffusion into particular grains (intra-particle diffusion), while the diffusion in the larger grains is taking part in intra-granular pores, since the larger grains are polymineralic. Also, all particle sizes are subject to mechanical stress during crushing which may give an increased porosity and therefore an increase in the level of the diffusivities compared to *e.g.* the observed diffusivities in through diffusion measurements.

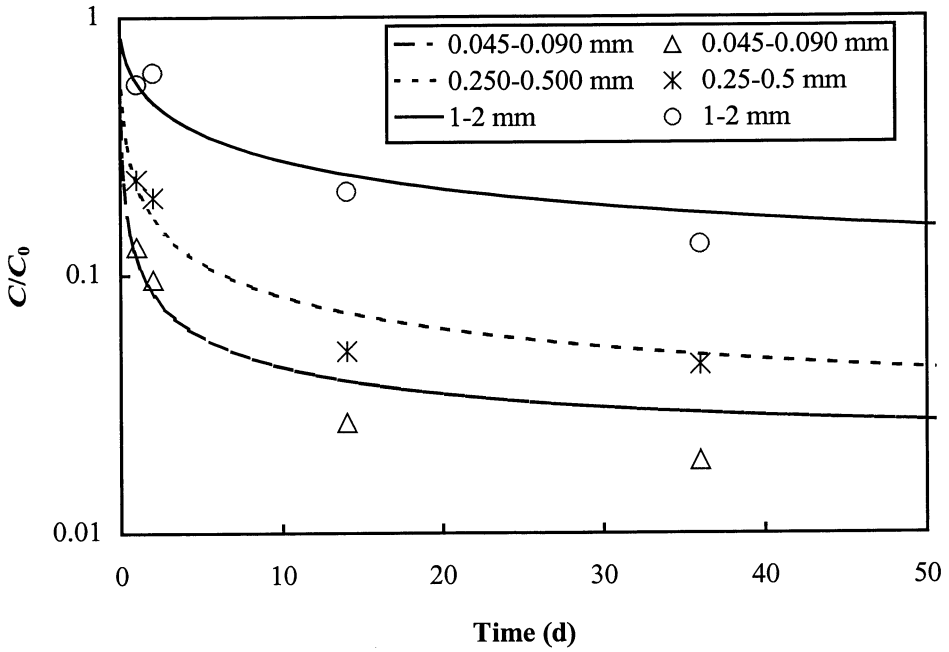

Figure 3-16 Sorption results of Cs onto three size fractions of Äspö diorite (symbols) and the fit of equation 3-27 to the data (lines).

Table 3-16 Apparent diffusivity, D_a, sorption coefficient, K_d, and calculated effective diffusivity, D_e, obtained from the fitting of the sorption results to equation 3-27.

Particle size (mm)	D_a ($m^2 \cdot s^{-1}$)	K_d ($m^3 \cdot kg^{-1}$)	D_e ($m^2 \cdot s^{-1}$)
Äspö diorite			
0.045-0.09	$2.5 \cdot 10^{-17}$	$3 \cdot 10^{-1}$	$2 \cdot 10^{-14}$
0.090-0.25	$1.2 \cdot 10^{-16}$	$1 \cdot 10^{-1}$	$4 \cdot 10^{-14}$
0.25-0.5	$1.9 \cdot 10^{-16}$	$3 \cdot 10^{-1}$	$2 \cdot 10^{-13}$
0.5-1	$1.0 \cdot 10^{-15}$	$1 \cdot 10^{-1}$	$3 \cdot 10^{-13}$
1-2	$2.7 \cdot 10^{-15}$	$8 \cdot 10^{-2}$	$6 \cdot 10^{-13}$
2-4	$1.5 \cdot 10^{-13}$	$1 \cdot 10^{-2}$	$3 \cdot 10^{-12}$
Fine-grained granite			
0.045-0.09	$1.5 \cdot 10^{-16}$	$6 \cdot 10^{-2}$	$3 \cdot 10^{-14}$
0.090-0.25	$1.4 \cdot 10^{-15}$	$3 \cdot 10^{-2}$	$1 \cdot 10^{-13}$
0.25-0.5	$1.1 \cdot 10^{-14}$	$2 \cdot 10^{-2}$	$6 \cdot 10^{-13}$
0.5-1	$8.8 \cdot 10^{-14}$	$1 \cdot 10^{-2}$	$2 \cdot 10^{-12}$
1-2	$4.5 \cdot 10^{-13}$	$8 \cdot 10^{-3}$	$1 \cdot 10^{-11}$
2-4	$2.5 \cdot 10^{-12}$	$7 \cdot 10^{-3}$	$4 \cdot 10^{-11}$

3.2.4.3 *Surface Sorption Diffusion Model*

The sorption and desorption results obtained from the Äspö diorite, fraction 1-2 mm, have been interpreted according to a sorption model (cf. Fig. 3-17) involving:

1. A fast equilibrium of distribution of the tracer between the water phase and the outer layer of the solid phase, representing the surface sorption.
2. One-dimensional diffusion of the sorbed tracers in pores in the solid material. The solid material consists of pores of different lengths (l), *i.e.*:

$$l = 0 \pm \sigma_p \qquad 3\text{-}29$$

where:

σ_p = standard deviation of the pore length (m).

3. Linear cation exchange sorption, *i.e.* sorption of radioactive tracers is accompanied by desorption non-radioactive species from the solid material and therefore no change of the composition of the water phase occurs.

The sorption/desorption-diffusion process is simulated to the following procedure:

1. For computer calculation purposes, the solid phase is divided into 11 discrete thin layers with pores of different lengths penetrating the layers. The first layer (d_0) is considered to be directly accessible for sorption and is thus meant to represent the surface of the solid phase. Therefore the thickness of the first layer is used as a fitting parameter, giving possibility to adjust the inner/outer surface ratio of the solid phase. The inner layers of the solid ($1 \leq n \leq 10$) are only accessible by diffusion. In the calculation, it is necessary to be able to vary the thickness of the inner layers, depending on the values that the fitting parameters d_0 and σ_p are given. The thickness of the n:th layer is calculated according to:

$$d_n = d_0 \cdot k^{(n-1)} \qquad 3\text{-}30$$

where the k is a parameter which is calculated in order to fulfil the equation:

$$3\sigma_p = d_0 + \sum_{n=1}^{10} d_0 \cdot k^{(n-1)} \qquad 3\text{-}31$$

This means that if $3\sigma_p > 11 \cdot d_0$, $k > 1$ and the thickness of the inner layers will be successively increasing. Consequently, if $3\sigma_p < 11 \cdot d_0$, $k < 1$ and the thickness of the inner layers will be successively decreasing. In any case, the first inner layer will

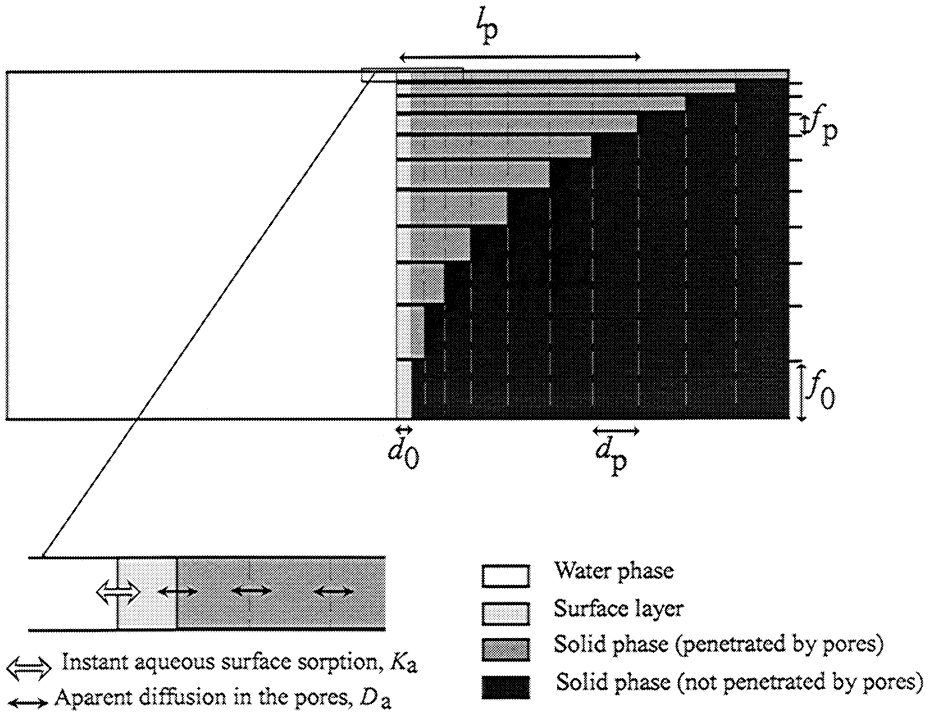

Figure 3-17 *Conceptual model used in the surface sorption – diffusion model (cf. Section 3.2.4.3)*

always have the same thickness as the surface layer, *i.e.*, $d_1 = d_0$. Using the described scheme, diffusion depth longer in than $3\sigma_p$ is not included in the calculation, *i.e.*, less than 0.5% of the inner surfaces is excluded from the calculation. The pores are given 11 different lengths and the length l_p of an individual pore type p ($0 \le p \le 10$) is given by:

$$l_p = \sum_{n=0}^{p} d_n \qquad 3\text{-}32$$

For each pore length (l_p) a probability factor (f_p) is calculated. Because of the normal distribution of the pore length, the probability of each pore length is calculated using Gaussian distribution, *i.e.*;

$$f_p = \frac{\int_{l_{p-1}}^{l_p} \sqrt{\frac{2}{\pi}} \cdot e^{-\left(\frac{l}{2\cdot\sigma_p}\right)} dl}{\int_{0}^{3\cdot\sigma_p} \sqrt{\frac{2}{\pi}} \cdot e^{-\left(\frac{l}{2\cdot\sigma_p}\right)} dl} \qquad 3\text{-}33$$

For p=0, 0 is used as the lower integration limit. The calculation yields a normalisation such that:

$$\sum_{n=0}^{10} f_p = 1 \qquad 3\text{-}34$$

2. The simulation of the diffusion is performed in small time steps, in which exchange of the tracer content occurs between the layers. A fast equilibrium of distribution of the tracer between the surface layer and the water phase is occurring, according to:

$$K_a = \frac{[M]_0 \cdot d_0}{[M]_w \cdot A} \qquad 3\text{-}35$$

where:

K_a = Surface distribution coefficient (m)
$[M]_0$ = Concentration of tracer in the surface layer (mole·m^{-1})
$[M]_w$ = Concentration of tracer in the aqueous phase (mole·m^{-3})
A = Surface area of the solid phase (m^2)

The sum of the amount of tracer present in the surface layer of the solid phase and the water phase is expressed as:

$$M_{0+w} = [M]_0 \cdot d_0 + [M]_w \cdot V \qquad 3\text{-}36$$

where:

M_{0+w} = Amount of tracer in the surface layer and the aqueous phase (mole)
V = Volume of the aqueous phase (m^3)

Combining equations 3-35 and 3-36 yields:

$$[M]_0 = \frac{M_{0+w}}{d_0 \cdot \left(1 + \frac{V}{K_a \cdot A}\right)} \qquad 3\text{-}37$$

The total concentration of tracer in the surface layer is then distributed between the different pores of different lengths, *i.e.*:

$$[M]_{0,p} = f_p \cdot [M]_0 \qquad 3\text{-}38$$

where:

$[M]_{0,p}$ = Concentration of tracer in the surface layer (mole·m^{-1}) in a pore with the length l_p.

3. The diffusion is simulated by exchange of tracer between the thin layers of the solid material. From each layer, n, subtractions and additions of tracer to and from the "neighbour" layer, n-1 and n+1, are performed, according to:

$$\mathbf{[M]_{n,p}} = [M]_{n,p} + D_a \cdot t_n \cdot \left(\frac{[M]_{n+1,p} - [M]_{n,p}}{\left(\frac{d_n + d_{n+1}}{2}\right)^2} + \frac{[M]_{n-1,p} - [M]_{n,p}}{\left(\frac{d_n + d_{n-1}}{2}\right)^2} \right) \qquad 3\text{-}39$$

(terms in bold indicates that a new value has been calculated using the old value of the same term)

where:

$[M]_{n,p}$ = Concentration of tracer in the present layer (mole·m^{-1})
$[M]_{n-1,p}$ = Concentration of tracer in the layer located on the inner side of the present layer (mole·m^{-1})
$[M]_{n+1,p}$ = Concentration of tracer in the layer located on the outer side of the present layer (mole·m^{-1})
d_n, d_{n+1}, d_{n-1}, = The thickness of the different layers of the solid phase (m)
t_n = The time step used (s)

For the case of diffusion to and from the surface layer (n=0), the layer n-1 does not exist. Therefore the diffusion has to be calculated according to:

$$\mathbf{[M]_{0,p}} = [M]_{0,p} + D_a \cdot t_n \cdot \left(\frac{[M]_{1,p} - [M]_{0,p}}{\left(\frac{d_1 + d_0}{2}\right)^2} \right) \qquad 3\text{-}40$$

For the case where the present layer represents the dead end of the pore (n=p), the concentration is calculated according to:

$$\mathbf{[M]_{n=p,p}} = [M]_{n=p,p} + D_a \cdot t_n \cdot \left(\frac{[M]_{n-1,p} - [M]_{n=p,p}}{\left(\frac{d_n + d_{n-1}}{2}\right)^2} \right) \qquad 3\text{-}41$$

4. In the calculations, the time step, t_n, has been moderated so that the maximum decrease of tracer concentration in any cell in one time step is lower than 1%. After the diffusion simulation has been performed for the present time step, a calculation is performed of the amounts of tracer mass present in the aqueous phase, solid phase and surface, according to:

$$[\mathrm{M}]_w = \frac{M_{tot} - \sum_{p=0}^{10}\sum_{n=0}^{p}[\mathrm{M}]_{p,n} \cdot d_n}{V} \qquad 3\text{-}42$$

where:

M_{tot} = total amount of tracer in the system (mole)

and:

$$M_{w+0} = [\mathrm{M}]_w \cdot V + \sum_{p=0}^{10}[\mathrm{M}]_{p,0} \cdot d_n \qquad 3\text{-}43$$

The new M_{w+0} is then used for the next diffusion simulation step, *i.e.*, returning to equation 3-37. When a diffusion simulation step has been performed, the total contact time, t_{tot}, is registered, according to:

$$t_{tot} = t_{tot} + t_n \qquad 3\text{-}44$$

If the t_{tot} corresponds to a time where sampling and measurement was performed in the experiment, the square of the difference between the measured and calculated value of the concentration of tracer in the water phase is calculated. The difference is weighted with either the experimental or the calculated value, depending on which one that is the smallest.

5. The desorption is simulated by setting the $[\mathrm{M}]_w$ to zero at the time when the original water phase was replaced by a non-spiked synthetic groundwater. The desorption is then simulated by calculating the surface sorption and diffusion according to the procedures described above.

6. Calculations are performed in order to minimise the square of the deviation of the experimental and calculated value, using the simplex method AMOEBA (Press *et al.* 1986) as the fitting routine.

Calculations have been performed based on the results obtained for the 1-2 mm size fractions of the Äspö diorite in the experiments using generic Äspö material. In the calculation the results of the tracers Ca, Rb, Cs and Ba were used. The apparent diffusivity (D_a) and the surface distribution coefficient (K_a) were used as fitting parameters for each tracer. Additionally, the thickness of the exchangeable surface layer (d_0) and the standard deviation of the pore length (σ_p) for the 1-2 mm faction were used as fitting parameters, *i.e.*, using the same value for all the cation tracers involved. This means that 10 fitting parameters were used in order to fit the results of 4 different tracers, *i.e.*, 2.5 fitting parameters per data set. This can be compared to the modelling using first order kinetics and the modelling using a homogeneous diffusion-sorption model (Section 3.2.4.1 and 3.2.4.2, respectively); in both models 2 fitting parameters were used in order to fit the results of a single tracer.

The results of the fitting calculations are given for Cs and Rb (cf. Fig 3-18). The fit is in no way perfect, but it is indicated that the present model can explain the levels of the desorption and the time dependence of the sorption and desorption. Furthermore, it is also possible that the indications of non-reversible sorption (see section 3.2.2.7) can be explained by diffusion taking place in the crushed solid material. It is, however, likely that the experimental results are influenced by an additional inhomogeneity which is not addressed by this comparatively simple model. It is likely that variations in sorption and diffusivity due to the mineralogical composition may occur.

The results obtained for the different fitting parameters in the modelling are given in Table 3-17. No evaluation of the uncertainty of the parameters has been performed. Therefore the values should be considered as very approximate. The only conclusion that can be made for the modelling is that a surface sorption – diffusion model can give a reasonable explanation for the time dependence of the sorption and desorption. However, further application of the model to other size fractions and other geologic materials is probably necessary in order to evaluate the usefulness of the proposed model.

The D_a-values obtained for the modelling of the batch sorption results deviate strongly from the values obtained in the diffusion experiments using intact rock material, chapter 4. It is possible that the diffusion in intact rock material takes place in the pockets between the grains of the crystals. In the crushed material these pockets do not exist any more and that the slower diffusion observed is because of diffusion into the individual grains; a much slower process. However, since the diffusion constants are only the result of the observation of slow sorption and desorption of the tracer and are not determined from any penetration studies, they have to be considered as very approximate.

Considerable differences in the D_a for Cs are also observed between the homogeneous sorption-diffusion model (section 3.2.4.2) and the present model. The reason for this is probably that the homogeneous surface sorption model does not involve any surface sorption and therefore has to address the fast loss in the beginning of the experiment as a diffusion process. A more elaborate modelling program is probably necessary to judge the usefulness and validity of the proposed sorption models.

Table 3-17 Constants derived from the fitting of the surface sorption–diffusion model to the experimentally obtained results

	D_a (m^2/s)	K_a (m)
Ca^{2+}	$1.3 \cdot 10^{-12}$	$7.2 \cdot 10^{-7}$
Rb^{+}	$3.6 \cdot 10^{-18}$	$3.2 \cdot 10^{-4}$
Cs^{+}	$3.6 \cdot 10^{-18}$	$4.5 \cdot 10^{-3}$
Ba^{2+}	$5.8 \cdot 10^{-20}$	$2.9 \cdot 10^{-4}$

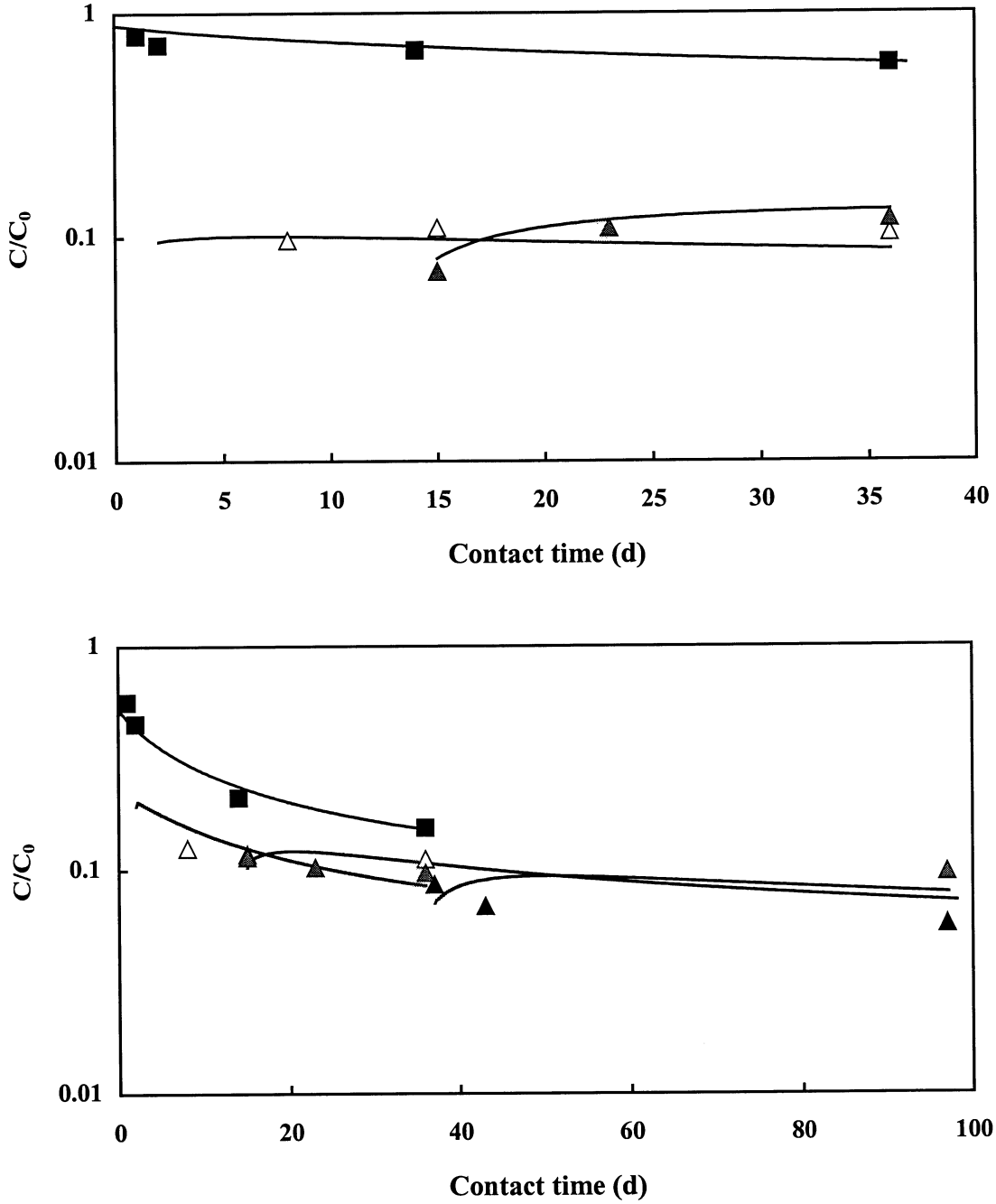

Figure 3-18 *C/C_0 (proportion of the originally added tracer remaining in solution) for the sorption experiment (filled squares) and the desorption experiments after a contact time of 2 days (open triangles), 14 days (grey triangles) and 36 days (filled triangles). The solid lines represent the C/C_0 obtained from the calculation described in section 3.2.4.3. The results are given for Rb (top) and for Cs (bottom) for the 1-2 mm size fraction of the Äspö diorite, generic Äspö material.*

3.3 Summary of the Batch Laboratory Experiments

The results from the laboratory experiments are summed up in the following paragraphs:

- For the sorbing tracers used, the following trend of increasing sorption coefficient is observed for the tracers used: $Na^{+}<Ca^{2+}\approx Sr^{2+}<<Ba^{2+}\approx Rb^{+}<Cs^{+}$. This trend is general for all the rock material involved in this investigation, generic or site-specific, although the sorptivity of the different materials may vary.
- For the generic rock material, it is observed that the tracers sorb more on the Äspö diorite than on the Fine-grained granite. For the Feature A site specific material, the mylonite and altered rock material originating from Äspö diorite are more sorptive than the corresponding altered material originating from the Fine-grained granite. A trend of increasing sorption coefficients with increasing content of biotite is observed. Furthermore, the alteration of biotite to chlorite (observed for the Feature A altered material) correlates with a decreasing sorption capacity.
- For the stronger sorbing species, *i.e.*, Ba^{2+}, Rb^{+} and Cs^{+}, increased sorption with increasing contact time has been observed. A modelling attempt has indicated that this could be a result of diffusion occurring in the particles of the crushed rock material. Diffusion could also explain the non- or slowly reversible sorption obtained for these tracers. However, slow chemical kinetics could also have an impact on the observed sorption characteristics.

4 Diffusion Experiments

The studies of the diffusion of non- and slightly sorbing tracers in Äspö rock material have been divided into three different experimental sections.

The experimental programme started with studies of diffusion in generic geologic Äspö material, Äspö diorite and Fine-grained granite (see section 2.1). Several diffusion cells were set up for the diffusion studies. In section, 4.1, the results of the through-diffusion experiments of the non- and very slightly sorbing tracers are described. Since the more strongly sorbing tracers used, *e.g.*, Ba and Cs, gave very limited breakthrough data in the diffusion experiment, penetration studies of the rock material had to be applied. Some of the diffusion cells were dismantled and the rock disc was analysed for the penetration of the tracer. The measurements of penetration depth, penetration profile and distribution of tracer in relation to the porosity are described in section 4.2.

The selection of Feature A as the TRUE-1 experimental fracture initiated diffusion studies addressed directly to the site-specific geology of that fracture. Therefore, an additional diffusion cell was set up, including a slab with site-specific Feature A rock material (*cf.* section 2.1.1.3). The results of the through diffusion studies of these experiments are given in section 4.3

4.1 Through Diffusion Experiments

4.1.1 Introduction

In the safety assessment of a repository for spent nuclear fuel, the surrounding rock will act as a barrier retarding released radionuclides. The retardation process in fractured rock is believed to be due to sorption of radionuclides on the fracture walls combined with diffusion into the fracture coatings and further into micropores of the rock (Neretnieks 1980). In order to perform a correct safety assessment, it is important to quantify and understand these water-rock interaction processes both in the laboratory scale and in the field scale. Important parameters in order to understand the retardation of radionuclides are parameters such as the flow-wetted surface and the sorption capacity of the fracture walls. These parameters can be determined from the results of *in-situ* experiments if the sorption properties of the used tracers are well understood. Byegård *et al.* (1993) proposed suitable tracers to be used for *in situ* field experiments and studied the sorption properties of these elements (Byegård *et al.* 1995).

Earlier studies have indicated that batch experiments using crushed material may overestimate the sorption distribution coefficient, K_d, compared to intact rock material (Bradbury and Stephen 1985). Crushing of the material creates new surfaces and may increase the accessibility to pores which may not be representative to the intact rock. The rock slabs used in the diffusion experiments are still somewhat disturbed, compared

to the intact rock, due to the pressure release induced when the core is drilled out of the bedrock and by subsequent treatment methods (cutting and grinding)

In the this study, the diffusion behaviour of the proposed tracers on the laboratory scale is presented. Diffusion of both sorbing and non-sorbing radioactive tracers is studied using a through-diffusion experimental technique. With this method the effective diffusivity, D_e, and the distribution coefficient, K_d, can be evaluated. Comparison of the results obtained for sorption measured with crushed material (Chapter 3) and through diffusion experiments are also conducted.

4.1.2 Experimental

A cylindrical rock disc was cast in an epoxy resin (Araldite F with triethylenetetraamin as a hardener, Ciba Geigy). After grinding the end surfaces, the cylinder was put in vacuum to remove gas trapped in pores and then saturated with the synthetic groundwater for at least one month. The rock disc was mounted between two water containers, see Fig. 4-1, sealed with o-rings on both sides. The volumes of the containers were 20 ml. One side of the diffusion cell was spiked with a sorbing tracer and/or tritiated water (HTO) as an inert reference. The concentration increase on the other side of the diffusion cell was monitored under stagnant groundwater conditions. A description of the different samples used (tracer, rock type and length) is given in Table 4-1. Samples of 2 ml and 10 µl were collected in the measurement container and the injection container, respectively. The removed sample volume was replaced with synthetic groundwater.

Three different lengths of the rock discs were used; 1,2 and 4 cm. Each side of the diffusion cell container was closed by a screw cap that was ventilated through a hole connected to a hose. The screw caps were closed by putting the hose on a thin pin. This was done in order to minimise pressure build-up when closing the reservoirs after sampling.

Radioactivity of HTO, $^{22}Na^{+}$, $^{45}Ca^{2+}$ and $^{86}Rb^{+}$ was measured with liquid scintillation counting (LKB Wallac, Rackbeta 1219) and. $^{85}Sr^{2+}$ was measured with a NaI-scintillation detector (Intertechnique, CG 4000). For the stronger sorbing tracers, *i.e.*, $^{133}Ba^{2+}$ and $^{137}Cs^{+}$, the concentration in the measurement container was too low to be measured using any of the methods described above. Instead, the whole volume in the measurement cell was isolated and was replaced with new synthetic groundwater. The sampled volume was contacted with small amounts (<10 mg) of ammonium molybdenum phosphate (AMP) or Na_2SO_4, in order to obtain precipitate of Cs-AMP or $BaSO_{4(s)}$, respectively. The precipitate was centrifuged to a small spot on the bottom of a test tube and was measured γ-spectometrically using a High Purity Germanium detector (EG&G Ortec).

Table 4-1 **Evaluated effective diffusivities, D_e, rock capacity factors, α, sorption coefficients, K_d and rock formation factors, F, for Äspö diorite (ÄD) and fine-grained granite (FGG). The errors are given as 1σ. Values within brackets indicates that steady state may not have been reached.**

Cell nr	Nuclide	Rock type	Cell size	D_e	α	K_d	$F_{(HTO)}$	$F_{(sorb)}$	$\frac{F_{(sorb)}}{F_{(HTO)}}$
			(cm)	(m^2/s)		(m^3/kg)			
1	HTO	FGG	1	$1.0\pm0.01\cdot10^{-13}$	$4.7\pm0.3\cdot10^{-3}$		$4.3\cdot10^{-5}$		
	Na-22			$6.4\pm0.01\cdot10^{-14}$	$1.1\pm0.02\cdot10^{-2}$	$2.6\pm0.2\cdot10^{-6}$		$4.8\cdot10^{-5}$	1.13
2	HTO	FGG	2	$7.5\pm0.12\cdot10^{-14}$	$4.4\pm0.3\cdot10^{-3}$		$3.1\cdot10^{-5}$		
	Na-22			$6.0\pm0.1\cdot10^{-14}$	$1.3\pm0.01\cdot10^{-2}$	$3.2\pm0.2\cdot10^{-6}$		$4.5\cdot10^{-5}$	1.44
3	HTO	ÄD	1	$1.4\pm0.01\cdot10^{-13}$	$4.4\pm0.3\cdot10^{-3}$		$6.0\cdot10^{-5}$		
	Na-22			$7.8\pm0.1\cdot10^{-14}$	$8.5\pm0.2\cdot10^{-3}$	$1.5\pm0.2\cdot10^{-6}$		$5.9\cdot10^{-5}$	0.98
4	HTO	ÄD	2	$1.2\pm0.01\cdot10^{-13}$	$4.3\pm0.2\cdot10^{-3}$		$5.1\cdot10^{-5}$		
	Na-22			$7.3\pm0.1\cdot10^{-14}$	$1.1\pm0.02\cdot10^{-2}$	$2.3\pm0.2\cdot10^{-6}$		$5.5\cdot10^{-5}$	1.08
5	HTO	ÄD	4	$3.2\pm0.12\cdot10^{-14}$	$8.6\pm0.8\cdot10^{-4}$		$1.3\cdot10^{-5}$		
	Na-22			$1.3\pm0.1\cdot10^{-14}$	$2.1\pm0.01\cdot10^{-3}$	$4.6\pm0.3\cdot10^{-7}$		$9.9\cdot10^{-6}$	0.75
6	Na-22	FGG	4	$6.2\pm0.1\cdot10^{-14}$	$7.0\pm0.1\cdot10^{-3}$			$4.7\cdot10^{-5}$	
7	Na-22	ÄD	4	$1.6\pm0.1\cdot10^{-14}$	$2.4\pm0.03\cdot10^{-3}$			$1.2\cdot10^{-5}$	
8	HTO	FGG	1	$1.2\pm0.03\cdot10^{-13}$	$3.4\pm1.0\cdot10^{-3}$		$5.1\cdot10^{-5}$		
	Sr-85			$3.5\pm0.1\cdot10^{-14}$	$2.5\pm0.02\cdot10^{-2}$	$8.2\pm0.5\cdot10^{-6}$		$4.5\cdot10^{-5}$	0.88
9	HTO	FGG	2	$6.2\pm0.35\cdot10^{-14}$	$2.4\pm0.5\cdot10^{-3}$		$2.6\cdot10^{-5}$		
	Sr-85			7.9±0.3E-15	$4.4\pm0.05\cdot10^{-3}$	$7.5\pm2.0\cdot10^{-7}$		$9.9\cdot10^{-6}$	0.39
10	HTO	ÄD	1	$1.9\pm0.03\cdot10^{-13}$	$9.8\pm1.1\cdot10^{-3}$		$8.1\cdot10^{-5}$		
	Sr-85			$6.3\pm0.1\cdot10^{-14}$	$2.9\pm0.03\cdot10^{-2}$	$6.9\pm0.5\cdot10^{-6}$		$7.9\cdot10^{-5}$	0.98
11	HTO	ÄD	2	$1.4\pm0.07\cdot10^{-13}$	$5.3\pm0.9\cdot10^{-3}$		$5.7\cdot10^{-5}$		
	Sr-85			$2.8\pm0.1\cdot10^{-14}$	$1.2\pm0.01\cdot10^{-2}$	$2.5\pm0.4\cdot10^{-6}$		$3.6\cdot10^{-5}$	0.63
14	HTO	FGG	1	$4.0\pm0.08\cdot10^{-13}$	$8.6\pm2.6\cdot10^{-3}$		$1.7\cdot10^{-4}$		
	Ca-45			$1.4\pm0.03\cdot10^{-13}$	$1.8\pm0.1\cdot10^{-2}$	$3.6\pm1.5\cdot10^{-6}$		$1.8\cdot10^{-4}$	1.06
15	HTO	ÄD	1	$1.2\pm0.03\cdot10^{-13}$	$5.5\pm1.2\cdot10^{-3}$		$5.2\cdot10^{-5}$		
	Ca-45			$4.3\pm0.1\cdot10^{-14}$	$2.1\pm0.1\cdot10^{-2}$	$5.5\pm0.8\cdot10^{-6}$		$5.4\cdot10^{-5}$	1.05
16	HTO	FGG	2	$2.2\pm0.07\cdot10^{-13}$	$5.3\pm0.8\cdot10^{-3}$		$9.2\cdot10^{-5}$		
	Ca-45			$7.3\pm0.12\cdot10^{-14}$	$1.4\pm0.08\cdot10^{-2}$	$3.5\pm0.6\cdot10^{-6}$		$9.3\cdot10^{-5}$	1.00
17	HTO	ÄD	2	$8.5\pm0.48\cdot10^{-14}$	$1.9\pm0.5\cdot10^{-3}$		$3.6\cdot10^{-5}$		
	Ca-45			$3.2\pm0.01\cdot10^{-14}$	$1.5\pm0.08\cdot10^{-2}$	$4.9\pm0.5\cdot10^{-6}$		$4.1\cdot10^{-5}$	1.15
18	HTO	FGG	1	$6.8\pm0.12\cdot10^{-14}$	$1.2\pm0.3\cdot10^{-3}$		$2.8\cdot10^{-5}$		
	Ba-133			a small breakthrough observed, not evaluated					
19	HTO	ÄD	1	$9.6\pm0.18\cdot10^{-14}$	$3.5\pm1.0\cdot10^{-3}$		$4.0\cdot10^{-5}$		
	Ba-133			($5\pm1\cdot10^{-16}$)	($2\pm0.5\cdot10^{-3}$)				
20	HTO	FGG	2	$4.3\pm0.21\cdot10^{-14}$	$8.9\pm1.8\cdot10^{-4}$		$1.8\cdot10^{-5}$		
	Ba-133			no breakthrough					
21	HTO	ÄD	2	$9.3\pm0.56\cdot10^{-14}$	$2.2\pm0.5\cdot10^{-3}$		$3.9\cdot10^{-5}$		
	Ba-133			no breakthrough					
22	HTO	FGG	1	$1.8\pm0.03\cdot10^{-13}$	$4.1\pm1.3\cdot10^{-3}$		$7.5\cdot10^{-5}$		
	Cs-137			($1.8\pm0.2\cdot10^{-14}$)	($5.6\pm0.5\cdot10^{-2}$)	($2\pm0.5\cdot10^{-5}$)			
23	HTO	ÄD	1	$1.4\pm0.01\cdot10^{-13}$	$2.1\pm0.5\cdot10^{-3}$		$5.7\cdot10^{-5}$		
	Cs-137			no breakthrough					
24	HTO	FGG	2	$5.1\pm0.25\cdot10^{-14}$	$1.1\pm0.3\cdot10^{-3}$		$2.1\cdot10^{-5}$		
	Cs-137			no breakthrough					

Continued on next page

Table 4-1 Continued from previous page

Cell nr	Nuclide	Rock type	Cell size (cm)	D_e (m^2/s)	α	K_d (m^3/kg)	$F_{(HTO)}$	$F_{(sorb)}$	$\frac{F_{(sorb)}}{F_{(HTO)}}$
25	HTO	ÄD	2	$1.0\pm0.05\cdot10^{-13}$	$3.2\pm0.6\cdot10^{-3}$		$4.2\cdot10^{-5}$		
	Cs-137			no breakthrough					
26	HTO	FGG	1	$7.2\pm0.12\cdot10^{-14}$	$4.9\pm0.6\cdot10^{-3}$		$3.0\cdot10^{-5}$		
	Rb-86			no breakthrough					
27	HTO	ÄD	1	$1.4\pm0.05\cdot10^{-13}$	$7.7\pm2.3\cdot10^{-3}$		$5.9\cdot10^{-5}$		
	Rb-86			no breakthrough					

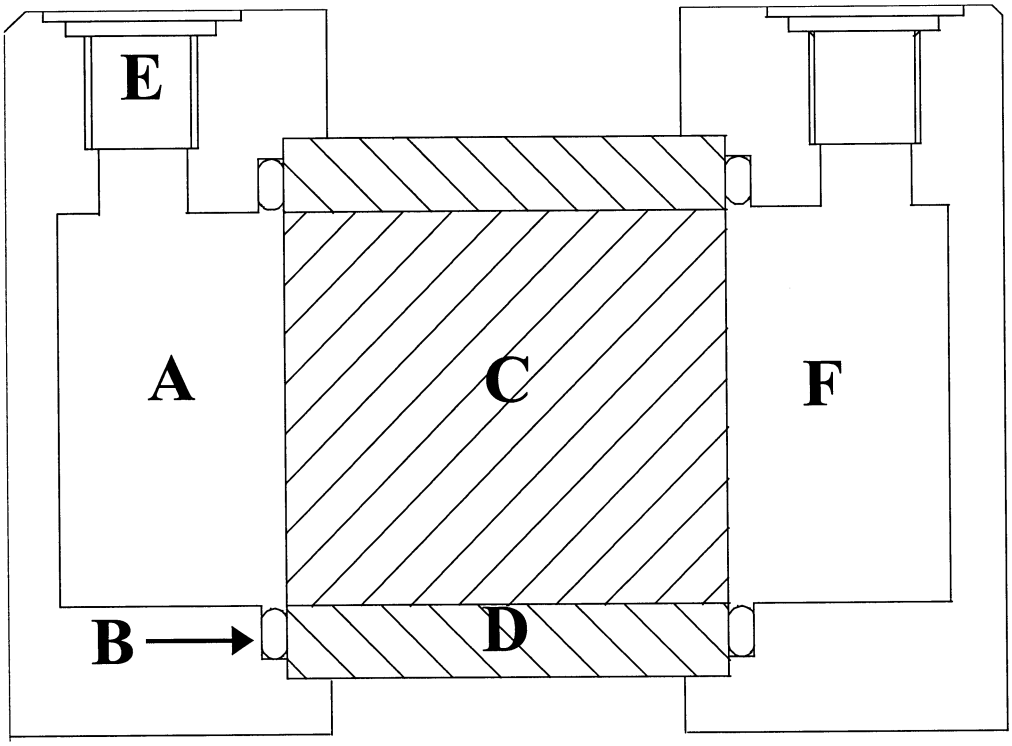

Figure 4-1. Schematic drawing of the diffusion cell. (A) injection container, (B) o-ring, (C) rock cylinder, (D) epoxy resin, (E) sampling hole, (F) measurement container.

4.1.3 Theory of Through-diffusion

The accumulated scaled ratio of concentration, C_r, of the diffusing species which has passed through the porous, homogeneous rock disc (initially at zero concentration) at time t, can be obtained by solving the diffusion equation for the boundary conditions: constant inlet concentration C_1 from $t = 0$, and outlet concentration C_2 ($C_2 \ll C_1$) at a distance l. The result is, (Crank 1975)

$$C_r = \frac{C_2 \cdot V_2}{C_1 \cdot A_s \cdot l_s} = \frac{D_e \cdot t}{l_s^2} - \frac{\alpha}{6} - \frac{2 \cdot \alpha}{\pi^2} \cdot \sum_{n=1}^{\infty} \frac{(-1)^n}{n^2} \cdot \exp\left\{ - \frac{D_e \cdot n^2 \cdot \pi^2 \cdot t}{l_s^2 \alpha} \right\} \qquad 4\text{-}1$$

where C_r is the scaled ratio of the concentration in the measurement container, C_2, relative to that of the injection container, C_1. A_s is the geometrical surface area of the sample which has thickness l_s and V_2 is the volume of the measurement container. $D_e = D_p \cdot \varepsilon^+$ is the effective diffusivity where D_p is the pore diffusivity, ε^+ is the "transport" porosity (the pores that are connected and contributes to the transport of the dissolved species from one side to the other), $\alpha = \varepsilon_t + K_d \rho$ is the rock capacity factor where ε_t is the total porosity (the sum of the transport porosity and the storage porosity), K_d is the sorption coefficient (cf. eq.3.2) and ρ is the density of the rock sample. The theory has previously been described in detail by *e.g.*, Skagius and Neretnieks (1986).

Equation (4.1) is only valid if: D_e is constant (independent of C and t), the concentration in the injection cell, C_1, is constant with time, the concentration in the measurement container, C_2, is negligible compared to C_1 for all times, no bulk flow (advection) occurs and if the rock sample is homogeneous. These assumptions seems to be reasonable, except for the assumption of homogeneous media which is not obvious, because the K-feldspar grains in the Äspö diorite are of the same size as the thickness of the samples, furthermore the fine-grained granite is brittle, containing microfissures and is foliated.

The effective diffusivity, D_e, and the rock capacity factor, α, were calculated by fitting the data to eq. (4.1). A steepest gradient method was used to minimise the error sum of squares according to the least square method. The errors of the parameters were estimated assuming normal distribution of the errors.

The total porosity used in the calculations was determined by the rock capacity factor for the non-sorbing tritiated water, for which $\alpha_{HTO} = \varepsilon_t$. K_d for the sorbing tracers could then be derived from the rock capacity factor for each sorbing tracer, *i.e.*;

$$K_d = \frac{\alpha - \alpha_{HTO}}{\rho} \qquad 4\text{-}2$$

4.1.4 Results and Discussion

Some typical breakthrough curves for HTO (cell 3), Na^+ (cell 3), Ca^{2+} (cell 15) and Sr^{2+} (cell 10) are presented in Fig.4-2. Ca^{2+} and Sr^{2+} are more retarded than Na^+ as expected from the K_d-values obtained in the batch experiments (Chapter 3). The K_d that have

been evaluated from the diffusion experiments are presented together with the diffusion data in Table 4-1.

The measurements of HTO showed that there was a large deviation in D_e and α between the different diffusion cells, even within the same rock type, the same length and with rock discs taken from the same drill core. In Fig. 4-2 all HTO data are plotted together for the two rock types. The plots show a tendency that an increase in D_e is associated with an increase in α for both materials. Since D_e is dependent on ε^+, the "transport" porosity, and α is the total porosity for HTO, it seems that both the storage and the transport porosity vary between the samples.

The spread in data, see Fig. 4-3, is larger for the fine-grained granite, which is probably due to the fact that it is brittle and even contain visible micro-fissures in some samples. There is a possibility for a decrease in D_e and α in the 4 cm cells containing Äspö diorite due to the fact that the 1-2 cm sized K-feldspar grains may give directly connecting grain boundary pores in the 1 and 2 cm cells but not in the 4 cm cells. The fine-grained granite is foliated with veins of chlorite which may give directly connecting diffusion pathways in the shorter cells but not in the 4 cm cells. However, more data would be needed to show this.

There is a tendency towards decreasing D_e and α with increasing cell lengths, see Fig.4-4 and Table 4-1. Increased D_e with decreasing cell lengths, indicates that the "transport" porosity is larger in the shorter samples.

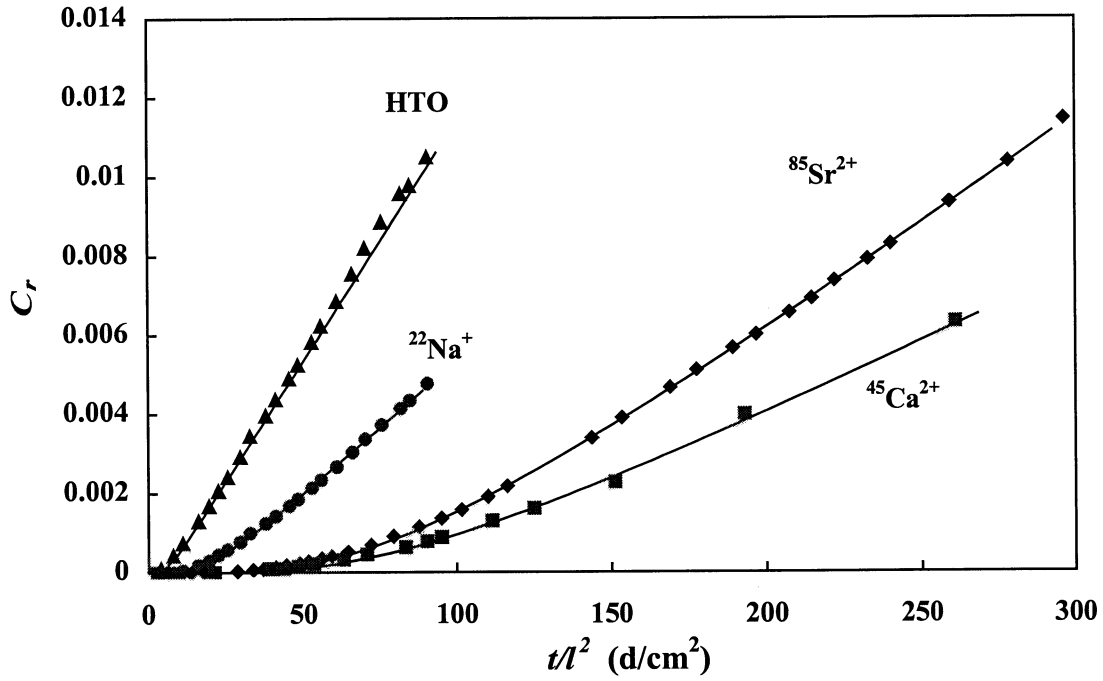

Figure 4-2 Measured reduced concentration (C_r) versus scaled diffusion time for HTO, Na^+, Ca^{2+} and Sr^{2+} in 1 cm cells of Äspö diorite. Solid lines are the fit of eq. (4-1).

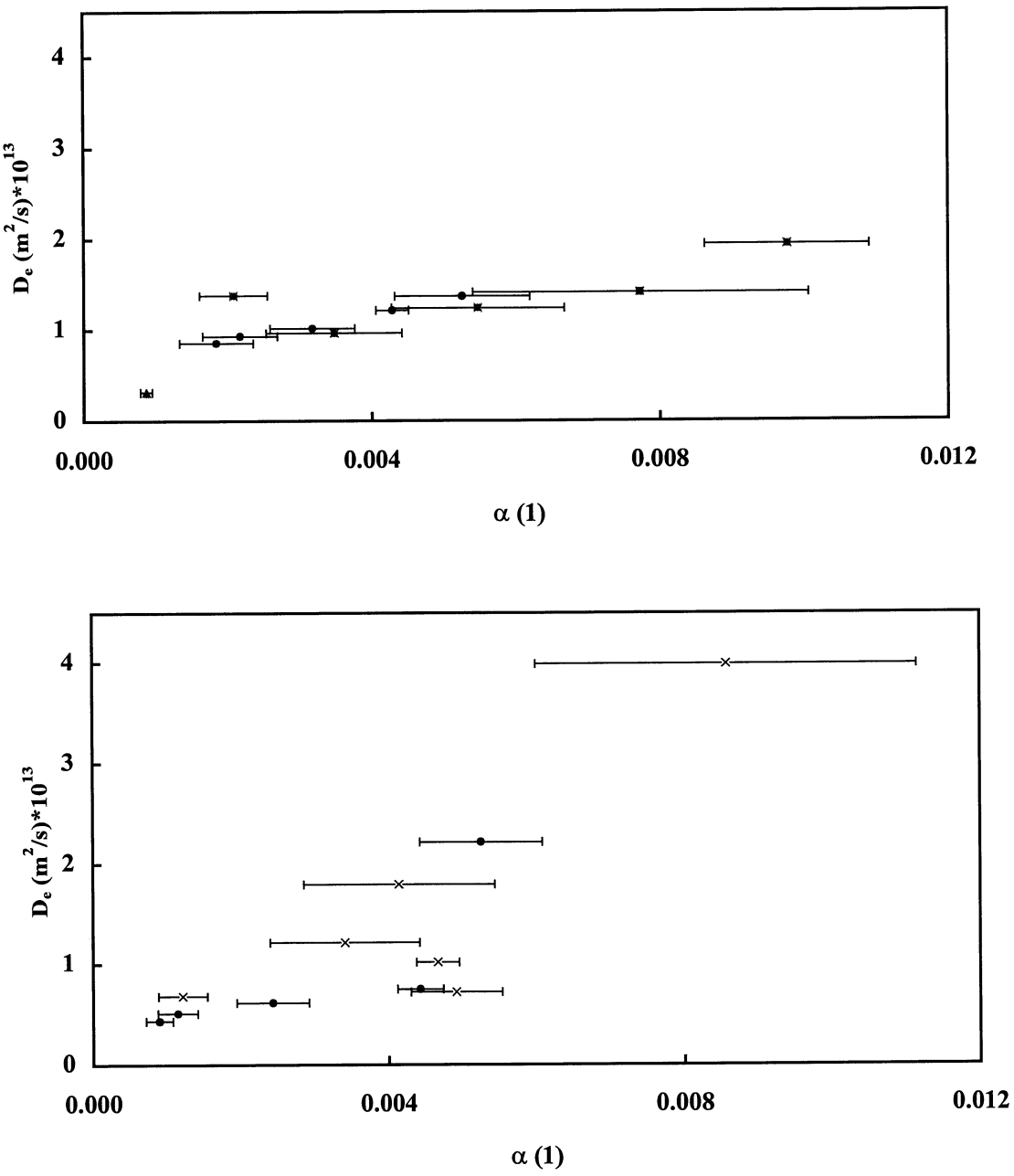

Figure 4-3 Effective diffusivity versus the formation factor for HTO in Äspö diorite (top) and Fine-grained granite (bottom) for 1 cm (×), 2 cm (●), and 4 cm (■) cells. Error bars represent 1σ. The uncertainties in D_e are of the same size as the height of the dots. The large deviations in α for the 1 cm cells are due to experimental problems with contamination of HTO in the glove box in combination with the short breakthrough time of HTO in the 1 cm cells.

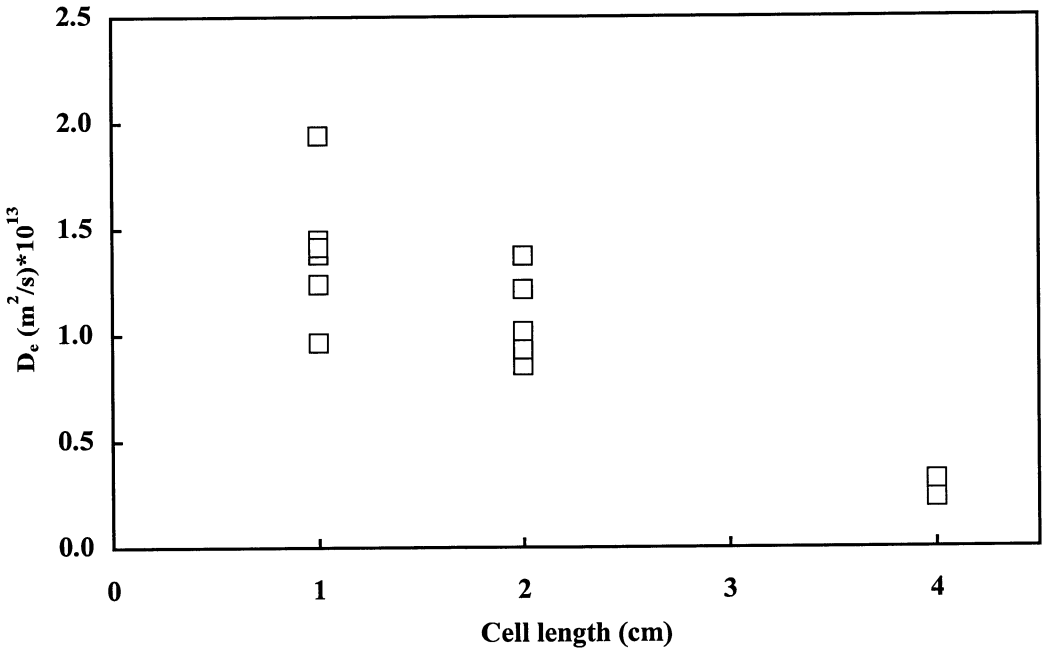

Figure 4-4 Effective diffusivity versus the cell length for HTO diffusion in Äspö diorite. One of the two 4 cm samples is calculated from Na^+ diffusion (cell 7) assuming that the formation factor for HTO is equal to the formation factor for Na^+. The uncertainties of the parameters are of the same size as the square dots.

The D_e (slopes of the concentration curves) tend to increase in the order $Ca^{2+} \approx Sr^{2+} < Na^+ <$ HTO. It is very important, when comparing the different sorbing tracers, to relate D_e to the D_e of HTO in each diffusion cell due to the variations in porosity between the cells. The difference in D_e between the different tracers could simply be an effect of the difference in bulk diffusivities, D_w, (the diffusion coefficient of the tracer in water) between the tracers. Instead the formation factor, F, calculated from both HTO and the sorbing tracer in each diffusion cell should be compared. The formation factor (properties of the material such as transport porosity, ε^+, tortuosity, τ, and pore constrictivity, σ) relates the effective diffusivity, D_e, to the water bulk phase diffusivity, D_w:

$$D_e = F \cdot D_w \;\; ; \;\; F = \frac{\varepsilon^+ \cdot \sigma}{\tau^2} \qquad 4\text{-}3$$

The formation factors, see Table 4-1 and Figure 4.5, for HTO and the accompanying sorbing tracer in the same diffusion cell, are generally of the same magnitude, ($F_{(sorb)}/F_{(HTO)} \approx 1$), which indicates that the difference in D_e between the sorbing tracers is only due to the difference in D_w and not due to the variation in material properties. Consequently, diffusivities for sorbing tracers can be estimated if the formation factor for a non-sorbing

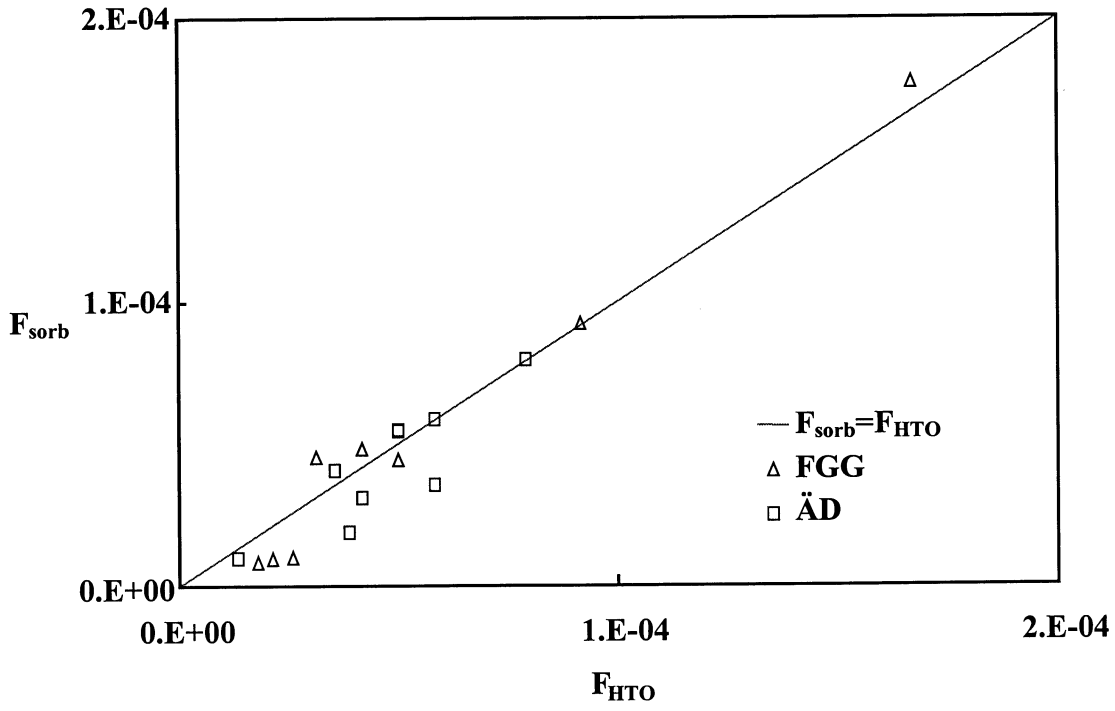

Figure 4-5 Formation factors obtained for Na^+, Ca^{2+}, Sr^{2+}, Cs^+ and Ba^{2+} in Äspö diorite and Fine-grained granite versus the formation factor for HTO in the corresponding diffusion cell.

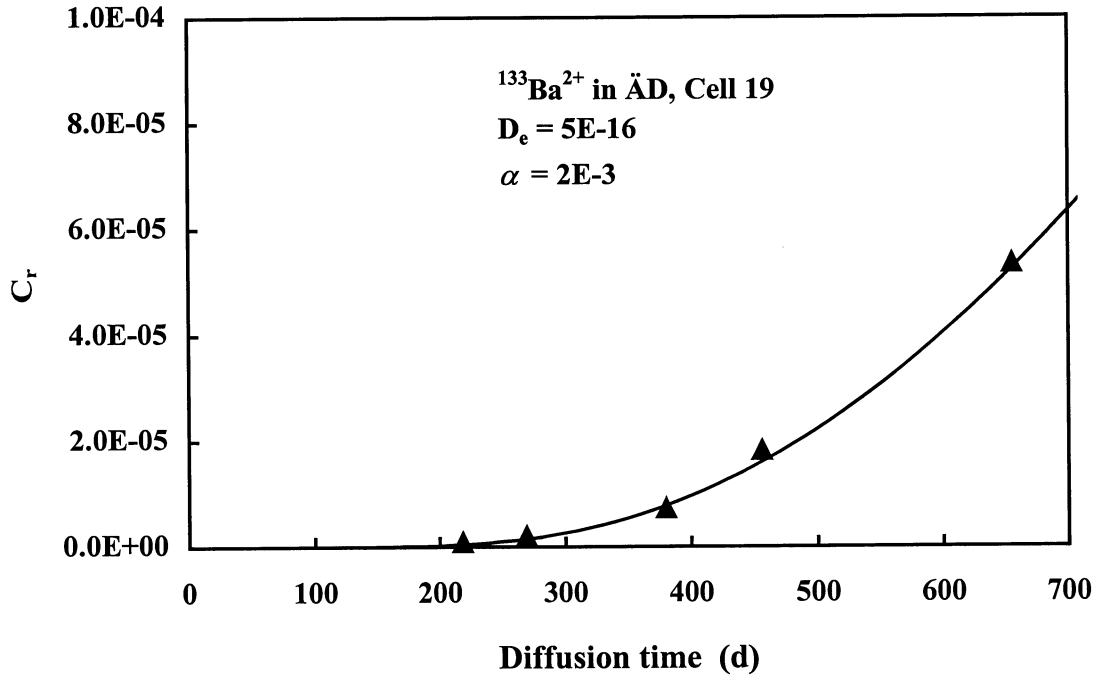

Figure 4-6 Through diffusion of $^{133}Ba^{2+}$ in Äspö diorite, (cell 19) The dots are the experimental data and the lines are the fit of the diffusion equation to the data.

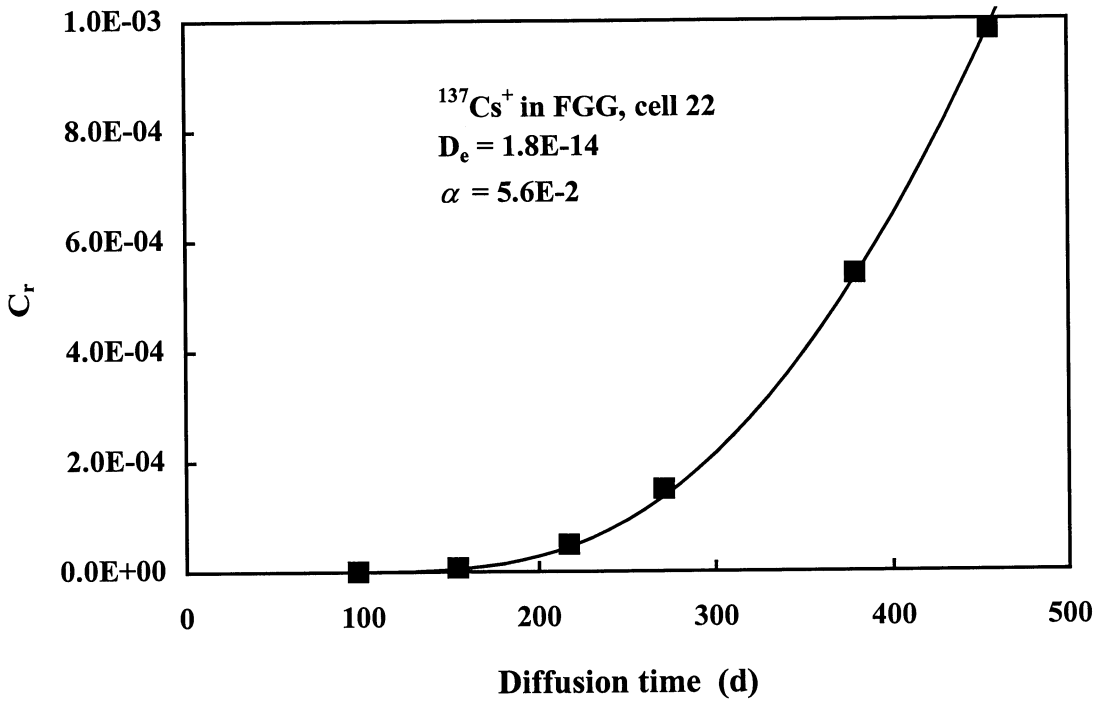

Figure 4-7 Through diffusion of $^{137}Cs^+$ in Fine-grained granite, cell 22. The dots are the experimental data and the lines are the fit of the diffusion equation to the data.

tracer is known. The bulk diffusion coefficients used in the calculations (D_w HTO=$2.4 \cdot 10^{-9}$, D_w Na^+=$1.33 \cdot 10^{-9}$, D_w Ca^{2+}=$0.79 \cdot 10^{-9}$ and D_w Sr^{2+}=$0.79 \cdot 10^{-9}$) were calculated from ionic conductivities at infinite dilution (Gray 1972).

No breakthrough was observed for Rb^+; this can probably be explained by the short half-life of Rb-86 (18.7 days) which makes it impossible to study this tracer in longer time perspectives. Breakthrough of Ba was obtained in the 10 mm cells of both Fine-grained granite and Äspö diorite (cells 18 and 19). However, the diffused amounts are large enough for evaluation only in the Äspö diorite sample (Fig. 4-6). The fitted diffusivity and retardation factor, α, are very low, and the α is even lower than the measured α for HTO diffusion in the same cell. Therefore no sorption coefficient can be evaluated. The very low retardation indicates that pores with very low sorption and low porosity have been the active diffusion pathways. Other parts of the porosity, like the biotite, may retard the Ba more strongly, and may therefore not contribute to the transport of tracer over the time frame in this experiment. Low sorption and diffusivity is observed also for Cs experiments in Fine-grained granite, cell 22 (Fig. 4-7). The diffusivity is lower than expected from the HTO transport, which indicates that the active pores in the transport (980301) are not the same as for the HTO measurement. However, a small K_d value of $2 \cdot 10^{-5}$ can be calculated from the retardation factor. The diffusion in different pathways is further discussed in section 4.2.3.3.

Table 4-2 Sorption coefficients, K_d, (eq. 3-2) for the 2-4 mm fraction, extrapolated $K_{d,i}$ (eq. 3-13) and average diffusion K_d for Na^+ Ca^{2+} and Sr^{2+}.

Tracer	Rock type	K_d, (m^3/kg) batch 2-4mm	$K_{d,i}$, (m^3/kg) batch, extrapolated	K_d (m^3/kg) diffusion exp.
Na^+	ÄD	$6.6\pm0.6\cdot10^{-6}$	$6.3\pm0.2\cdot10^{-6}$	$1.4\pm0.6\cdot10^{-6}$
	FGG	$4.0\pm0.5\cdot10^{-6}$	$3.3\pm0.4\cdot10^{-6}$	$2.9\pm0.4\cdot10^{-6}$
Ca^{2+}	ÄD	$3.8\pm1\cdot10^{-5}$	$3.2\pm1\cdot10^{-5}$	$5.2\pm1.3\cdot10^{-6}$
	FGG	$1\pm0.3\cdot10^{-5}$	$9\pm0.5\cdot10^{-6}$	$3.6\pm1.5\cdot10^{-6}$
Sr^{2+}	ÄD	$3.4\pm0.8\cdot10^{-5}$	$2.8\pm1.3\cdot10^{-5}$	$4.7\pm0.8\cdot10^{-6}$
	FGG	$1.3\pm0.5\cdot10^{-5}$	$1.1\pm0.2\cdot10^{-5}$	$4.5\pm0.6\cdot10^{-6}$

The K_d-values evaluated from the diffusion experiments correspond best to the batch K_d-values obtained with the largest size fractions (2-4 mm). This indicates that the large particle size is the most representative for estimating K_d for bulk rock. Possibly, this is due to the fact that the largest size fraction consists of whole mineral grains. This is not the case for the smaller size fractions where the mineral grains have been divided during the sample preparation.

When estimating K_d which is valid for the bulk rock from batch experiments, the $K_{d,i}$ value should be most correct to use since the largest size fractions consist of only about 10% outer surface. With this method (described in section 3.2.2.6) the $K_{d,i}$ can be estimated without measuring the surfaces of the size fractions. A summary of the batch K_d for the largest size fraction, the evaluated $K_{d,i}$ and the average diffusion K_d are presented in Table 4.2. The diffusion K_d for both the Äspö diorite and the fine-grained granite tend to increase in the same order as observed in the batch experiments. It should also be noted that the $K_{d,i}$ gives an overestimation compared to the diffusion K_d by a factor of 2-6.

4.1.5 Conclusions

Prediction of K_d, for weakly, ion exchangeable sorbing tracers in laboratory diffusion experiments, based on laboratory batch experiments, may overestimate the matrix diffusion related K_d if small size fractions are used. The comparisons show that large size fractions are the most representative for estimating the K_d in bulk rock samples possibly due to that these fractions consists of polymineralic grains.

The observed differences in D_e between HTO and Na^+, Ca^{2+} or Sr^{2+} are related to differences in water diffusivity, D_w, and no influences of the material properties were observed on the D_e.

There are tendencies of decreasing D_e and α with increasing cell lengths, indicating that the transport porosity (and the storage porosity) decreases with increasing cell lengths. It is probable that the shorter samples overestimates the D_e and α since the length of the samples are of the same size as the heterogeneity of the samples.

4.2.1 Penetration of Ca, Cs and Ba into the Rock

4.2.1 Introduction

The properties of the rock matrix along actual and potential groundwater pathways are the most relevant parameters determining the ability of the geosphere to retard radionuclides released from repositories at depth in crystalline bedrock. Porosity data give information on the ability of the rock matrix to retard radionuclides by diffusion into the rock matrix. However, bulk porosity data alone are not sufficient to evaluate which mineral phases which are potentially able to sorb radionuclides. Knowledge of intra- and inter granular porosities and the spatial distribution of the pore space in is necessary. A relevant property to be quantified is the accessible internal volume determining diffusive transport in the host rock.

In this work the open pore system, its geometry and relation with mineralogy, is studied at centimetre scale using the ^{14}C-PMMA method (Hellmuth *et al.* 1993, 1994, Rasilainen *et al.*, 1996), which gives quantitative information on magnitudes and spatial distribution of porosity in the rock matrix. The results of the characterisation of the pore system are used as a basis for evaluation of the diffusion results obtained by analysing the breakthrough curves or concentration profiles of the rock samples. By using HTO (^{3}HHO) as an inert tracer in the diffusion experiments, the porosity in the rock samples can be determined. Thus, distribution coefficients, K_d, and effective diffusivities, D_e, can be evaluated from the concentration profiles according to common diffusion theory. The distribution coefficients obtained from the diffusion experiments are compared with distribution coefficients obtained from measurements on crushed material.

4.2.2 Experimental

4.2.2.1 Materials

Drill cores (∅ 35.1 mm) of Fine-grained granite and Äspö diorite were obtained from the Äspö Hard Rock Laboratory (HRL).

The tracers used were tritiated water, HTO, $^{137}Cs^+$, $^{45}Ca^{2+}$ and $^{133}Ba^{2+}$. The radioactive tracers were injected in concentrations that gave a negligible increase of the natural elemental concentrations in the groundwater. Elemental concentration gradients and non-linear sorption phenomena in the diffusion cells were thus avoided. All concentrations mentioned in the results refer to the concentration of the radioactive tracers.

A synthetic groundwater representative for the Äspö 340 m level, Table 2-7, was used in the experiments. In order to obtain non-oxic conditions, all experiments were performed in glove boxes with N_2-atmosphere at an ambient temperature (20-25 ^{o}C).

4.2.2.2 ^{14}C-PMMA method

One sample of Äspö diorite and one of Fine-grained granite were impregnated with ^{14}C-labelled methylmethacrylate (^{14}C-MMA), and the total porosities and spatial porosity distributions were determined (Hellmuth *et al.*, 1993, 1994, Rasilainen *et al.*, 1996). The samples consisted of two rock cores having a length of 40 mm. The method employs impregnation of vacuum dried rock samples by ^{14}C-MMA, radiation polymerisation, autoradiography and digital image processing techniques. Migration pathways can be identified and visualised and porosity histograms of the matrix (2D images) can be obtained.

MMA is a monomer with a low viscosity. Its contact angle on silicate surfaces is low leading to a rapid impregnation of the bulk rock specimen. It behaves in the rock matrix like a non-sorbing tracer. Transferring the MMA monomer at a slow rate ensures degassing of the monomer and initially infiltration of vapour only. The impregnation time was 7 days. After impregnation, the samples were irradiated with gamma rays from a ^{60}Co source to polymerise the monomer in the rock matrix. The required dose was 50 kGy.

Irradiation of the rocks with ^{60}Co causes strong thermoluminescence of K-feldspar and other rock forming minerals, which later exposes autoradiographic film. To avoid this, the thermoluminescence was released by heating the samples to 120°C for three hours before sawing. The samples were sawed in three pieces with a diamond saw (Buehler, Isomet, Low Speed Saw). The surfaces were exposed on a β film (Hyperfilm-βmax, Amersham), which is a high performance autoradiographic film for low energy β-emitting radionuclides. The exposure times were 9 to 22 days.

4.2.2.3 Digital image processing and calculation of porosity

A table scanner measures the intensities of autoradiographs in 256 grey levels, with an optical resolution of 600 dpi. The resolution of ^{14}C-PMMA autoradiographs is about 20 to 30 μm.

Interpretation of the results is based on digital image analysis of autoradiographs which starts from discretising the autoradiograph into pixels (about 30x30μm). Basically all the intensities of the subdomains are converted into corresponding optical densities which in turn are converted into activities with the help of measured calibration curves for each exposure. Finally, the activities are converted into porosities. In principle the interpretation is based on studying the abundance of tracer in each subdomain. The rock is approximated by a homogeneous mixture of minerals and pore space. This assumption is applicable when the pore apertures are below the limit of lateral resolution of autoradiography. The method has successfully been applied in several other studies (Hellmuth *et al.*, 1993, 1994, and Rasilainen *et al.*, 1996).

4.2.2.4 Diffusion experiments

The rock discs were cast with an epoxy resin and mounted between two water containers. One side of the diffusion cell was spiked with a sorbing tracer and HTO as an inert reference. The concentration increase on the other side of the diffusion cell was monitored under stagnant groundwater conditions. The setup for the through diffusion experiments is thoroughly described in section 4.1. Three different lengths of the rock slabs were used: 1,2 and 4 cm.

For the tracers where no breakthrough could be observed, the concentration profiles in the rock samples were measured. The samples were first sawn parallel to the diffusion direction. One of the two parts was used for autoradiography, and the other part was sawn into slices of approx. 0.5-1 mm thickness. Concentration profiles were determined by measuring the radioactivity content in the slices using a HPGe-detector. Radioactivity of HTO and $^{45}Ca^{2+}$ was measured using liquid scintillation counting (LKB Wallac, Rackbeta 1219) and $^{133}Ba^{2+}$ and $^{137}Cs^{+}$ were measured using a HPGe-detector (EG&G, ORTEC, USA).

4.2.2.5 Theory of In-diffusion

The analytical solution to the transport equation for the in-diffusion experiments assuming a linear sorption isotherm, a homogeneous porosity of the solid, constant C_0 during the experiment and a semi-infinite boundary at the sealed end of one sample is (Crank, 1975),

$$\frac{C_x}{C_{x=0}} = \alpha \cdot \mathrm{erfc}\left(\frac{x}{2\sqrt{\frac{D_e}{\alpha}t}}\right) \qquad 4\text{-}4$$

where C_x is the measured average concentration of a slice at distance x and time t, $C_{x=0}$ is the constant concentration in the pore water in the first thin layer at the surface of the solid, $\alpha = \varepsilon + K_d\rho$ is the rock capacity factor and erfc is the error function complement (erfc = 1-erf). The apparent diffusivity, D_a, is related to the effective diffusivity, D_e, the total porosity ε, the density of the bulk rock, ρ , and the sorption distribution coefficient, K_d, by

$$D_a = \frac{D_e}{\varepsilon + K_d \cdot \rho} = \frac{D_e}{\alpha} \qquad 4\text{-}5$$

D_e and α were obtained by fitting eq. 4-4 to the measured data. The porosity data that were used for evaluation of K_d was determined from through diffusion experiments with HTO, see Table 4-1.

4.2.3 Results and Discussion

4.2.3.1 Porosity Distribution in Äspö diorite and Fine-grained granite

Photographs of sawed rock surfaces and the corresponding autoradiographs of ^{14}C-MMA impregnated samples of Äspö diorite and Fine-grained granite are shown in Figure 4-8.

The Äspö diorite shows a heterogeneous and mineral specific porosity distribution. The measured total porosity is 0.4±0.1 %. Mineral grainboundaries were not observed to form the main migration pathways in the diorite matrix. Quartz and large K-feldspar crystals were not impregnated and can be classified as non-porous minerals with this method. The dark (porous) areas in the autoradiographs form a connected network of migration pathways with relatively high porosity. This network is the consequence of a complex mixture of minerals dominated by biotite, plagioclase and chlorite all having small (<0.5 mm) grain sizes. The highest porosities observed in the network were 1.5-3%, found near large quartz and feldspar mineral crystals. In comparison with the Fine-grained granite, the Äspö diorite has a much wider porosity distribution, see Figure 4-8. A slight direction dependence of the porosity was found, but larger pieces of rock samples should be examined to ensure this.

The porosity pattern of Fine-grained granite was uniformly distributed although a slight foliation could be observed in the autoradiographs. This is also clearly seen in the texture of sawn rock surfaces. The high porosity minerals are not observed to form a connected network as observed in the Äspö diorite. The porosity is low, 0.2±0.1 %, indicating very small pore apertures in all minerals and the differences in porosity between minerals was not clearly shown using the ^{14}C-PMMA method. The highest porosities are 0.8 to 1.0 % determined in some points, which were smaller than 0.5 mm in diameter. Intensive dark spots in autoradiographs (see Fig. 4-8 and 4-9) were excluded from the quantitative analysis because they are due to natural radioactivity (Thorium series).

No obvious differences in absolute porosity are observed between the different methods used in this study, see Table 4-3. The uncertainty in the ^{14}C-PMMA method is associated with the spatial distribution of porosities. The diffusion porosity (through diffusion in resin cast samples) shows a much larger distribution between different samples than the water saturation porosity. This may be caused by variability in the connectivity of the pores in different samples, due to the heterogeneity of the pore system in the centimetre scale. In Äspö diorite the diffusion porosity seems to be about 60% of the water saturation porosity. This indicates that all of the porosity measured with the water saturation method is not available for diffusion. Thus, the porosity measurement by HTO diffusion shows a directional dependence, since only the flat surfaces of the cast rock cylinders are in direct contact with water.

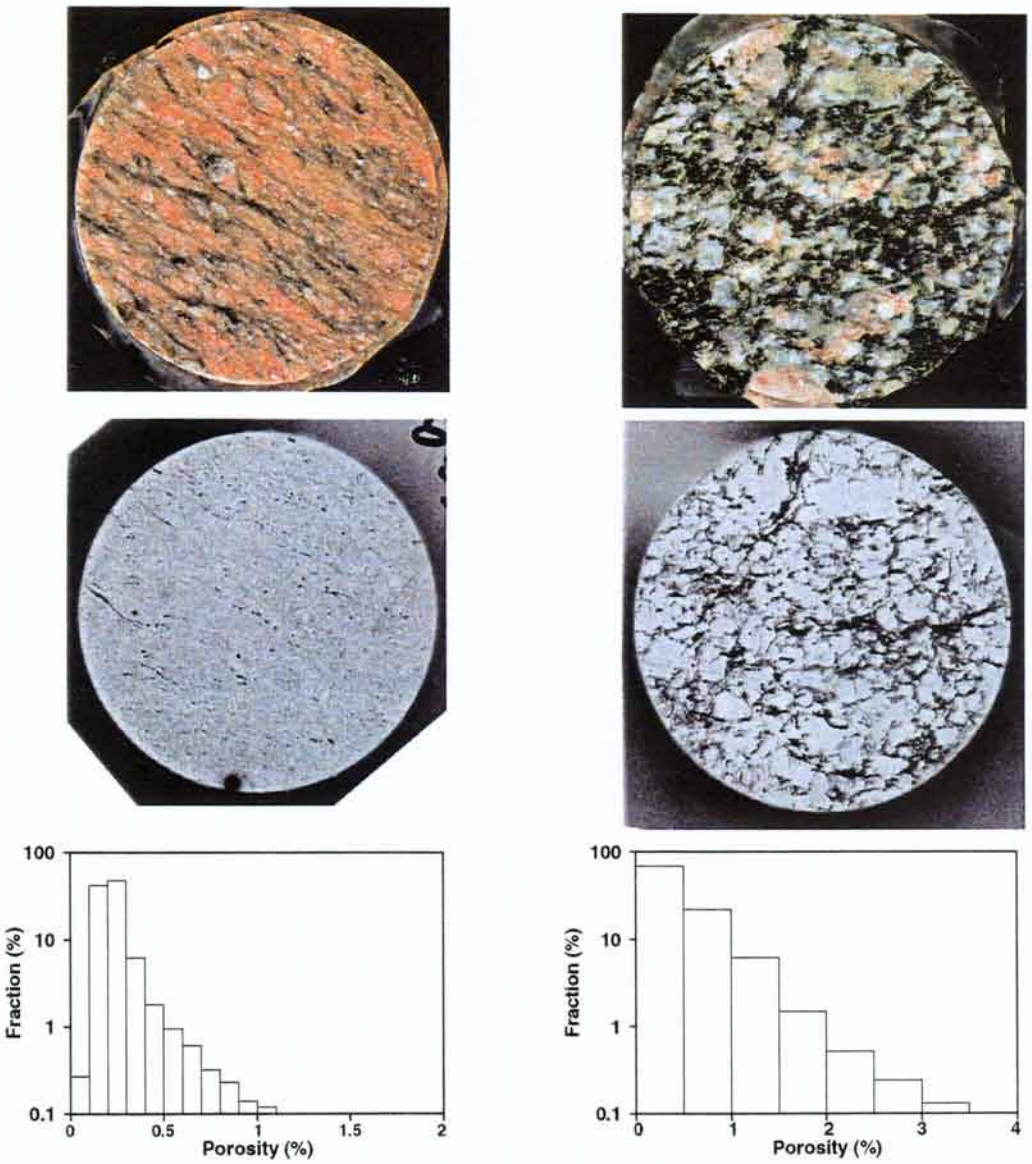

Figure 4-8. Photograph (top), corresponding autoradiograph (middle) and porosity distribution (bottom) of ^{14}C-PMMA impregnated samples of Äspö diorite (right) and Fine-grained granite (left).

Table 4-3. Comparison of porosities measured with different techniques: water saturation, through diffusion measurements and the ^{14}C-PMMA method.

Rock type	Water saturation[a] (% ±1 σ between samples)	Through diffusion[b] (% ±1σ between samples)	^{14}C-PMMA method[c] (% ±1 σ)
ÄD	0.55 ± 0.06	0.35 ± 0.15	0.4 ± 0.1
FGG	0.25 ± 0.01	0.3 ± 0.2	0.2 ± 0.1

[a] Measured on 1,2 and 4cm thick drill core slices, Äspö diorite 6 samples, Fine-grained granite 10 samples.
[b] From HTO through diffusion in 5 samples of 2cm thickness for each rock type.
[c] Measured on 4cm thick drill core samples.

As the matrix of Fine-grained granite is uniformly distributed, smaller variations in diffusion data than for Äspö diorite are expected. However, a few filled fissures observed in the Fine-grained granite may have caused the variability in porosity measured with the through diffusion method. In some samples of Fine-grained granite, the diffusion porosity is larger than the water saturation porosity. This may be due to porosity created at the boundary between the epoxy resin and the rock. Some observations of sorption/diffusion in the boundary of Fine-grained granite have been made from autoradiographs of sorbing tracers. However, investigations of some autoradiographs from the of measurement container side of the diffusion slab shows that the exposure from the boundary is low compared to the exposure of the other areas of the slab. Therefore the amounts transported in the boundary is considered to give a negligible contribution to the total mass transport of the tracers.

4.2.3.2 Concentration profiles of $^{45}Ca^{2+}$

Photographs of sawn rock surfaces (sawn parallel to the diffusion direction) and the corresponding autoradiographs of Äspö diorite (cell 17) and Fine-grained granite (cell 16) using $^{45}Ca^{2+}$ as tracer are shown in Figure 4-9. The through diffusion rate of $^{45}Ca^{2+}$ was close to steady state (constant transport rate) before the diffusion cells were dismantled. Nearly linear concentration profiles were expected, which was also found by activity analysis of the sawn rock slices (*cf.* Figure 4-10).

The migration pathways observed for $^{45}Ca^{2+}$ within Äspö diorite are consistent with the pore system that was characterised using the ^{14}C-PMMA method. In quartz and potassium feldspar grains of Äspö diorite, no tracer activities were found by autoradiography. As will be described below for $^{137}Cs^{+}$ and $^{133}Ba^{2+}$, two pathways can be distinguished in the evaluation of intensities in the autoradiographs, *i.e.* two major tracer concentration intervals.

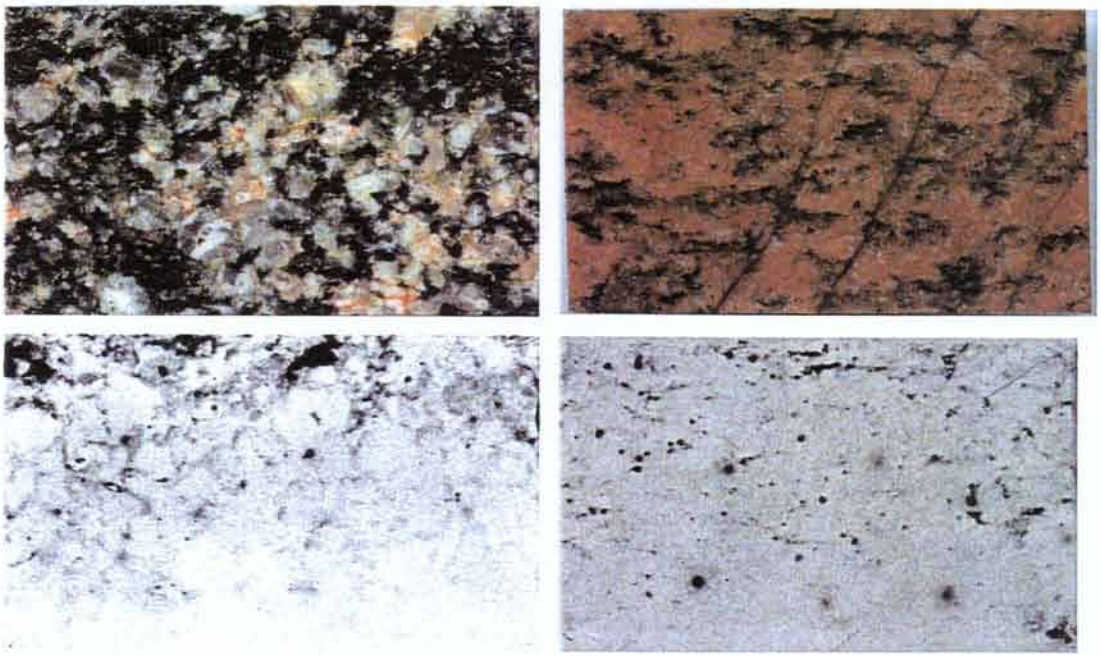

Figure 4-9. *Photograph (top) and corresponding autoradiograph (bottom) of through diffusion of $^{45}Ca^{2+}$ in cell 17, Äspö diorite (left) and cell 16, Fine-grained granite (right). Direction of diffusion is from top to bottom.*

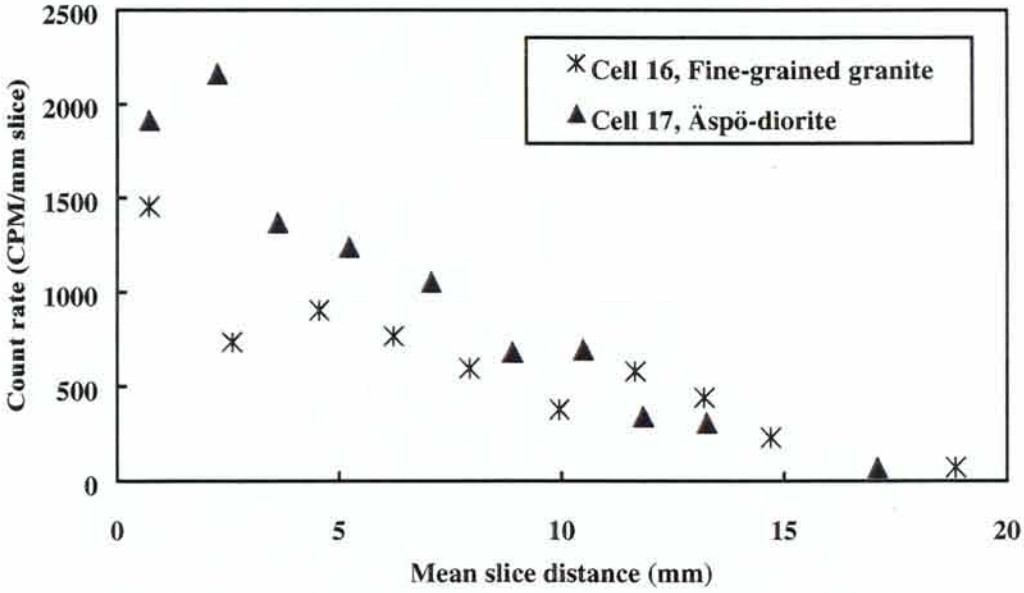

Figure 4-10 *Concentration profile of obtained for the through diffusion of $^{45}Ca^{2+}$ in cell 17, Äspö diorite and cell 16, Fine-grained granite*

The distribution of $^{45}Ca^{2+}$ in Fine-grained granite shows some consistency with the ^{14}C-PMMA autoradiographs, but the activities are too low to get a reliable evaluation of the concentration profile by autoradiography. Activities were only found in dark spots, associated with plagioclase containing muscovite or sericite. The sample of Fine-grained granite contained visible filled micro-fissures, crossing the bulk rock structure of the sample. No activity increase caused by sorption appears however, in the micro-fissures observed in the autoradiograph. However, in other samples micro fissure fillings that had higher porosity have been observed by the ^{14}C-PMMA method.

4.2.3.3 *Concentration profiles of $^{133}Ba^{2+}$ and $^{137}Cs^{+}$*

The penetration profiles obtained in the 2cm cells for $^{133}Ba^{2+}$ and $^{137}Cs^{+}$ are shown in Figs. 4-11 and 4-12. None of the profiles could be fitted satisfactorily using one set of D_e and α (equivalent to a single D_a). Similar results for granites have been obtained in other studies (Ittner *et al.*, 1990, Idemitsu *et al.*, 1992 and Tsukamoto *et al.*, 1993). The measured profiles appear to consist of two parts, one slower process for the short penetration depths and one faster process for the deeper penetration. Assuming that the experimentally obtained concentration profiles are the sum of diffusion in the two separate networks, approximate values of D_e and α can be obtained by curve fitting of Eq. 4-4 to the measured data. The results are summarised in Table 4-4

It is obvious that the darker intensities of the autoradiographs show different migration pathways than the light intensities, see *e.g.* Fig. 4-13 where the optical densities for Cs is plotted vs. penetration depth. The dark part corresponds to the sorptive mineral part of the matrices, where pores with high porosity and high sorption capacity minerals, *e.g.* biotite in the Äspö diorite, are found. This part provides the migration pathways for the slow process, which gives the dominating mass transport in the sample. Comparatively high D_e (due to high porosity) and high K_d (due to high sorption capacity) are expected for this part of the matrix, which is in good agreement with the fitted data. The D_a is low due to the high K_d. Contrary to the slow process; the fast process has a somewhat lower D_e, but a high D_a due to a much lower K_d. It is indicated by ^{14}C-PMMA impregnation that this pore system has low porosity, which is in agreement with the low D_e. According to the low K_d-values, the fast process part is supposed to contain low capacity minerals. The pathways of the slow process are thus the most important in terms of retention capacity, since they have the highest porosity and sorption capacity.

Double migration pathways are sufficient to reproduce the shape of the concentration profiles obtained for the rock types used in these experiments, which is indicated by the superposition of the theoretical profiles in Figs. 4-11 and 4-12. Multiple pathways have also been considered in other studies (Tsukamoto *et al.*, 1993 and Atkinsson *et al* 1988). In reality, the porosity is a complex combination of variable apertures with a heterogeneous spatial distribution. Since D_e is a function of the porosity, a distribution of D_e together with a description of the connectivity of the porosity and the distribution of the sorbing minerals should be accounted for. Then, the simple model used for evaluation of this work generally is not applicable, since by definition it is only valid for homogeneous material.

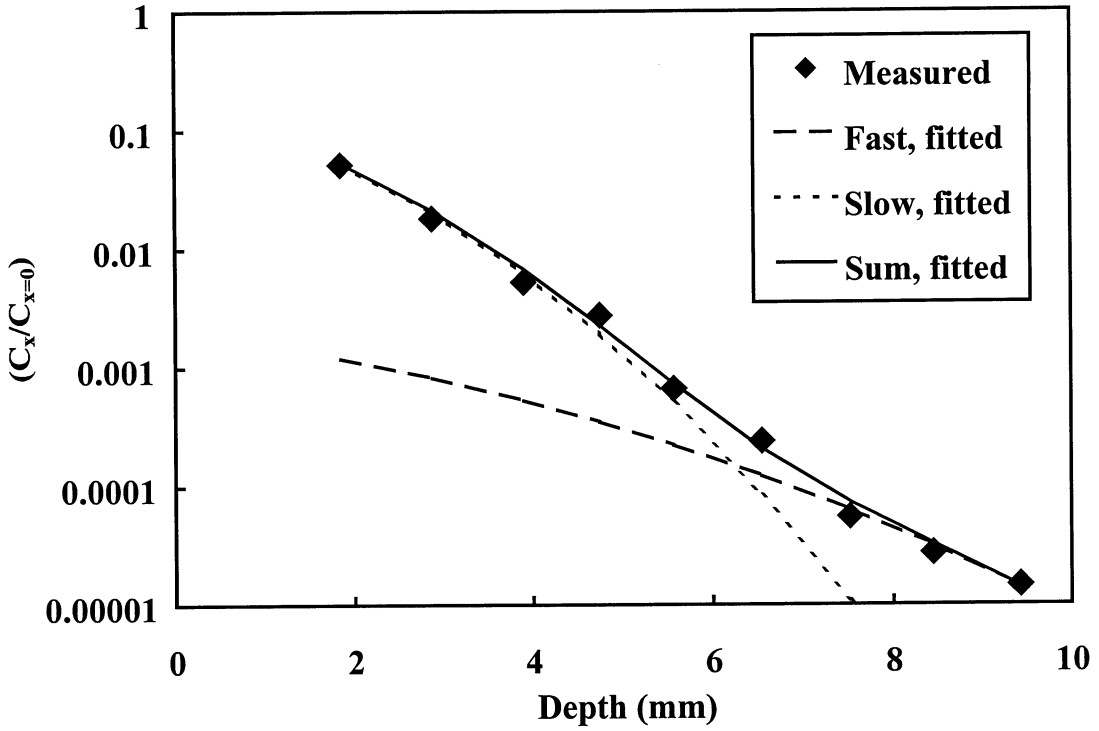

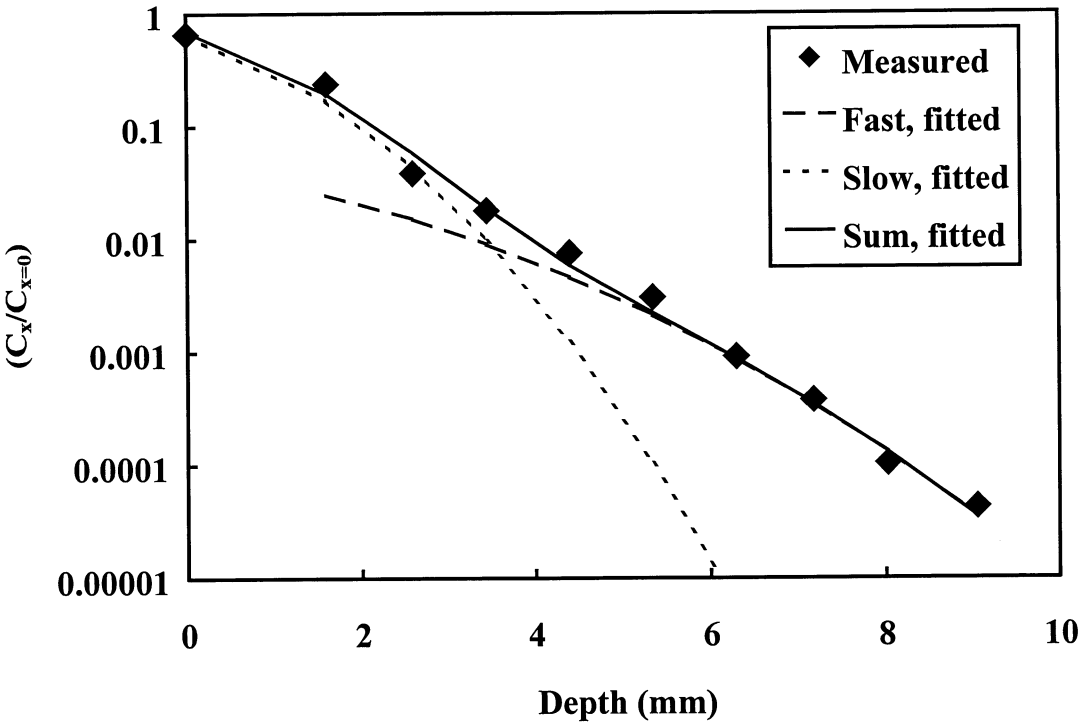

Figure 4-11. Concentration profiles of Ba^{2+} in Äspö diorite, cell no 21, (bottom) and Fine-grained granite, cell no 20, (top). Diffusion time 472 days.

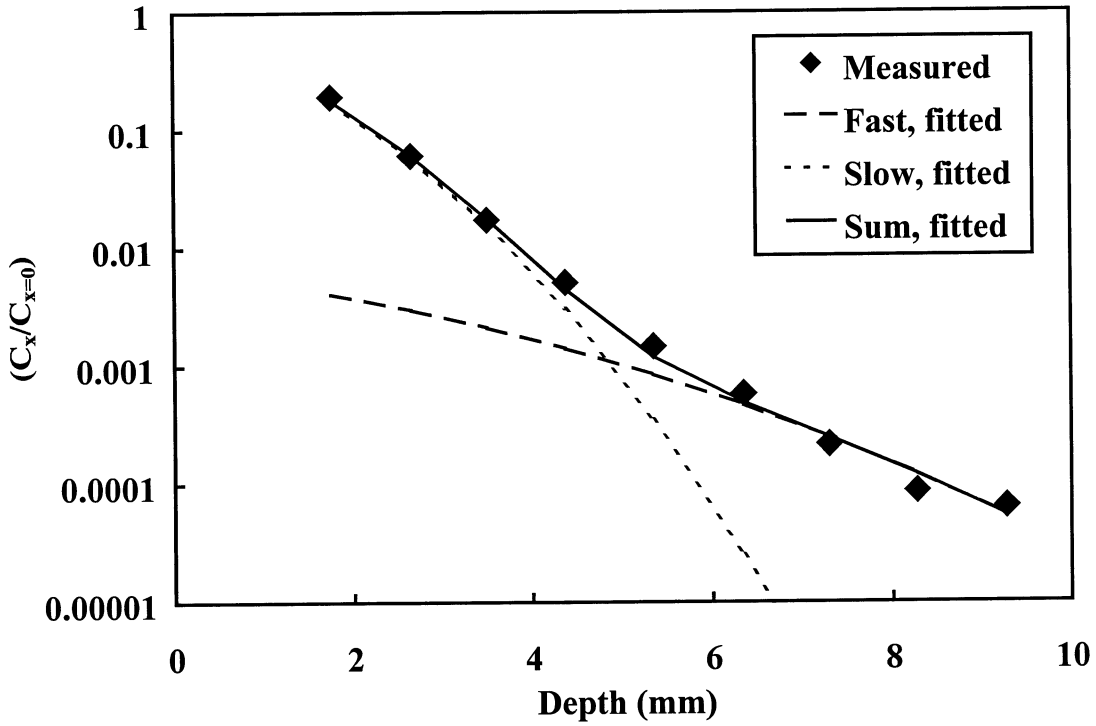

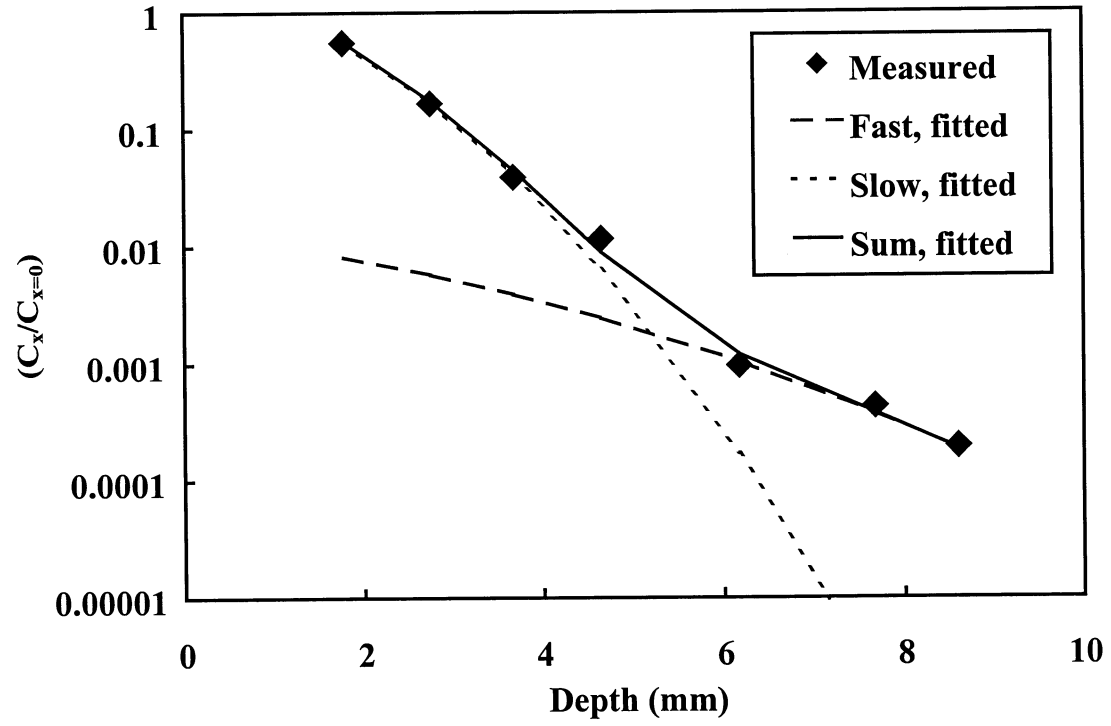

Figure 4-12. *Concentration profiles of Cs^+ in Äspö diorite, cell no 25 (bottom) and Fine-grained granite, cell no 24, (top). Diffusion time 472 days.*

Table 4-4. Summary of parameters derived from fitting of the two pathways model to the experimental results. The porosities are based on the through diffusion experiments with HTO in the same diffusion cells, (*cf.* Table 4.1). For comparison, For cell number 19 and 22, through diffusion data of $^{133}Ba^{2+}$ and $^{137}Cs^{+}$ from 1 cm cells are presented.

				Slow process (short penetration)				Fast process (deep penetration)			
Cell no	Ele-ment	Rock Type	ε	D_e (m^2/s)	α (1)	K_d (m^3/kg)	D_a (m^2/s)	D_e (m^2/s)	α (1)	K_d (m^3/kg)	D_a (m^2/s)
20	Ba^{2+}	FGG	$9\cdot10^{-4}$	$7\cdot10^{-15}$	0.16	$6\cdot10^{-5}$	$4\cdot10^{-14}$	$3\cdot10^{-16}$	$2\cdot10^{-3}$	$4\cdot10^{-7}$	$1.5\cdot10^{-13}$
21	Ba^{2+}	ÄD	$2.2\cdot10^{-3}$	$1.6\cdot10^{-14}$	0.65	$2\cdot10^{-4}$	$2\cdot10^{-14}$	$4\cdot10^{-15}$	$4.5\cdot10^{-3}$	$2\cdot10^{-5}$	$9\cdot10^{-14}$
24	Cs^{+}	FGG	$1.1\cdot10^{-3}$	$2\cdot10^{-14}$	0.69	$3\cdot10^{-4}$	$3\cdot10^{-14}$	$1\cdot10^{-15}$	$6.7\cdot10^{-3}$	$2\cdot10^{-6}$	$1.5\cdot10^{-13}$
25	Cs^{+}	ÄD	$3.2\cdot10^{-3}$	$6.5\cdot10^{-14}$	2.2	$8\cdot10^{-4}$	$3\cdot10^{-14}$	$2\cdot10^{-15}$	0.13	$4\cdot10^{-6}$	$1.5\cdot10^{-13}$

				Through diffusion measurement			
				D_e (m^2/s)	α (1)	K_d (m^3/kg)	D_a (m^2/s)
19	Ba^{2+}	ÄD	$3.5\cdot10^{-3}$	$5\cdot10^{-16}$	$2\cdot10^{-3}$	-	$2.5\cdot10^{-13}$
22	Cs^{+}	FGG	$4.1\cdot10^{-3}$	$1.8\cdot10^{-14}$	0.06	$2\cdot10^{-5}$	$3\cdot10^{-13}$

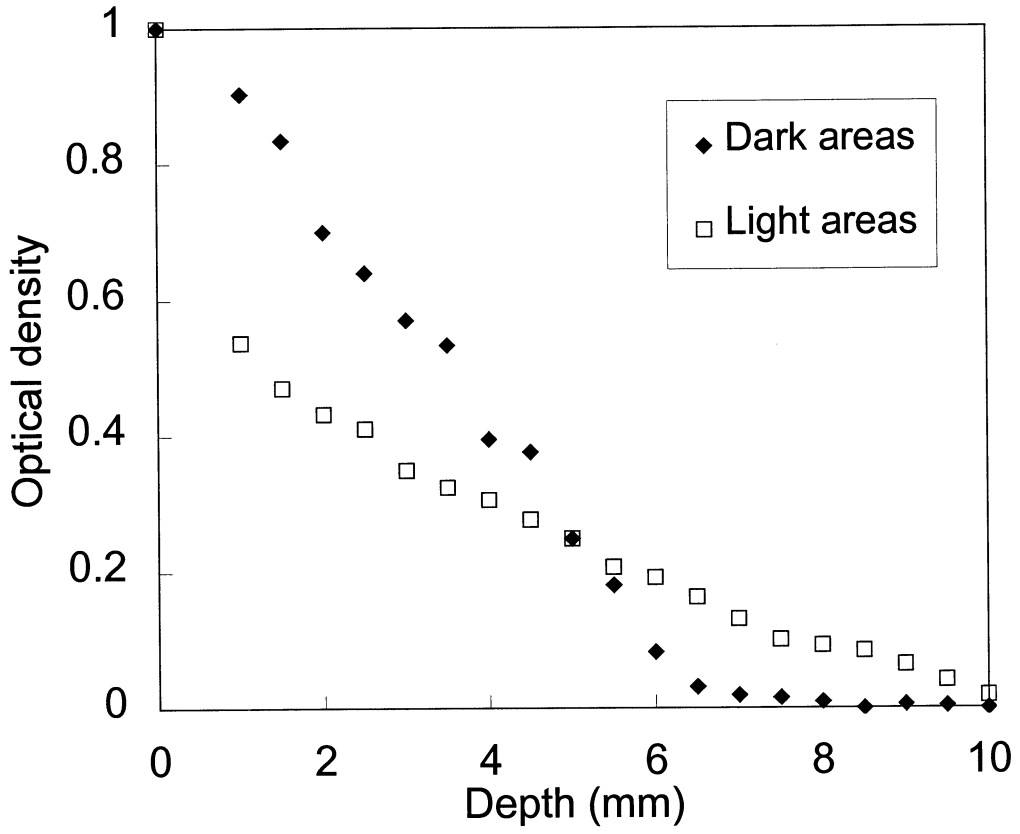

Figure 4-13 Optical density versus penetration depth from autoradiograph of $^{137}Cs^{+}$ profile in Äspö diorite.

Through diffusion of $^{133}Ba^{2+}$ in Äspö diorite and of $^{137}Cs^{+}$ in Fine-grained granite was evaluated after 22 months diffusion time, see Fig. 4-6 and 4-7. The obtained D_a is of the same order as the D_a from the fast process in the concentration profiles, which indicates that at this time, the slow pathways may not yet fully contribute to the transport.

A comparison of the formation factor ($F = D_e / D_w$, where D_w is the water diffusivity) for $^{137}Cs^{+}$ and $^{133}Ba^{2+}$ with the formation factor for HTO, shows a factor of ~2 smaller factor for Cs^{+} and Ba^{2+}. This indicates that the pore system is similar for the diffusion of Cs^{+}, Ba^{2+}, and HTO, see Fig 4-5. Consequently, by using the rock formation factor and water diffusivities, the D_e can be reasonably well estimated for Na, Ca, Sr, Ba and Cs.

A comparison of K_d-values obtained from batch experiments with crushed material is presented in Table 4-5. Approximately one order of magnitude lower K_d-values are obtained from diffusion experiments compared to batch experiments using large particle size fractions. Even larger differences are often observed for smaller size fractions (<2mm). This is probably a result of increased surface areas due to the crushing of the geological material, which was also observed by BET measurements. Similar results were obtained for Na^{+}, Ca^{2+} and Sr^{2+} (see section 4.1). By definition K_d describes the reversible distribution of a species between a solid phase and solution. Since this work (see Table 4-5) and earlier batch experiments (Byegård *et al.*, 1995) indicate that among the alkaline and alkaline earth metals, Cs, Ba, and Rb are to some extent irreversibly sorbed within the time frame of the experiments, the usefullness of batch K_d in transport and diffusion experiments can be questioned. The K_d values evaluated from diffusion experiments are therefore more adequate for predicting the transport rate. However, since irreversible sorption is observed for some of the studied elements it is not possible to state that the total mass is transported by the observed diffusion rate. A significant part of the mass can according to the batch experiments result be irreversibly lost by sorption and therefore not be transported at all.

Qualitative estimation of mineral specific sorption of Cs^{+} and Ba^{2+} was made from the autoradiographs. Sorbing minerals were difficult to identify. All autoradiographs show dark and light areas indicating double migration pathways. In Äspö diorite, it was found that large K-feldspar grains do not sorb Cs^{+} and Ba^{2+} and that the dark intensities were found in biotite rich regions. Cs^{+}, which has the highest K_d-value of the studied tracers, shows the most mineral-specific sorption in the Fine-grained granite. In the Fine-grained granite, dark veins of plagioclase containing inclusions of chlorite and muscovite are found to contain the radionuclides, but it was difficult to distinguish and identify the specific minerals containing Cs^{+}.

4.2.3 Conclusions

Evaluation of radionuclide transport in crystalline rock using models for homogeneous materials can give erratic results since large heterogeneities are observed at all scales of crystalline rock matrices. In order to use models which presume homogeneous materials, one has to know that effects of heterogeneity are such that the use of overall bulk parameters will give representative results. In this work, two different pathways, also experimentally observed, were used to describe the diffusion in centimetre scale. It is found that the knowledge of non-uniform distributions of porosity and sorptive

Table 4-5 Comparisons of the distribution coefficient, K_d, determined for Ba^{2+} and Cs^+ using different methods. The distribution coefficients for the batch sorption and desorption experiments are determined using a contact time of 14 days (cf. section 3.2.2). K_d for the diffusion experiments is evaluated from the short penetration depths (slow migration pathways).

Radio-Nuclide	Rock Type	K_d batch exp. (m^3/kg)	K_d desorption batch exp. (m^3/kg)	K_d diffusion exp. (m^3/kg)
$^{133}Ba^{2+}$	FGG	$6 \cdot 10^{-4}$	$4 \cdot 10^{-4}$	$6 \cdot 10^{-5}$
$^{133}Ba^{2+}$	ÄD	$9 \cdot 10^{-4}$	$5 \cdot 10^{-4}$	$2 \cdot 10^{-4}$
$^{137}Cs^+$	FGG	$6 \cdot 10^{-3}$	$1 \cdot 10^{-3}$	$3 \cdot 10^{-4}$
$^{137}Cs^+$	ÄD	$3 \cdot 10^{-2}$	$4 \cdot 10^{-3}$	$8 \cdot 10^{-4}$

minerals are of great importance for the understanding of diffusion in crystalline rock. The conclusions are summarised below:

- The in-diffusion results can not satisfactorily be described by one set of D_e and α, using a homogeneous model. However, using common transport modelling, a double porosity network could be used to describe the results using a double set of D_e and α.

- The non-uniform distributions of porosity and sorptive minerals are reflected in the large differences in K_d and in D_e between the slow and fast pathways.

- Batch experiments may overestimate the sorbed fraction for alkali- and alkaline earth-metals in crystalline rock, compared to the sorbed fraction evaluated from diffusion experiments. This is probably caused by the creation of new surfaces when crushing the material for batch experiments.

- The use of batch K_d in transport modelling requires consideration of necessary surface correction and non- or slowly reversible sorption effects observed for some elements (Cs, Ba, Rb) within the time frame of the performed experiments. Further studies of the sorption mechanisms together with long-term kinetic studies are therefore essential in order to estimate reliable transport parameters for *e.g.* Cs^+.

- Areas with porous mineral are found to be consistent with the areas with sorbing minerals in Äspö diorite. Autoradiographic studies indicate two main migration pathways having different porosities and retention capacities. The penetration of the cations $^{45}Ca^{2+}$, $^{133}Ba^{2+}$ and $^{137}Cs^+$ follows the migration pathways (fast/slow) that are found with the ^{14}C-PMMA method used for porosity determination in Äspö diorite.

- In Fine-grained granite, the different porous phases can not be clearly found with the ^{14}C-PMMA method and the porosity pattern was uniform although a slight foliation was observed. Only diffusion of Cs^+ (which has the highest K_d-value of the studied tracers) shows mineral-specific sorption in the Fine-grained granite, where dark veins in the autoradiographs correspond to the foliation of the mineral texture.

4.3 Through Diffusion Experiment using Feature A Site-Specific Material

4.3.1 Experimental

The rock sample consists of a piece of rock making up the intersection of borehole KXTT1 with Feature A. Both sides of the sample have been in contact with groundwater. The uneven fracture surfaces are nearly parallell, and the thickness of the sample in the diffusion direction varies between approximately 16 to 20 mm. A part (~10%) of the start side has a depression, with 10 mm thickness at the thinnest point between the two sides.

Prior to casting the sample, the mantle surfaces were primed with epoxy resin (Araldit F with triethylenetetraamin as a hardener, Ciba Geigy). The casting of the sample was made inside a polymethylmethacrylate ring. To avoid contamination of the fracture surfaces with epoxy resin, a wall of tixotropic resin (particle filled resin that do not flow) was built round the bottom surface, in order to seal on to the underlying teflon tray. In the same way, the upper surface was protected by a thin wall of tixotropic resin after the first addition of resin. A second addition was needed to complete the casting. The resin was then grounded before the cast sample was mounted between two water containers. A picture of the cast sample is shown in Fig. 4-14.

Before addition of tracers, the sample was pre-equilibrated with synthetic groundwater under N_2-atmosphere. The composition of the water used is given in Table 2-7 (Feature A site-specific groundwater) The volume of each water container was 50 ml.

One side of the diffusion cell was spiked with a tracer cocktail and the activity increase on the other side of the diffusion cell was monitored. Liquid scintillation counting was used for HTO meaurements (LKB Wallac, Rackbeta 1219) and $^{22}Na^{+}$, $^{47}Ca^{2+}$, $^{82}Br^{-}$, $^{85}Sr^{2+}$, $^{86}Rb^{+}$, $^{131}I^{-}$, $^{133}Ba^{2+}$, $^{137}Cs^{+}$, ^{169}Yb-EDTA, ^{160}Tb-DTPA, ^{177}Lu-DOTA and $^{186}ReO_4^{-}$ were measured using a HPGe detector (EG&G ORTEC, 25%). The tracers were added in amounts that would give negligible increases of the concentrations in the synthetic groundwater. Fluorecent dye tracers (Uranine, Amino G Acid and Rhodamine WT) were also used in the experiment, but the start concentrations were too low to be able to obtain reliable concentration measurements in the measurement container in the diffusion cell.

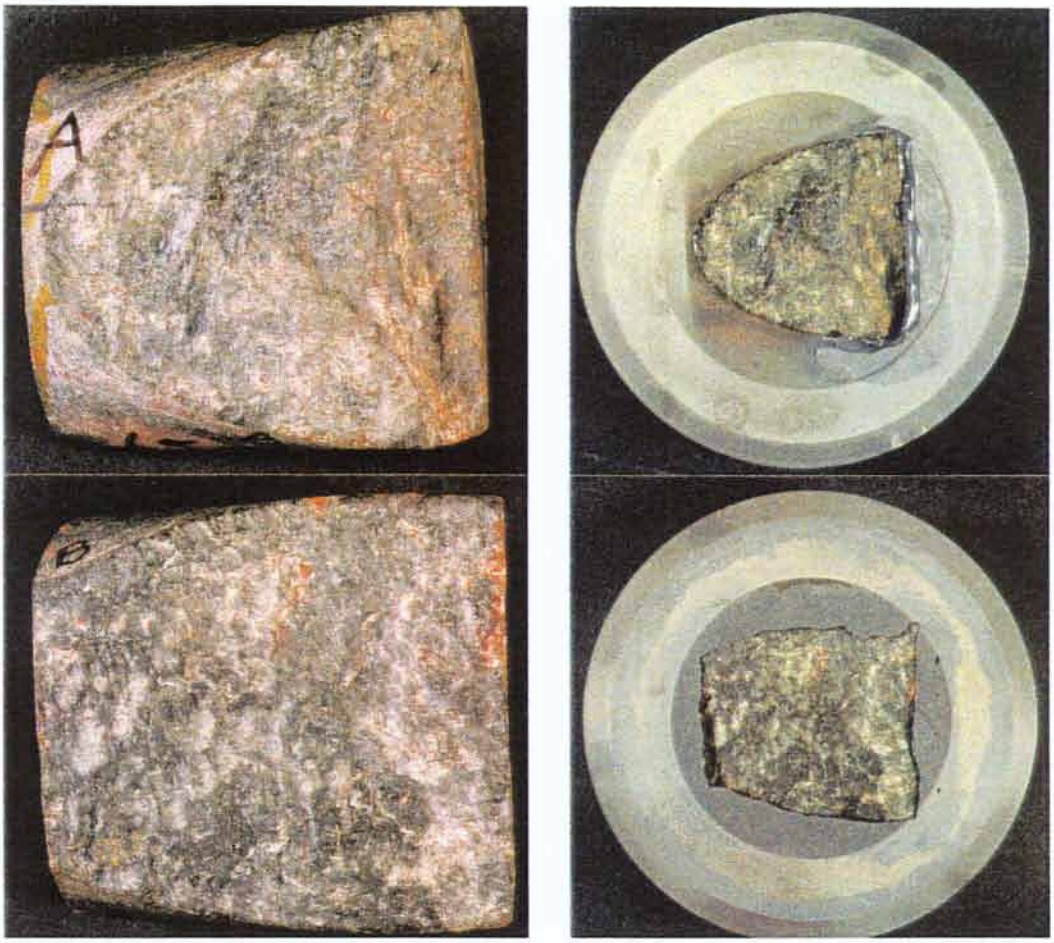

Figure 4-14 The high concentration side (top) and the low concentration side (bottom) of the KXTT1 diffusion cell. The left photographs show the both sides of the diffusion slab prior to casting and the right photographs show the diffusion slab after casting.

4.3.2 Results and discussion

All tracers except ^{86}Rb (decayed) were detected in the measurement container within 3 months. The breakthrough curves are presented in Fig. 4-15. Due to short half lifes, some of the radionuclides could only be monitored for a few weeks.

An attempt was made to evaluate the breakthrough curves using the one-dimensional solution to the diffusion equation (eq. 4-1), assuming that the length of the sample is 18 mm. Obviously, this is an oversimplification, but the evaluation gives an indication of the range in diffusivities. The results of the evaluation are presented in Table 4-6.

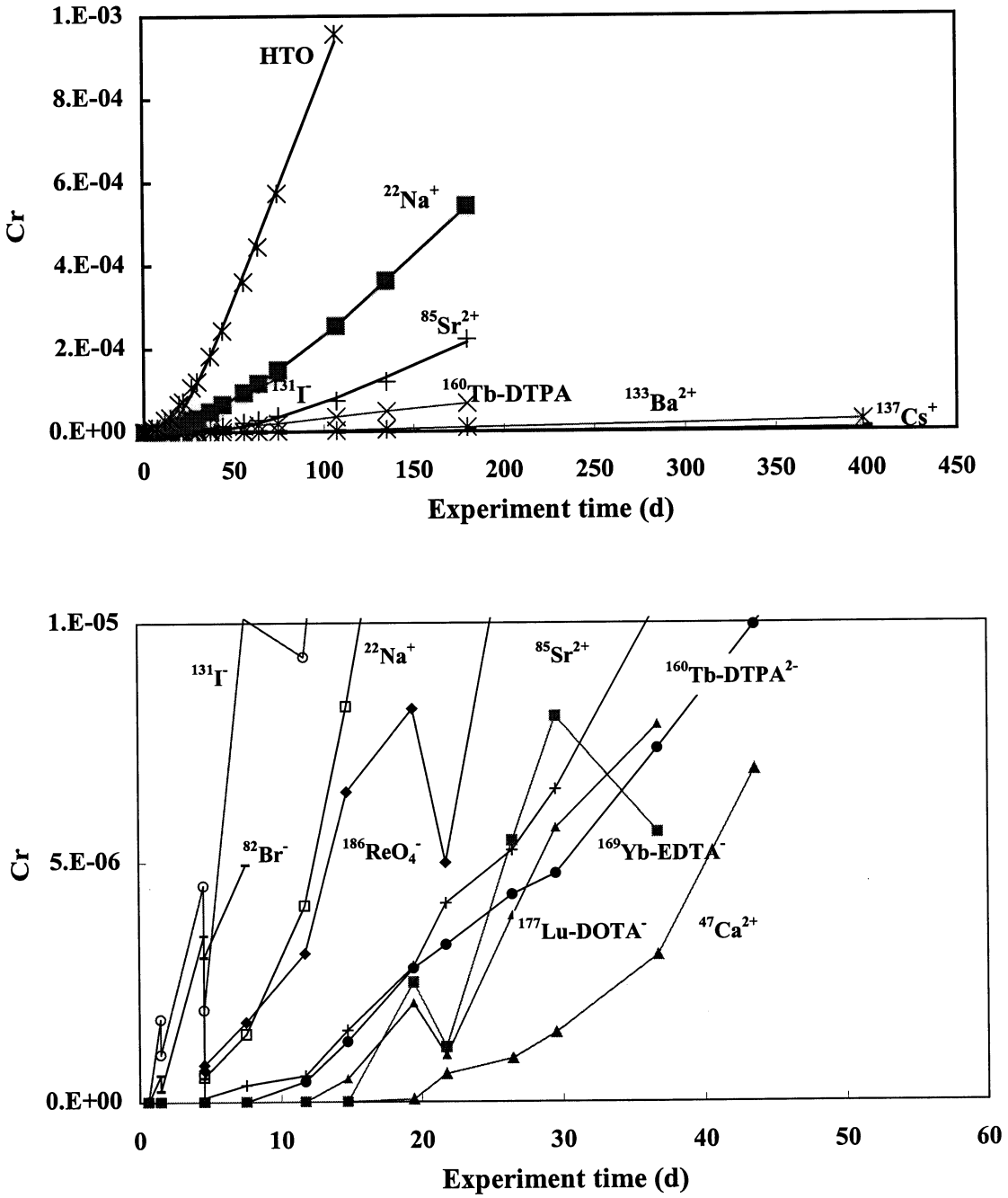

Figure 4-15 Scaled ratio of concentration versus experimental time. The lower figure is an enlargement of the first 2 months. The lines for HTO, Na and Sr in the top figure is the fit of the data to a one-dimensional diffusion equation (4-1).

Table 4-6 Evaluation of breakthrough data by a least square fitting of the data to the one-dimensional solution of the diffusion equation. $D_{w,i}$ is the free water diffusivity of ion i at infinite dilution.

Tracer	D_e exp. (m^2/s)	α (1)	$D_{w,i}$ / $D_{w,HTO}$ (m^2/s)	$D_{e,i}/D_{e,HTO}$ (m^2/s)
HTO	$4 \cdot 10^{-14}$	$1.5 \cdot 10^{-3}$	1	1
$^{137}Cs^+$	n.e.	n.e.	0.85	-
$^{131}I^-$	$4 \cdot 10^{-15}$	$1 \cdot 10^{-3}$	0.8	0.1
$^{82}Br^-$	n.e.	n.e.	0.8	-
$^{22}Na^+$	$1 \cdot 10^{-14}$	$< \alpha_{HTO}$	0.55	0.25
$^{186}ReO_4^-$	n.e.	n.e.	0.4	-
$^{133}Ba^{2+}$	n.e.	n.e.	0.22	-
$^{85}Sr^{2+}$	$7 \cdot 10^{-15}$	$< \alpha_{HTO}$	0.2	0.18
$^{47}Ca^{2+}$	$7 \cdot 10^{-15}$	$< \alpha_{HTO}$	0.2	0.18
^{169}Yb-DTPA	n.e.	n.e.	<0.1	-
^{160}Tb-EDTA	$1 \cdot 10^{-15}$-$2 \cdot 10^{-15}$	$< \alpha_{HTO}$	<0.1	0.02-0.05
^{177}Lu-DOTA	n.e.	n.e.	<0.1	-

The range of the measured diffusivity are within the expected range of the calculated diffusivity, if the tracer diffusivity in water relative to the water diffusivity in water ($D_{w,i}/D_{w,HTO}$) is assumed to be valid also for the measured effective diffusivities ($D_{e,i}/D_{e,HTO}$). The diffusivities are low, which is in accordance with the low porosity. Sodium and especially iodide show lower diffusivities than expected. In the case of iodide, anion exclusion is likely to occur, since the porosity of the sample is low. Anion exclusion is supported by the similar behaviour of bromide as of iodide.

The diffusivities of Ba and Cs were not evaluated quantitatively due to too small accumulated amounts of tracer. The preliminary fits to the present data show very low diffusivity and sorptivity. However, a breakthrough has occurred and the small amounts diffused indicates that some diffusion pathways that have low sorptivity and low diffusivity exists in the sample. More sorptive pathways may not yet have contributed to the breakthrough of the more sorbing tracers. The breakthrough could also be affected by the diversivity of the geometrical lengths of the sample. It is obvious that the inhomogeneous composition of the sample disables the evaluation using the ordinary solution to the diffusion equation.

For the other more weakly sorbing elements as Ca, Sr and Na, the retardation factor, α, is smaller than for HTO. No sorption coefficients can therefore be calculated for those elements. A general low sorption is also found in the batch experiments with the crushed material Feature A material (cf. chapter 3)

The diffusivity of the large Tb-EDTA is low, which is in agreement with diffusivities for other large molecules. The retardation factor for the Tb-EDTA complex is low, which indicates that it is the diffusion of Tb-EDTA that has been measured and not diffusion of Tb^{3+}.

Compared to the diffusion experiments using generic material, the observed porosity, diffusivities and sorption capacity in the KXTT1 sample are lower, as a consequence of the geologic past of the material. The low porosity of the mylonite results in low effective diffusivities and the abscence of biotite lead to low sorption capacity.

Parts of the KXTT1-material may be altered without mylonitization, having a higher porosity than the mylonite. However, in a material composed of two layers of length l_1 and l_2, having the diffusivities $D_{e,1}$ and $D_{e,2}$ in each layer, the total diffusivity $D_{e,tot}$ for diffusion through the two layers can be described as (Skagius and Neretnieks 1985)

$$\frac{l_1}{D_{e,1}} + \frac{l_2}{D_{e,2}} = \frac{l_1 + l_2}{D_{e,tot}} \qquad 4\text{-}6$$

Consequently, the the total diffusivity is largely determined by the layer with the smallest diffusivity, *i.e.* the largest resistance to diffusion. In the case of the KXTT1 material, the mylonite layer will determine the total diffusivity of the sample.

5 General Conclusions

A general conclusion of the experiments is that it will be difficult to apply a simple fully reversible sorption-diffusion model to interpret the *in situ* results of the TRUE experiments with sorbing tracers. The laboratory experiments indicate that the important parameters, sorption and diffusivity, are far more complex than to be described by a simple sorption coefficient and a single diffusion rate.

Comparison of the results of the batch sorption and the diffusion experiments indicates that the sorption of the cations is considerably lower in the diffusion experiments. This finding is also supported by the observation in the batch experiments of the increased sorption with decreasing particle size. It can therefore be concluded that the crushing process increases the availability of sorption sites on the inner surfaces of the rock material. It is therefore possible that the results obtained from sorption experiments on crushed material may overestimate the *in situ* sorption of radionuclides. However, the increase of sorption with contact time observed may indicate that that the inner surfaces can become available for sorption in the performance assessment time scale but not in the laboratory experiment time scale. The main scope of this study is to provide data to be used for the prediction and evaluation of the TRUE *in situ* experiments. It is therefore recommended to use sorption and diffusion data obtained from the diffusion experiment or from the batch experiments using the larger size fractions of the crushed geological material.

In the coarser fractions of the Äspö diorite many grains are polymineralic and diffusion along the grain boundaries can thus be expected to contribute to the sorption. Along with these ideas, it was initially expected that a larger increase in K_d versus time should be recorded for the 1-2 mm fraction than for the finest fraction (0.045-0.09mm). Instead the reverse was observed; the finest fractions show the highest increase in K_d versus time. However, the studies of the distribution of porosity in intact Äspö diorite, using the ^{14}C-PMMA method, show that a network of biotite and plagioclase grains, both showing high intra-granular porosity, largely constitutes the porosity whereas grain boundary porosity is not found to be important. This observation indicates that the increase in K_d with time for the crushed finer, monomineralic fractions can be explained by the fact that in these samples a much larger pore volume is open for diffusion and interaction. This is also supported by the higher K_d values in the finer fractions which cannot be explained by the higher biotite content in the fine fractions. Instead the larger available surfaces including the inner pore spaces seems to be the most important factor.

6 Selection of Site-Specific Transport Parameters for Modelling

Estimations of transport parameters for the TRUE experiments with sorbing tracers are primarily based on the laboratory experiments with Äspö diorite (batch and through diffusion experiments) using non-oxic conditions, ambient temperature (20-25 °C) and a saline synthetic "Äspö-like" groundwater with an ionic strength of ~0.25 and pH 7.5. Data are also available for the batch experiments with crushed site specific material taken from drill core intersections with Feature A. For the latter experiments, a synthetic groundwater with an ionic strength of ~0.17, representing the site specific conditions, was used.

6.1 Diffusivity (D_e)

The effective diffusivities for the different tracers are based on mean values from through diffusion measurements in rock cylinders of Äspö diorite of 1 and 2 cm lengths. It is observed that D_e decreases with increasing cell lengths used in the experiments, but since the porosity in the vicinity of a natural fracture is largest near the fracture, the 1 and 2 cm samples may be the most representative (which is a guess, since the Äspö diorite used in the laboratory experiments was fresh and unaltered, which is not the case for the fracture material).

The diffusivity and porosity results from the KXTT1 Feature A site specific diffusion cell show four times lower diffusivity and porosity than for the Äspö diorite, *i.e.*,. ($D_e^{HTO} \approx 4 \cdot 10^{-14}$, $\varepsilon \approx 0.001$) and ($D_e^{HTO} \approx 1.2 \cdot 10^{-13}$, $\varepsilon \approx 0.004$) for the site specific material and the Äspö diorite, respectively. An estimation of effective diffusivities based on this single sample would therefore be to reduce the diffusivities for the tracers obtained for Äspö diorite with a factor of three in order to obtain the effective diffusivities of the Feature A site specific material.

D_e for the sorbing tracers have been calculated from the relation

$$D_e^{sorb} = D_w^{sorb} \cdot F \qquad 6\text{-}1$$

where the formation factor for Äspö diorite has been calculated according to:

$$F = \frac{D_e^{HTO}}{D_w^{HTO}} = \frac{1.2 \cdot 10^{-13}}{2.4 \cdot 10^{-9}} = 5 \cdot 10^{-5} \qquad 6\text{-}2$$

and the formation factor for the Feature A site specific material has been calculated according to:

$$F = \frac{D_e^{HTO}}{D_w^{HTO}} = \frac{4 \cdot 10^{-13}}{2.4 \cdot 10^{-9}} = 1.7 \cdot 10^{-5} \qquad 6\text{-}3$$

where D_w is the diffusivity of the tracer in the water phase (Gray 1972). The estimated diffusivities are presented in Table 6-1.

The diffusivities are valid for water with an ionic strength less than 0.5. and a temperature of 20-25 °C. A lowering of the temperature with 10 °C would theoretically give approximately 25% lower diffusivities.

Table 6-1 Matrix sorption and diffusion data obtained from through diffusion experiments in rock cylinders of Äspö diorite and Feature A site specific material.

Tracer	K_d (m^3/kg)	D_w (m^2/s)**	ÄD D_e (m^2/s)***	Feature A D_e (m^2/s)***
HTO	-	$2.4 \cdot 10^{-9}$	$1.2 \cdot 10^{-13}$	$4 \cdot 10^{-14}$
Na^+	$1.4 \cdot 10^{-6}$	$1.33 \cdot 10^{-9}$	$6.7 \cdot 10^{-14}$	$2.2 \cdot 10^{-14}$
Rb^+	$4 \cdot 10^{-4}$*	$2.03 \cdot 10^{-9}$	$1.0 \cdot 10^{-13}$	$3 \cdot 10^{-14}$
Cs^+	$6 \cdot 10^{-3}$****	$2.02 \cdot 10^{-9}$	$1.0 \cdot 10^{-13}$	$3 \cdot 10^{-14}$
Ca^{2+}	$5.2 \cdot 10^{-6}$	$0.79 \cdot 10^{-9}$	$4.0 \cdot 10^{-14}$	$1.3 \cdot 10^{-14}$
Sr^{2+}	$4.7 \cdot 10^{-6}$	$0.79 \cdot 10^{-9}$	$4.0 \cdot 10^{-14}$	$1.3 \cdot 10^{-14}$
Ba^{2+}	$2 \cdot 10^{-4}$****	$0.83 \cdot 10^{-9}$	$4.2 \cdot 10^{-14}$	$1.4 \cdot 10^{-14}$

Data valid for 20-25 °C (K_d for 10-30 °C), I=0.25 and pH=7.5.

* from $K_{d(2\text{-}4mm)}/5$, other K_d are mean values from diffusion experiments.

** calculated water diffusivities at infinite dilution (Gray 1972)

*** $D_e = F \cdot D_w$, $F = 5 \cdot 10^{-5}$ for the Äspö diorite and $F = 1.7 \cdot 10^{-5}$ for the Feature A site specific material.

**** from penetration depth studies (section 4.2)

6.2 Sorption Coefficients (K_d, K_a)

The results of the batch experiments with crushed site specific material show that the sorption strength is similar to that of the Äspö diorite, see Table 6-3. Therefore, the estimations of K_d are based on laboratory experiments with Äspö diorite. Sorption coefficients are dependent on ionic strength and pH. The presented sorption data are reasonably valid for a saline groundwater with I = 0.1-0.4, pH = 7-9 and a temperature of 10-30 °C.

K_d for sorption within the rock matrix (related to matrix diffusion), is based on K_d evaluated from through diffusion experiments in rock cylinders of Äspö diorite (Na, Ca and Sr) and on the penetration studies of Äspö diorite (Cs and Ba). Since no "diffusion K_d" for Rb is available, the K_d for this elements has been estimated based on the K_d measured for the largest particle fraction (2-4 mm) in the batch experiments. These batch K_d values have been divided by a factor of 5, which was the observed relation between the diffusion K_d and batch K_d for Na, Ca and Sr. The estimated K_d values are presented in Table 6-1.

An attempt to estimate surface related sorption coefficients, K_a, has been made. As a base the geometrical area and the BET-surface area of the largest particle size and the geometrical surface area of the injection side of the diffusion cells have been used. However, in a real fracture, the size of the surfaces may vary drastically depending on whether the fracture contains crushed particles, clay minerals etc. K_a values determined from experiments with crushed material often tend to overestimate the surface areas.

Assuming spherical shape of the particles of the solid phase used in the batch experiments (section 3.2.2.6) , K_d can be described as

$$K_d = K_{di} + K_a \cdot \frac{6}{\rho \cdot d_p} \qquad 6\text{-}4$$

where K_{di} is the sorption onto inner surfaces and K_a is the sorption onto the outer surfaces. K_a evaluated from eq. 6-4 (the slope of a plot of K_d vs $1/d_p$) and from initial sorption onto the injection side of a diffusion cell (Cs sorption) and the TRUE-1 diffusion cell (Cs, Rb) are presented in Table 6-2. K_a has also been calculated from K_d data for the 2-4 mm fraction after the shortest sorption time (1 d), when the penetration into the rock matrix is small. However, a slight diffusion into the pores may lead to an overestimation of K_a even after this contact time. K_a has also been calculated related to the measured BET-surfaces of the 2-4 mm fractions (Kr-gas adsorption).

A comparison of K_d for the 1-2 mm particle size fraction of site specific material (mylonite and altered granite) and Äspö diorite is presented in Table 6-3. The 1-2 mm fraction was used for this experiment. The synthetic groundwater used had the same composition as the Feature A groundwater. A volume of 8.5 ml of synthetic groundwater was contacted to 2 g of solid material. The K_d-values are obtained from

measuring the losses of tracers in the liquid phase and calculating the K_d from the mass balance. The values presented are given for a contact time of 9 days.

The ion exchange is assumed to be in instantaneous equilibrium, since generally, ion exchange reactions are considered to have fast kinetics. If the transport of the sorbing tracer from the bulk of the groundwater to the fracture surface is slow, this may be interpreted as non-equilibrium in the sorption.

6.3 Porosity (ε)

The mean porosity for the 1 and 2 cm diffusion cells of Äspö diorite ($\varepsilon = 0.4 \pm 0.1\%$) was evaluated from the experiments with tritiated water, for which the rock capacity factor equals the total porosity. The "diffusion" porosity of the single diffusion cell with site specific material is 0.1%.

Table 6-2 Surface sorption coefficients (K_a) for Äspö diorite and Feature A site specific material.

Tracer	Crushed material, Geom. surf. 14 d.[1] K_a (m)	Diff.cell, geom.surf. 10 d.[2] K_a (m)	TRUE-A diff.-cell, geom.surf. 5 d.[2] K_a (m)	Crushed material, geom.surf. 1 d.[3] K_a (m)	Crushed material, BET-surf. 14d.[4] K_a (m)
Na^+	$7\cdot10^{-7}$			$5\cdot10^{-6}$	$2\cdot10^{-7}$
Rb^+	$5\cdot10^{-4}$		$4\cdot10^{-3}$	$1\cdot10^{-3}$	$6\cdot10^{-5}$
Cs^+	$8\cdot10^{-3}$	$9\cdot10^{-3}$	$1\cdot10^{-2}$	$8\cdot10^{-3}$	$5\cdot10^{-4}$
Ca^{2+}	$4\cdot10^{-6}$			$3\cdot10^{-5}$	$3\cdot10^{-6}$
Sr^{2+}	$8\cdot10^{-6}$			$2\cdot10^{-5}$	$4\cdot10^{-6}$
Ba^{2+}	$2\cdot10^{-4}$			$6\cdot10^{-4}$	$4\cdot10^{-5}$

Data valid for 10-30 °C, I=0.25 . (I=0.17. for TRUE-A diff.cell), and pH=7.5

[1] From eq.6-4, plot of K_d vs $1/d_p$ for the four largest particle fractions. For Na^+, Ca^{2+} and Sr^{2+} the desorption coefficient, $K_{d(des1)}$,(eq. 3-8)has been used while for the other tracers, sorption K_d (eq. 3-3), has been used

[2] Initial sorption onto the surface of the injection side of the diffusion cell.

[3] From K_d/A_{geom} 2-4 mm particle size. A_{geom}=0.67 m^2/kg.

[4] From K_d/A_{BET} 2-4mm particle size. A_{BET}=26 m^2/kg.

In those cases where no value is given the sorption was below the detection limit.

Table 6-3 Sorption K_d (eq. 3-3) for the tracers in contact with Äspö diorite, mylonite and altered granite, using Feature A site specific conditions

Tracer	**Äspö-Diorite**		**Mylonite T2**		**Alt. Diorite T3**	
	K_d (m^3/kg)	**+/-**	**K_d (m^3/kg)**	**+/-**	**K_d (m^3/kg)**	**+/-**
Na^+	$<2.8\cdot10^{-5}$		$<2.2\cdot10^{-4}$		$<6.0\cdot10^{-5}$	
Ca^{2+}	$<4.4\cdot10^{-5}$		$<5.3\cdot10^{-4}$		$<6.3\cdot10^{-4}$	
Rb^+	$1.4\cdot10^{-3}$	$3.5\cdot10^{-4}$	$2.1\cdot10^{-3}$	$4.3\cdot10^{-4}$	$3.8\cdot10^{-4}$	$3.1\cdot10^{-4}$
Sr^{2+}	$<2.3\cdot10^{-4}$		$<2.6\cdot10^{-4}$		$<9.4\cdot10^{-5}$	
Cs^+	$1.4\cdot10^{-2}$	$1.2\cdot10^{-3}$	$8.0\cdot10^{-3}$	$5.6\cdot10^{-4}$	$3.1\cdot10^{-3}$	$2.3\cdot10^{-4}$
Ba^{2+}	$1.2\cdot10^{-3}$	$1.2\cdot10^{-4}$	$1.3\cdot10^{-3}$	$1.3\cdot10^{-4}$	$1.8\cdot10^{-3}$	$1.4\cdot10^{-4}$

Acknowledgement

Marja Siitari-Kauppi (Laboratory of Radiochemistry, University of Helsinki, Finland) is acknowledged for assistance with the ^{14}C-PMMA impregnation technique used for porosity studies, and for valuable discussions.

List of Abbreviations and Symbols

Abbr.	Meaning	Sort	Used in chapter
A	Area of the solid phase	m^2	3
A_s	Geometrical surface area of the diffusion slab	m^2	3
C	Concentration of tracer in the aqueous phase	mole/l	3
CEC	Cation exchange capacity	µeq/g	3
C_r,	Accumulated scaled ratio of concentration	mole/l	4
C_x	Measured average concentration of a slice of the diffusion slab at distance x	mole/l	4
$C_{x=0}$	Concentration in the pore water in the first thin layer at the surface of the diffusion slab	mole/l	4
C_0	Concentration of tracer in the aqueous phase in contact with no solid phase	mole/l	3
C_1	Concentration in the injection cell	mole/l	4
C_2	Concentration in the measuring cell	mole/l	4
D_a	Apparent diffusivity	m^2/s	3,4
D_e	Effective diffusivity	m^2/s	4,6
D_p	Pore diffusivity	m^2/s	4
D_w,	Diffusivity of the tracer in water	m^2/s	4
d_n	Thickness of the layer n in the solid phase (modelling in 3.2.4)	m	3
$<d_p>$	Average particle diameter of the solid phase	m	3
d_0	Thickness of the first directly exchangeable layer of the solid phase (modelling in 3.2.4)	m	3
F	Formation factor,	-	4
f_p	Probability factor of the pre type p	-	3
K_a	Distribution coefficient for the tracer between the surface area of the solid phase and the volume of the aqueous phase	m	3,6
K_d	Distribution coefficient for the tracer between the mass of the solid phase and the volume of the aqueous phase	m^3/kg	3,4,6
$K_{d(des1)}$	Distribution coefficient obtained from desorption experiments (see chapter 3)	m^3/kg	3
$K_{d(des2)}$	Distribution coefficient obtained from desorption experiments (see chapter 3)	m^3/kg	3
$K_{d,i}$	Distribution coefficient regarding only the inner surfaces of the solid phase (see chapter 3)	m^3/kg	3
K_s	Selectivity coefficient	[1)]	3
k	Factor used in equation 3.26	-	3
k_1	Rate constant for the sorption reaction	s^{-1}	3
k_{-1}	Rate constant for the desorption reaction	$kg \cdot m^{-3} \cdot s^{-1}$	3
l	Lengths of the pores in the solid phase	m	3

List of abbreviations, continued from previous page

Abbr.	Meaning	Sort	Used in chapter
l_p	Length of the pore type p	m	3
l_s	Length of the diffusion slab	m	4
m	Mass of the solid phase	kg	3
N_{ndes}	Percentage of the non- or very slowly desorbable of the sorbed tracer	%	3
q_n	Argument in eq. (3.25)	-	3
R_{aq}	Counting rate of the sampled water from samples with solid phase present	cpm	3
R_{des}	Counting rate of the sampled desorption solution	cpm	3
$R_{des(exp)}$	Expected counting rate of the desorption solution assuming fully reversible sorption	cpm	3
$R_{des(p)}$	Counting rate of the sampled desorption solution after the p-1 exchange of the desorption solution	cpm	3
R_s	Counting rate of the solid phase measurement	cpm	3
R_0	Counting rate of the sampled water from samples with no solid phase present	cpm	3
r	Radius of a sphere	m	3
S	Cation exchange site with the charge 1-	eq	3
t	Sorption or diffusion contact time	s	3,4
t_n	Time step used (modelling in 3.2.4)	s	3
t_{tot}	Total time (modelling in 3.2.4)	s	3
V	Volume of the aqueous phase	m^3	3
V_s	Volume of the sampled aqueous phase	m^3	3
V_2	Volume of the measuring container	m^3	4
α	Rock capacity factor	-	3,4
ε_t	Total porosity	-	3,4,6
ε^+	Transport porosity	-	4
ρ	Density of the solid phase	kg/m^3	3
σ	Pore constrictivity,		4
σ_p	Standard deviation of the length of the pores in the solid material.	m	3
τ	Tortuosity		4

[1)] Sort of selectivity coefficient is dependent on the definition, see 3.1.12

References

Atkinson A, Nickerson AK, 1988. Diffusion and Sorption of Cesium, strontium and iodine in Water-Saturated Cement, *Nuclear Technology*, **81**, 100

Banwart S, (ed) 1995. The redox experiment in block scale – Final report from the 3 years project, SKB Progress Report PR 25-95-06.

Bradbury, MH, Stephen, IG, 1985. Diffusion and permeability based sorption measurements in intact rock samples, Mat. Res. Soc. Symp. Proc. **50**, Pittsburgh, PA, 1985, 81-90.

Brunauer S, Emmet PH, Teller E, 1938. Adsorption of Gases in Multimolecular Layers, J.Am. Chem. Soc. 60, 309

Byegård J, 1993. The possibility of using slightly sorbing cations in tracer experiments in the Äspö Hard Rock Laboratory - A litterature survey and some basic considerations, Äspö Hard Rock Laboratory Progress Report PR-25-93-14

Byegård J, 1993 Tracer Handbook, SKB Progress Report PR 25-92-11.

Byegård J, Skarnemark G, Skålberg M, 1995. The use of some ion-exchange sorbing tracer cations in in-situ experiments in high saline groundwaters, Mat. Res. Soc. Symp. Proc. 353, Pittsburgh, PA, 1077-1084

Bäckblom G, Olsson O, 1994. Program for Tracer Retention Understanding Experiments. Äspö Hard Rock Laboratory Progress Report PR-25-94-24.

Cornell RM, 1993. Adsorption of cesium on minerals: A review. J Radioanal. Nucl. Chem., 171, 483-500.

Crank J, 1975. The Mathematics of Diffusion, 2nd ed., Oxford University Press, NewYork, 50-51

Eliasson T, 1993. Mineralogy, geochemistry and petrophysics of red coloured granite adjacent to fractures. SKB Technical Report, TR 93-06

Gray DE, 1972. American Institute of Physics Handbook, McGraw-Hill , New York (1972)

Hellmuth KH, Lukkarinen S., Siitari-Kauppi M., 1994. Rock matrix studies with carbon-14-polymethylmethacrylate (PMMA); Method, development and applications. Isotopenpraxis Environ. Health Stud., 30: 47-60

Hellmuth KH, Siitari-Kauppi, M, Lindberg, A, 1993. Study of porosity and migration pathways in crystalline rock by impregnation with ^{14}C-polymethyl-methacrylate, J. of Contaminant Hydrology, 13, pp 403-4183

Idemitsu K, Furuya H, Hara T, Inagaki Y, 1992. Migration of cesium, strontium and cobalt in water-saturated Inada Granite, J. Nucl. Sci. Technol. 29, 454-460

Ittner T, Torstenfelt B, Allard B, 1990. Diffusion of strontium, iodine and cesium in granitic rock, Radiochim. Acta 49, 101-106

Ittner T, Byegård J, 1997. First TRUE stage – Test of tracer sorption on equipment, Äspö Hard Rock Laboratory Progress Report HRL-97-28.

Johansson H, Byegård J, Skarnemark G, Skålberg M, 1996. Matrix diffusion of some alkali- and alkaline earth-metals in granitic rock, Mat. Res. Soc. Symp. Proc. 465, Pittsburgh, PA, 871-878.

Neretnieks I, 1980. Diffusion in the rock matrix - an important factor in radionuclide retardation? J. Geophys. Res., 85, 4379

Nilsson AC, 1997. Results of the analyses of groundwater sampled in the TRUE-1 site, Äspö Hard Rock Laboratory Technical Note TN-97-08t.

Press WH, Teukolsky SA, Vetterling WT, Flannery BP, 1986. Numerical Recipes , Cambridge University Press.

Rasilainen K, Hellmuth KH, Kivekäs L, Melamed A, Ruskeeniemi T, Siitari-Kauppi M, Timonen J., Valkiainen M, 1996. An interlaboratory comparison of methods for measuring rock matrix porosity. Espoo: VTT (Technical Research Centre of Finland) Energy, 1996, VTTRN 1776

Skagius K, Neretnieks, I, 1982. Diffusion in crystalline rocks of some sorbing and nonsorbing species, SKB Technical Report 82-12.

Skagius K, Svedberg G, Neretnieks I, 1982. A study of strontium and cesium sorptionon granite, Nucl. Tecn., 59, 389-398.

Skagius K, Neretnieks I, 1986. Porosities and diffusivities of some nonsorbing species in crystalline rocks, Water Resources Res., 22:3, 389-398

Smellie JAT, Laaksoharju M, Wikberg P, 1995. Äspö, SE Sweden: a natural groundwater flow model derived from hydrogeochemical observations, J. of Hydrology, 172, 147-169

Stanfors R, Liedholm M, Munier R, Olsson P, Stille H, 1993. Geological - structural evaluation of data from section 700-1475 m. SKB Progress Report 25-93-05.

Stanfors R, Liedholm M, Munier R, Olsson P, Stille H, 1993. Geological - structural evaluation of data from section 1475-2265 m. SKB Progress Report 25-93-10.

Tsukamuto M, Ohe T, 1993. Effects of biotite distribution on cesium diffusion in granite, Chemical geology, 107, 29-46

Winberg A, 1994. Tracer Retention Understanding Experiments (TRUE)– Test plan for the first TRUE stage, Äspö Hard Rock Laboratory Progress Report 25-94-35

Winberg A, 1996. First TRUE Stage – Tracer Retention Understanding Experiments – Descriptive structural-hydraulic models on block and detailed scales of the TRUE-1 site, Äspö Hard Rock Laboratory International Cooperation Report 96-04

List of SKB reports

Annual Reports

1977-78
TR 121
KBS Technical Reports 1 – 120
Summaries
Stockholm, May 1979

1979
TR 79-28
The KBS Annual Report 1979
KBS Technical Reports 79-01 – 79-27
Summaries
Stockholm, March 1980

1980
TR 80-26
The KBS Annual Report 1980
KBS Technical Reports 80-01 – 80-25
Summaries
Stockholm, March 1981

1981
TR 81-17
The KBS Annual Report 1981
KBS Technical Reports 81-01 – 81-16
Summaries
Stockholm, April 1982

1982
TR 82-28
The KBS Annual Report 1982
KBS Technical Reports 82-01 – 82-27
Summaries
Stockholm, July 1983

1983
TR 83-77
The KBS Annual Report 1983
KBS Technical Reports 83-01 – 83-76
Summaries
Stockholm, June 1984

1984
TR 85-01
Annual Research and Development Report 1984
Including Summaries of Technical Reports Issued during 1984. (Technical Reports 84-01 – 84-19)
Stockholm, June1985

1985
TR 85-20
Annual Research and Development Report 1985
Including Summaries of Technical Reports Issued during 1985. (Technical Reports 85-01 – 85-19)
Stockholm, May 1986

1986
TR 86-31
SKB Annual Report 1986
Including Summaries of Technical Reports Issued during 1986
Stockholm, May 1987

1987
TR 87-33
SKB Annual Report 1987
Including Summaries of Technical Reports Issued during 1987
Stockholm, May 1988

1988
TR 88-32
SKB Annual Report 1988
Including Summaries of Technical Reports Issued during 1988
Stockholm, May 1989

1989
TR 89-40
SKB Annual Report 1989
Including Summaries of Technical Reports Issued during 1989
Stockholm, May 1990

1990
TR 90-46
SKB Annual Report 1990
Including Summaries of Technical Reports Issued during 1990
Stockholm, May 1991

1991
TR 91-64
SKB Annual Report 1991
Including Summaries of Technical Reports Issued during 1991
Stockholm, April 1992

1992
TR 92-46
SKB Annual Report 1992
Including Summaries of Technical Reports Issued during 1992
Stockholm, May 1993

1993
TR 93-34
SKB Annual Report 1993
Including Summaries of Technical Reports Issued during 1993
Stockholm, May 1994

1994

TR 94-33

SKB Annual Report 1994

Including Summaries of Technical Reports Issued during 1994

Stockholm, May 1995

1995

TR 95-37

SKB Annual Report 1995

Including Summaries of Technical Reports Issued during 1995

Stockholm, May 1996

1996

TR 96-25

SKB Annual Report 1996

Including Summaries of Technical Reports Issued during 1996

Stockholm, May 1997

List of SKB Technical Reports 1998

TR 98-01

Global thermo-mechanical effects from a KBS-3 type repository. Summary report

Eva Hakami, Stig-Olof Olofsson, Hossein Hakami, Jan Israelsson

Itasca Geomekanik AB, Stockholm, Sweden

April 1998

TR 98-02

Parameters of importance to determine during geoscientific site investigation

Johan Andersson[1], Karl-Erik Almén[2], Lars O Ericsson[3], Anders Fredriksson[4], Fred Karlsson[3], Roy Stanfors[5], Anders Ström[3]

[1] QuantiSci AB

[2] KEA GEO-Konsult AB

[3] SKB

[4] ADG Grundteknik KB

[5] Roy Stanfors Consulting AB

June 1998

TR 98-03

Summary of hydrochemical conditions at Aberg, Beberg and Ceberg

Marcus Laaksoharju, Iona Gurban, Christina Skårman

Intera KB

May 1998

TR 98-04

Maqarin Natural Analogue Study: Phase III

J A T Smellie (ed.)

Conterra AB

September 1998

TR 98-05

The Very Deep Hole Concept – Geoscientific appraisal of conditions at great depth

C Juhlin[1], T Wallroth[2], J Smellie[3], T Eliasson[4], C Ljunggren[5], B Leijon[3], J Beswick[6]

[1] Christopher Juhlin Consulting

[2] Bergab Consulting Geologists

[3] Conterra AB

[4] Geological Survey of Sweden

[5] Vattenfall Hydropower AB

[6] EDECO Petroleum Services Ltd.

June 1998

TR 98-06

Indications of uranium transport around the reactor zone at Bagombe (Oklo)

I Gurban[1], M Laaksoharju[1], E Ledoux[2], B Made[2], A L Salignac[2],

[1] Intera KB, Stockholm, Sweden

[2] Ecole des Mines, Paris, France

August 1998

TR 98-07

PLAN 98 – Costs for management of the radioactive waste from nuclear power production

Swedish Nuclear Fuel and Waste Management Co

June 1998

TR 98-08

Design premises for canister for spent nuclear fuel

Lars Werme

Svensk Kärnbränslehantering AB

September 1998

TR 98-09

Test manufacturing of copper canisters with cast inserts Assessment report

Claes-Göran Andersson

Svensk Kärnbränslehantering AB

Augusti 1998

TR 98-10
Characterization and Evaluation of Sites for Deep Geological Disposal of Radioactive Waste in Fractured Rocks
Proceedings from The 3rd Äspö International Seminar, Oskarshamn, June 10–12, 1998-11-10
Svensk Kärnbränslehantering AB
September 1998

TR 98-11
Leaching of 90-year old concrete mortar in contact with stagnant water
Jan Trägårdh, Björn Lagerblad
Swedish Cement and Concrete Research Institute
July 1998

TR 98-12
Geological-structural models used in SR 97
Uncertainty analysis
Pauli Saksa, Jorma Nummela
FINTACT Ltd
October 1998

TR 98-13
Late Quaternary changes in climate
Karin Holmgren and Wibjörn Karlén
Department of Physical Geography
Stockholm University
December 1998

TR 98-14
Partitioning and transmutation (P&T) 1997
Åsa Enarsson, Anders Landgren, Jan-Olov Liljenzin, Mats Skålberg, Lena Spjuth
Department of Nuclear Chemistry, Chalmers University of Technology, Gothenburg
and
Waclaw Gudowski, Jan Wallenius
Department of Nuclear and Reactor Physics, Royal Institute of Technology, Stockholm
May 1998

TR 98-15
Studies of surface complexation of H^+, NpO_2^+, Co^{2+}, Th^{4+} onto TiO_2 and H^+, UO_2^{2+} onto alumina
Anna-Maria Jakobsson, Yngve Albinsson
Department of Nuclear Chemistry, Chalmers University of Technology, Sweden
and
Robert S Rundberg
Los Alamos National Laboratory, USA
November 1998

TR 98-16
Backfilling with mixtures of bentonite/ ballast materials or natural smectitic clay?
Roland Pusch
Geodevelopment AB
October 1998

TR 98-17
Groundwater degassing in fractured rock:
Modelling and data comparison
Jerker Jarsjö and Georgia Destouni
Water Resources Engineering
Royal Institute of Technology, Stockholm
November 1998

ISSN 0284-3757
CM Gruppen AB, Bromma, 1999